

Coupling Chemistry for Surface Immobilization in Scanning

Probe Lithography

Zur Erlangung des akademischen Grades eines

DOKTORS DER NATURWISSENSCHAFTEN

(Dr. rer. nat.)

von der KIT-Fakultät für Chemie und Biowissenschaften

des Karlsruher Instituts für Technologie (KIT)



genehmigte

DISSERTATION

Von

M.Sc. SEYED MOHAMMAD MAHDI DADFAR

Karlsruhe, 2019

Dekan: Prof. Dr. Reinhard Fischer

Referent: PD Dr. Dr. Michael Hirtz

Korreferent: Prof. Dr. Annie Powell

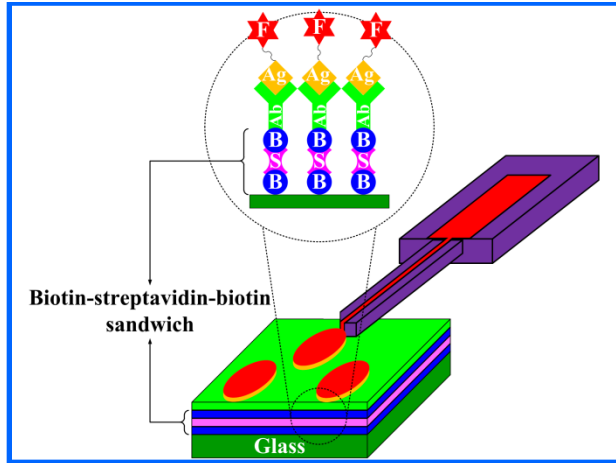
Tag der mündlichen Prüfung: 26.07.2019

To my family especially my father and my mother that I owe them

Acknowledgements

None of the work explained in this thesis would have been possible without the help of many different people and the support of the funding agency. I would like to thank very much PD Dr. Dr. Michael Hirtz for giving me the opportunity to do PhD under his guidance. I very appreciate his guidance during the past few years. I furthermore appreciate the amount of freedom that he has given me regard to the experiments performed during my PhD. I am pretty sure that he is the best supervisor that I have ever had. I would also to thank him for being such a nice person who is always willing answer questions and showing interest in my work. I honestly hope that we can continue to work together for many more years to come. I would furthermore like to thank Prof. Dr. Harald Fuchs for helping me during the past few years. I would like to thank Prof. Dr. Annie Powell for helping me during my PhD time at KIT. I am very grateful for her interests in my work and very much appreciate for her kind and pleasant nature and I have always enjoyed spending time with her. Also, I would like to thank Vanessa Trouillet for performing XPS measurement and Georgia Lewes-Malandrakis for diamond preparation. Furthermore, I would like to thank my colleagues especially, Dr. Sylwia Sekula, Dr. Uwe Bog, Dr. Ravi Kumar, Dr. Masooma Ibrahim, Hui-Yu Liu, Dr. Jianmei Chen, Dr. Yangxin Wang, Navid Hussain, Dr. Ghulam Abbas, Chunting Zhong, Firas Al-Zeidaneen and Bingquan Yang, for supporting me during my time at KIT. At the end I would finally like to thank very much Deutsche Forschungsgemeinschaft (DFG) for the kind support and Karlsruhe house of young scientist (KHYS) for supporting me to visit two scientific groups at Denmark and Netherlands.

Die vorliegende Arbeit wurde in der Zeit von April 2016 bis July 2019 am Institut für Nanotechnology, des Karlsruher Instituts für Technologie (KIT) unter Anleitung von PD Dr. Dr. Michael Hirtz angefertigt.



TOC

| Content | Page |
|---|-------------|
| Zusammenfassung | 5 |
| Chapter 1..... | 7 |
| Introduction..... | 7 |
| 1.1. Lithography, DPN and μ CS | 8 |
| 1.2. Surface and material functionalization..... | 8 |
| 1.3. Click chemistry: history and types..... | 12 |
| 1.4. Biomarkers for hepatocellular carcinoma (HCC) | 14 |
| 1.5. Diamond substrate for printing | 15 |
| Chapter 2..... | 17 |
| Thesis overview and research objectives | 17 |
| Chapter 3..... | 20 |
| Functionalization of DBCO-terminated glass surface | 20 |
| 3.1. Introduction | 21 |
| 3.2. Results and discussion | 24 |
| 3.2.1. XPS and contact angle measurements | 24 |
| 3.2.2. Array immobilization of TAMRA-azide and Cy5 thiol | 27 |
| 3.2.3. Protein coupling by biotin-azide and biotin-thiol | 32 |
| 3.3. Summary | 35 |
| Chapter 4..... | 36 |
| Functionalization of thiol-terminated glass surface..... | 36 |
| 4.1. Introduction | 37 |
| 4.2. Results and discussion | 40 |
| 4.2.1. Contact angle measurements | 40 |
| 4.2.2. XPS measurements..... | 42 |
| 4.2.3. Array immobilization of FAM-DBCO and TAMRA-maleimide | 43 |
| 4.2.4. Protein coupling by biotin-DBCO and biotin-maleimide..... | 45 |
| 4.3. Summary | 48 |
| Chapter 5..... | 49 |
| Functionalization of epoxy-terminated glass surface | 49 |

| | |
|---|----|
| 5.1. Introduction | 50 |
| 5.2. Results and discussion | 53 |
| 5.2.1. Characterization of surfaces by contact angle and AFM..... | 53 |
| 5.2.2. Array immobilization of Cy5 thiol, R6G and TAMRA-azide | 54 |
| 5.2.3. Protein coupling by biotin-thiol, biotin-amine and biotin-azide | 59 |
| 5.3. Summary | 61 |
| Chapter 6..... | 62 |
| Fluorescent immunosensors for detection of alpha-fetoprotein (AFP)..... | 62 |
| 6.1. Introduction | 63 |
| 6.2. Results and discussion | 64 |
| 6.2.1. Generation of biotinylated surfaces..... | 64 |
| 6.2.2. Characterization of surfaces by AFM | 64 |
| 6.2.3. Characterization of surfaces by XPS..... | 65 |
| 6.2.4. Comparison of immobilization routes for sandwich application | 65 |
| 6.2.5. Evaluation of sensitivity | 69 |
| 6.3. Summary | 74 |
| Chapter 7..... | 75 |
| Functionalization of DBCO-, thiol- and epoxy terminated diamond surface | 75 |
| 7.1. Introduction | 76 |
| 7.2. Results and discussion | 77 |
| 7.2.1. Contact angle measurement | 77 |
| 7.2.2. Array immobilization on the diamond surfaces | 77 |
| 7.2.3. Protein coupling on the diamond surfaces | 80 |
| 7.3. Summary | 85 |
| Chapter 8..... | 86 |
| Summary..... | 86 |
| Chapter 9..... | 89 |
| Experimental section | 89 |
| 9.1. Materials..... | 90 |
| 9.2. Methods..... | 92 |

| | |
|--|----|
| 9.2.1. Functionalization of DBCO-terminated glass surface (chapter 3) | 92 |
| 9.2.1.1. Substrate preparation | 92 |
| 9.2.1.2. Ink solution preparation | 93 |
| 9.2.1.3. Pattern writing via μ CS..... | 93 |
| 9.2.1.4. Click reaction between azides and alkyne | 93 |
| 9.2.1.5. Click reaction between thiols and alkyne | 93 |
| 9.2.1.6. Protein binding on microarrays | 94 |
| 9.2.2. Functionalization of thiol-terminated glass surface (chapter 4)..... | 94 |
| 9.2.2.1. Preparation of substrate | 94 |
| 9.2.2.2. Preparation of ink solution..... | 94 |
| 9.2.2.3. Microarray printing via μ CS | 94 |
| 9.2.2.4. Microarray immobilization via click reaction | 95 |
| 9.2.2.5. Protein binding on biotinylated microarrays..... | 95 |
| 9.2.3. Functionalization of epoxy-terminated glass surface (chapter 5) | 95 |
| 9.2.3.1. Cleaning and activation of glass slide surfaces | 95 |
| 9.2.3.2. Preparation of epoxy-coated glasses..... | 95 |
| 9.2.3.3. Ink solution preparation | 96 |
| 9.2.3.4. Microarray immobilization via click reaction | 96 |
| 9.2.3.5. Protein binding on biotinylated microarrays..... | 96 |
| 9.2.4. Fluorescent immunosensors for detection of AFP (chapter 6)..... | 97 |
| 9.2.4.1. Preparation of biotinylated substrates..... | 97 |
| 9.2.4.2. Biotin immobilization | 97 |
| 9.2.4.3. Antibody attachment via sandwich | 98 |
| 9.2.4.4. Microarray writing via μ CS | 98 |
| 9.2.4.5. Preparation of fluorescently labeled AFP ink | 98 |
| 9.2.5. Functionalization of DBCO-, thiol- and epoxy-terminated diamond surfaces (chapter 7)..... | 99 |
| 9.2.5.1. Preparation of hydrogen- and oxygen-terminated diamonds | 99 |
| 9.2.5.2. Functionalization of diamonds | 99 |
| 9.3. Characterization techniques..... | 99 |
| 9.3.1. Contact angle measurement | 99 |

| | |
|---|-----|
| 9.3.2. X-ray photoelectron spectroscopy (XPS) | 99 |
| 9.3.3. Atomic force microscopy (AFM)..... | 100 |
| 9.3.4. Fluorescence microscopy | 100 |
| 9.3.5. Statistical analysis | 100 |
| References..... | 101 |
| Appendix A: List of abbreviations | 109 |
| Appendix B: List of Figures | 113 |
| Appendix C: List of Tables..... | 119 |
| Curriculum Vitae..... | 120 |
| List of publications | 125 |

Zusammenfassung

Die Funktionalisierung von Oberflächen und Materialien durch kovalentes Anbinden organischer Monolagen hat viele Anwendungen in der chemischen/biologischen Sensorik, gezielter Arzneimittelfreigabe, selektive Gasseparation, Krebsdiagnostik, u.a. Hier sind Klick-Chemie-Reaktionen, besonders die, welche ohne Metall-Katalyse auskommen, machtvolle Kandidaten. Diese Arbeit beschäftigt sich mit der Funktionalisierung von Glas- und Diamantoberflächen mittels verschiedener Klick-Reaktionen mit dem Ziel mikroskalige Muster für Sensoranwendungen zu erzeugen. Vor der Funktionalisierung wurden die Oberflächen mittels Estrifizierungs- und Silanisierungstechniken mit passenden funktionalen Gruppen modifiziert. Die Glasoberflächen wurden in drei Gruppen unterteilt: Die erste Gruppe wurde mittels dibenzocyclooctyne-Azid (DBCO-Azid) modifiziert, einem cyclooctyne mit Carboxylgruppe (DBCO-terminierte Glasoberflächen). Die zweite Gruppe wurde mit (3-mercaptopropyl)trimethoxysilan (MPTMS) modifiziert, einem Mercaptosilan (thiol-terminierte Glasoberflächen). Zuletzt, die dritte Gruppe, welche mit (3-glycidiloxypropyl)trimethoxysilan (GPTMS), einem Glycidoxysilan modifiziert wurde (epoxy-terminierte Glasoberflächen). Auf dieser Grundlage wurden dann in verschiedenen Experimenten alle Glasoberflächen mittels Mikrokanalspitzen Spotting (μ CS) mit unterschiedlichen fluoreszierenden und nicht-fluoreszierenden Tinten funktionalisiert: Die DBCO-terminierten Glasoberflächen mit Tinten welche Azid- oder Thiolgruppen enthalten, die thiol-terminierten Glasoberflächen mit Tinten welche Maleimid oder DBCO-Gruppen enthalten, und die epoxy-terminierten Glasoberflächen mit Tinten welche Thiol-, Amin- oder Azidgruppen enthalten. Experimente mit verschiedenen Fluorophoren haben gezeigt, dass alle Routen erfolgreich in kurzer Zeit und bei geringer Temperatur die funktionalen Gruppen an die Oberflächen binden konnten. In diesen Experimenten wurden auch die optimalen Reaktionsbedingungen für die jeweiligen Routen ermittelt. Um die Verwendbarkeit der Ansätze und mittels ihrer erzeugten Mikrostrukturen in biologischen und biomedizinischen Anwendungen zu untersuchen wurden Protein-bindungs-experimente durchgeführt. Ein Vergleich in Streptavidin-Bindungsexperimenten auf verschiedenen Biotin-Spot Arrays (Biotin-Azid und Biotin-Thiol auf DBCO-terminierten Oberflächen, Biotin-Maleimid und Biotin-DBCO auf thiol-terminierten Oberflächen und Biotin-Thiol, Biotin-Amin und Biotin-Azid auf epoxy-terminierten Oberflächen) enthüllte die höchsten Dichten an immobilisierten Biotin für das System Biotin-Maleimid auf thiol-terminierten

Oberflächen, sowie Biotin-Amin auf den epoxy-terminierten Oberflächen. Die erstere eine thiol-ene Michael Addition (TEMA) und die letztere eine Ringöffnung des Epoxids durch ein Amin. Mit Hinblick auf die erhaltenen Resultate zur Funktionalisierung der verschiedenen Glasoberflächen mit fluoreszierenden und nicht-fluoreszierenden Tinten, wurde ein sensibler Immunosensor für die Nachweise von Alphafetoprotein (AFP) entworfen und hergestellt. AFP ist der meistverbreitete Biomarker für das Screening und die Diagnose des hepatozellulären Karzinoms (HCC). Für den Aufbau dieses Immunosensors wurden drei (bio)chemische Techniken, die Klick-Chemie, die Biotin-Streptavidin-Biotin Sandwich Technik, sowie das Prinzip der Antigen-Antikörper Interaktion, kombiniert. Abschließend wurden die Experimente auf den Glasoberflächen auf DBCO-, thiol- und epoxy-terminierten Diamantoberflächen wiederholt, da diese einen exzellenten Transducer in optischen Sensoren darstellen. Die durch diese Arbeit erreichten Ziele und erhaltenen Ergebnisse sind beim Entwurf und der Herstellung von Biosensoren für die Proteindetektion und anderen biologischen/biomedizinischen Anwendungen anwendbar.

Chapter 1

Introduction

1.1. Lithography, DPN and μ CS

Lithographic methods - which rely on patterning of a resistive film, followed by a chemical etch of the substrate - are at the heart of modern-day microfabrication, and molecular electronics (Figs 1.1 and 1.2). Dip-pen technology, in which desired inks on a sharp object are transported to a substrate via capillary forces, has been used extensively throughout history to transport molecules on macroscale dimensions. Merging these two techniques has developed a new type of scanning probe microscopy-based nanolithographic method known as dip-pen nanolithography (DPN). However, DPN was first used to deposit thiols on gold surfaces but was quickly adapted for a wide range of biological inks. In DPN, an atomic force microscope (AFM) tip is used as a “nib”, a solid-state substrate as a “paper” and molecules with a chemical or physical affinity with the solid-state substrate as “ink”. Surface immobilization of bioactive molecules by spotting and printing methods is a base technique for the preparation of structured, bioactive surfaces. Capillary transport of biomolecules from the AFM tip to the solid-state substrate in DPN is used to directly “write” patterns with nanometer resolution. DPN is a perfect technique to create a potentially useful tool for creating and functionalizing nanoscale devices and biologically active chips (Fig. 1.3) ^[1]. Contactless techniques like microchannel cantilevers spotting (μ CS) allow for the deposition of femtoliter sized droplets of ink, offering high throughput spotting at larger length scales. In this technique as shown in Figs. 1.4 and 1.5, after loading of the microchannel cantilevers, spotting is performed by bringing the substrate into contact with the apex of the microchannel cantilever of the surface patterning tool (SPT) for controlled amount of time and allow the ink to flow down to the substrate by capillary forces ^[2]. The NLP 2000 System is a versatile desktop nanolithography platform designed for patterning a variety of materials using the proven technique of DPN (Fig 1.6).

1.2. Surface and material functionalization

In the last decade, the search for efficient functionalization routes of surfaces and materials through the covalent attachment of organic monolayers has dramatically increased because of numerous applications in chemical/biological sensing, drug delivery, selective gas separation, cancer detection, etc. In this regard, using click reactions, especially those that require no metal catalyst, is a powerful and widely used tool ^[3]. Before functionalization, the surface should be modified using attachment of suitable functional groups through esterification or silanization techniques. In silanization approach, hydroxyl-terminated surface reacts with methoxy or ethoxy

groups of organosilane molecules. In esterification, molecules containing COOH react with hydroxyl groups of surface. Fig. 1.7 shows examples of silane coupling agents used in the silanization technique.

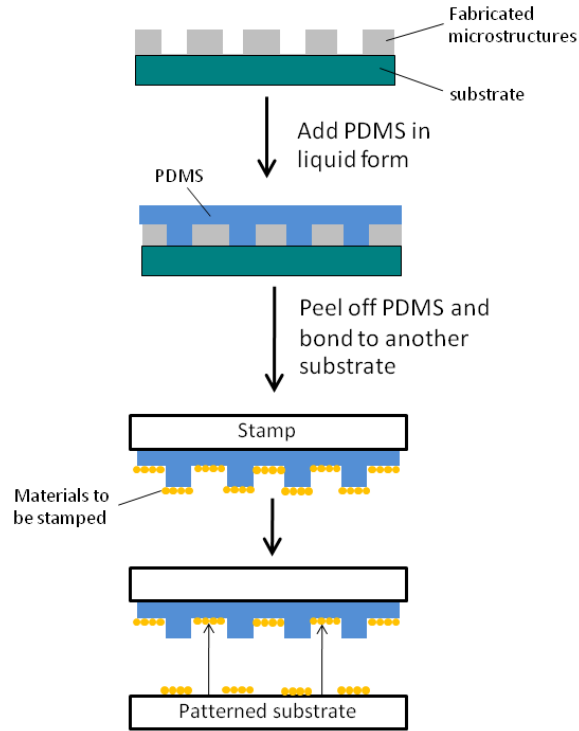


Figure 1.1. Schematic illustration of soft lithography [\[1b\]](#)

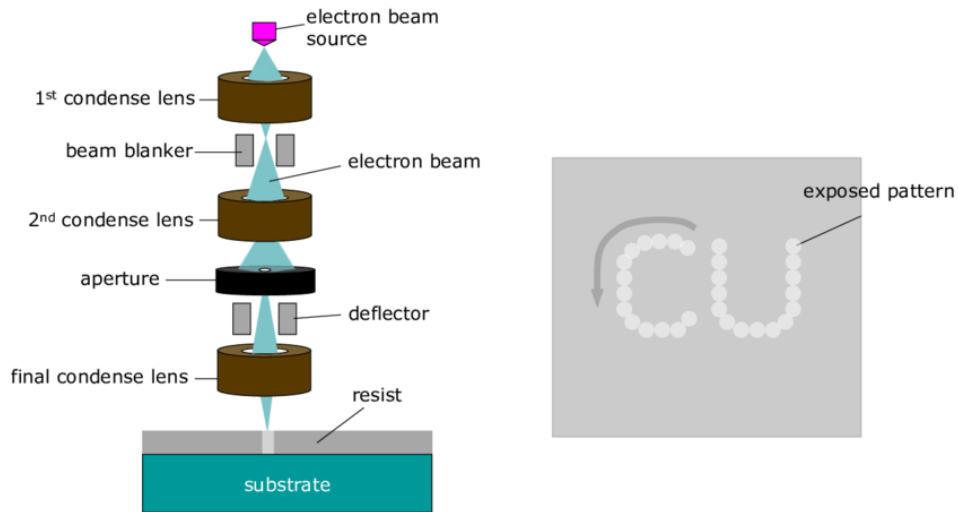


Figure 1.2. Schematic illustration of electron beam lithography [\[1b\]](#)

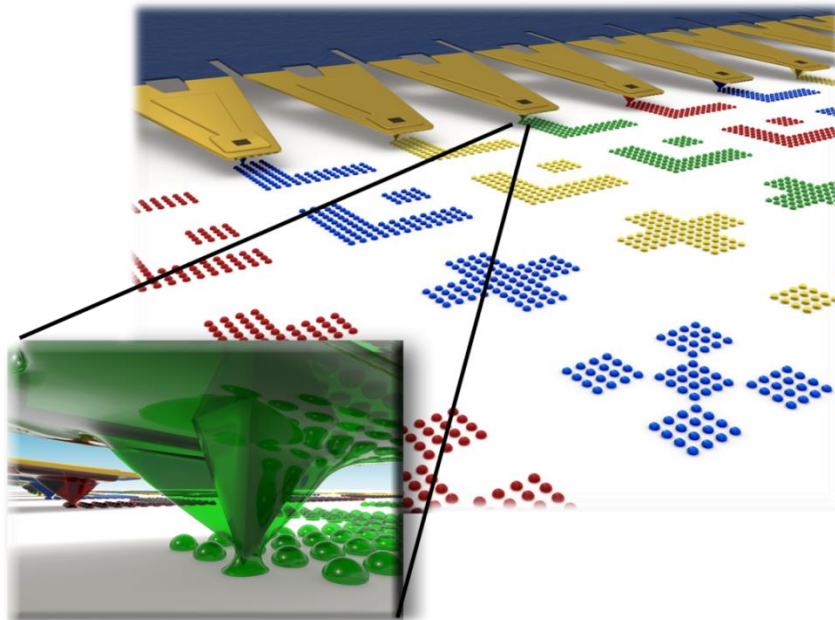
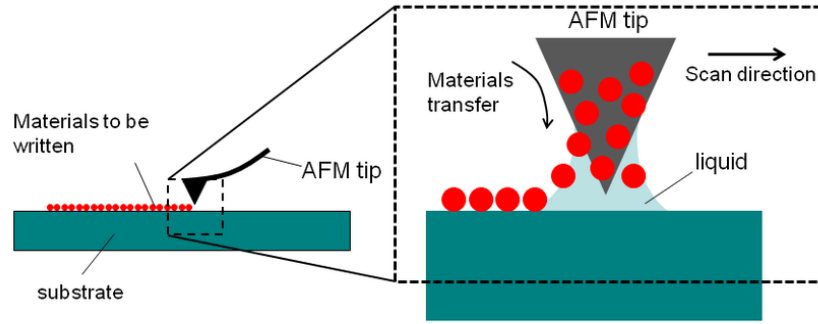


Figure 1.3. Schematic illustration of dip-pen nanolithography [\[1b\]](#)

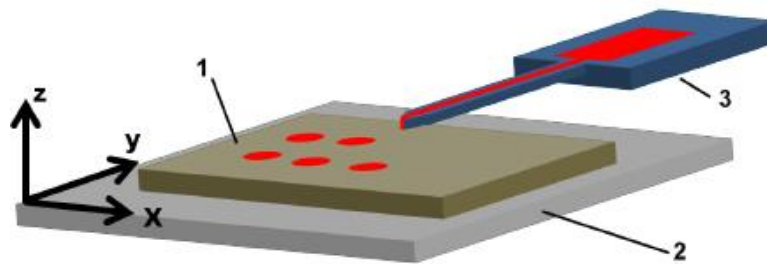


Figure 1.4. Dye delivery by microchannel cantilever. The substrate (1) is placed on the stage (2), which can be actuated in the x-, y- and z-direction with a precision of less than 100 nm. The substrate can be brought into contact with the apex of the microchannel cantilever of the SPT (3) By raising the stage in the z-direction [\[2a\]](#).

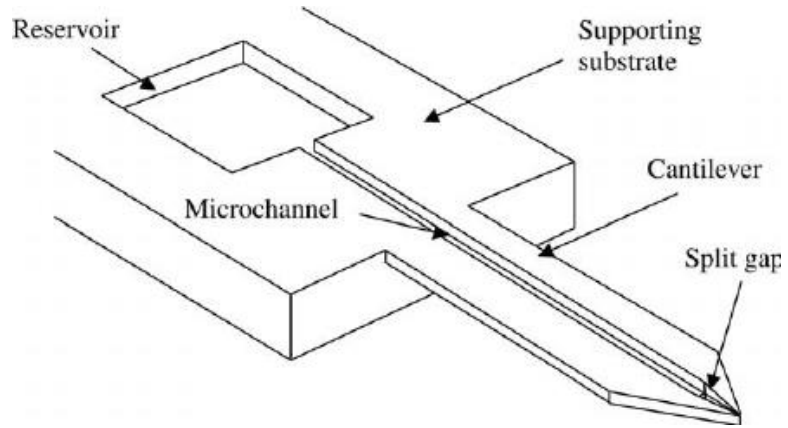


Figure 1.5. Schematic of quill-type cantilever-based SPT [2b]

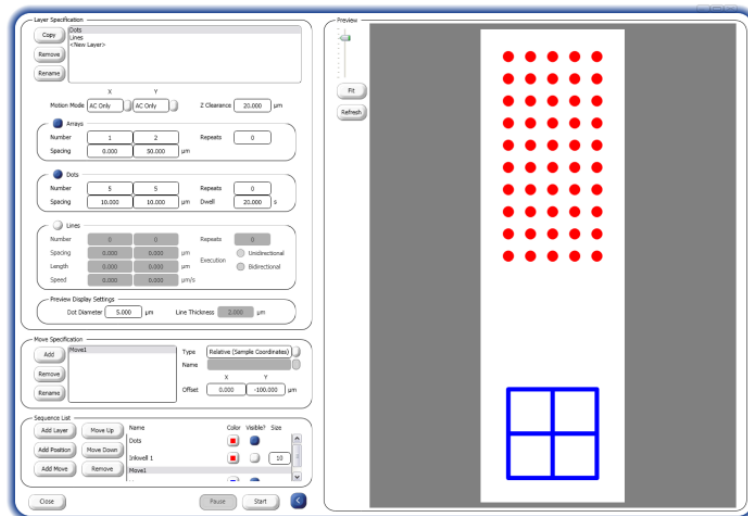
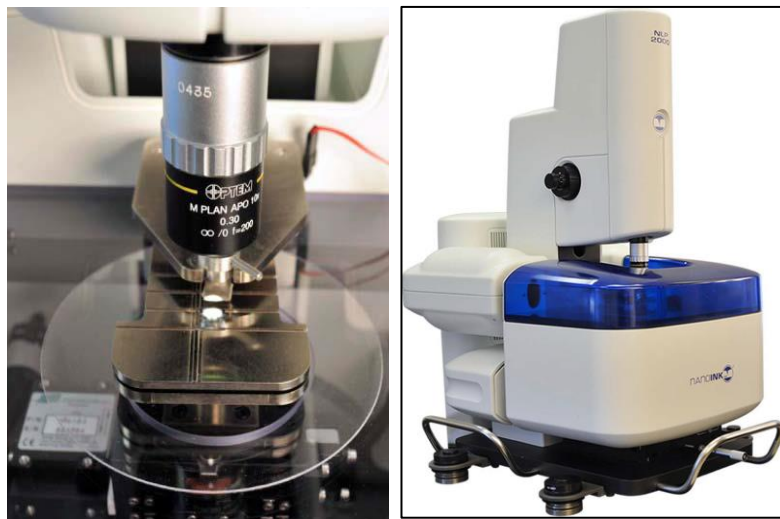


Figure 1.6. A NLP 2000 System along with related software

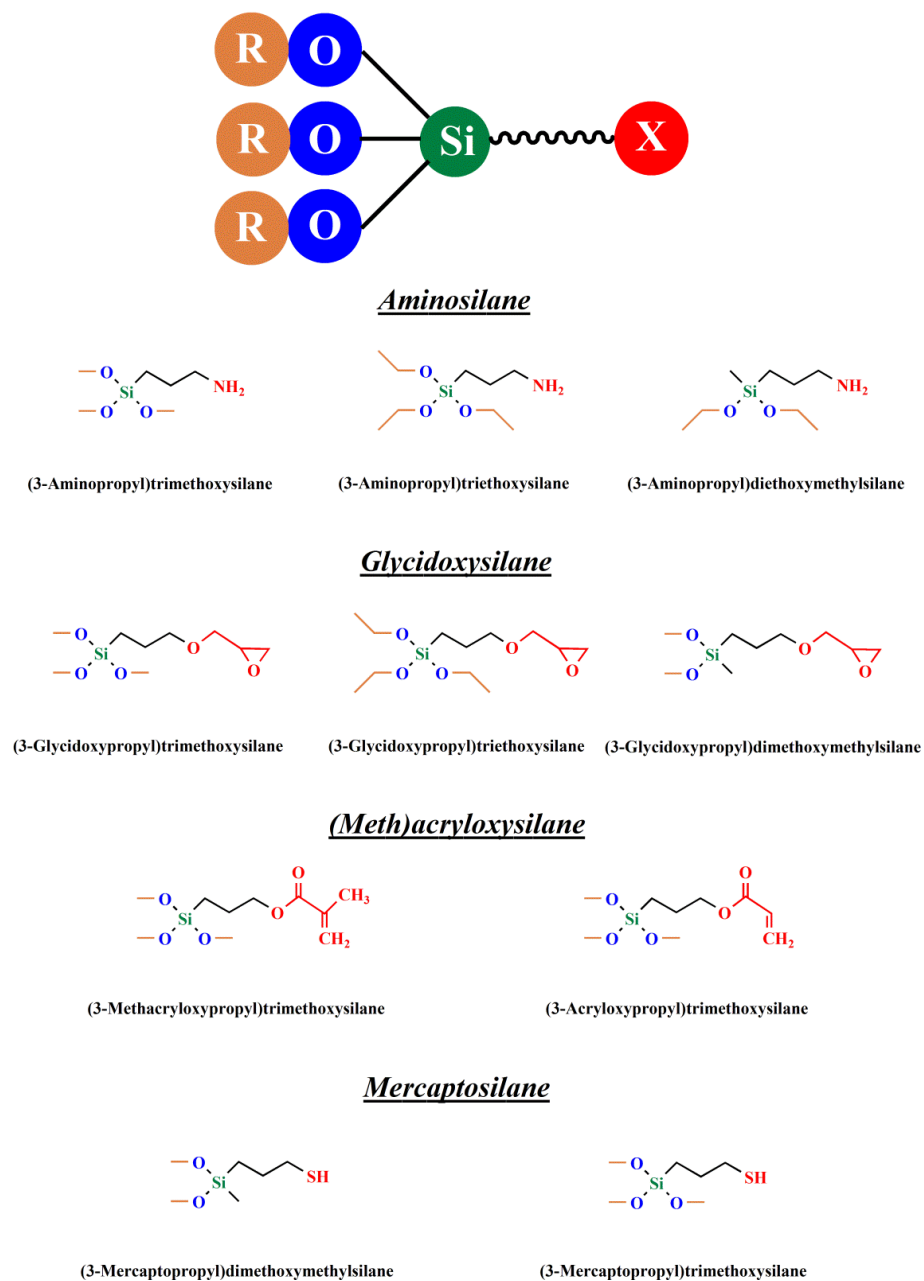


Figure 1.7. Examples of silane coupling agents used in the silanization technique

1.3. Click chemistry: history and types

Click chemistry reactions - which were introduced by Kolb, Finn, and Sharpless in 2001 ^[4] - are excellent candidates for functionalization of surfaces and materials due to having unique characteristics such as mild reaction conditions, compatibility with different kinds of solvents specially water, high reaction rate, and easy post-treatment and for many applications. Click reactions provide high yields without generation of by-products, need readily accessible starting

materials and reagents, and do not require any complicated purification techniques [3]. There are different kinds of click chemistry reactions. Fig. 1.8 summarizes the most significant metal-free click reactions used in the modification of solid surfaces and materials during the last ten years including strain-promoted azide-alkyne cycloaddition (SPAAC), thiol-ene coupling (TEC), thiol-yne coupling (TYC), thiol-ene Michael addition (TEMA), and Diels-Alder (DA) cycloaddition. In summary, the catalyst-free click reactions have been established as an elegant methodology in the modification of surfaces and particles in the last decade. Hence, it is to be expected that this field will develop not only in quantity, but also in variety [3a, 5].

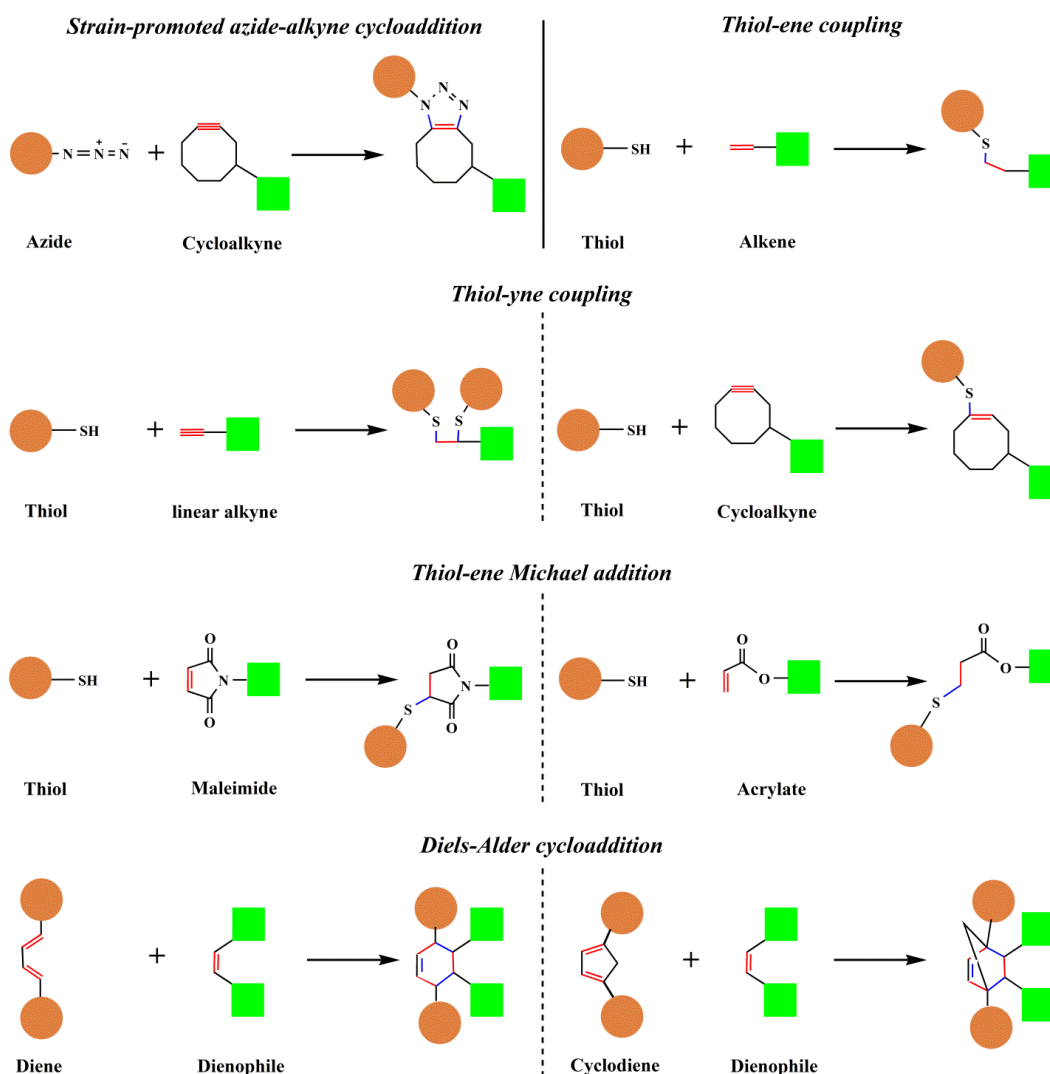


Figure 1.8. Most significant metal-free click reactions used in the modification of solid surfaces and materials during the last ten years. Newly formed bonds after performing click reaction are highlighted in blue.

1.4. Biomarkers for hepatocellular carcinoma (HCC)

Hepatocellular carcinoma (HCC) is the major cause of morbidity and mortality in patients with chronic liver disease, the sixth most common cancer, and the fourth leading cause of cancer-related deaths worldwide. The last release of the Global Cancer Observatory (GCO) database in September 2018 estimated about 840,000 new cases and 780,000 deaths of liver cancer in 2018 for both sexes and all ages (Fig. 1.9) ^[6]. Cirrhosis of the liver, hepatitis B virus (HBV) and hepatitis C virus (HCV) infections, heavy alcohol consumption, ingestion of aflatoxin and certain diseases like hemochromatosis, alpha 1-antitrypsin deficiency (A1AD or AADT) and nonalcoholic steatohepatitis (NASH) are the most important risk factors for HCC development ^[7].

Life expectancy of HCC patients depends on the stage of the disease at detection. Diagnosis of HCC at early stage through surveillance methods provides highly effective treatment and prolongs the lifetime of patients; whereas, as the disease is detected in advanced stage, available therapies are restricted to palliative care and local treatment and have no satisfactory effect ^[8]. Current methods of the HCC diagnosis are divided into two main categories: imaging and biomarker tests. Cancer biomarkers are measurable molecules or substances which present in cells, tissues, or body fluids and the level of them predicts the presence of cancer or even indicates the stage of cancer. Whereas the measurement of biomarkers level always leads to a specific numeric value, the obtained result, although not necessarily accurate, is generally more objective than images produced by imaging techniques, whose interpretation of them is often subjected to the judgment and experience of physicians. Additionally, there is a strong economic argument for the acceptance of biomarkers in cancer detection, especially in the countries where advanced imaging instruments are limited or even unavailable ^[8-9].

Recent studies identified a number of biomarkers in the early detection of HCC including alpha-fetoprotein (AFP) ^[10], Lens culinaris agglutinin-reactive alpha-fetoprotein (AFP-L3) ^[10b, 11], des-gamma-carboxy prothrombin (DCP) ^[10a, 10b, 11b], glypican-3 (GPC-3) ^[12], cytokeratin 19 (CK19) ^[12b], golgi protein 73 (GP73) ^[13], microRNA (miRNA) ^[14], osteopontin (OPN) ^[10c, 15], Annexin A2 ^[16], midkine (MDK) ^[17] and others.

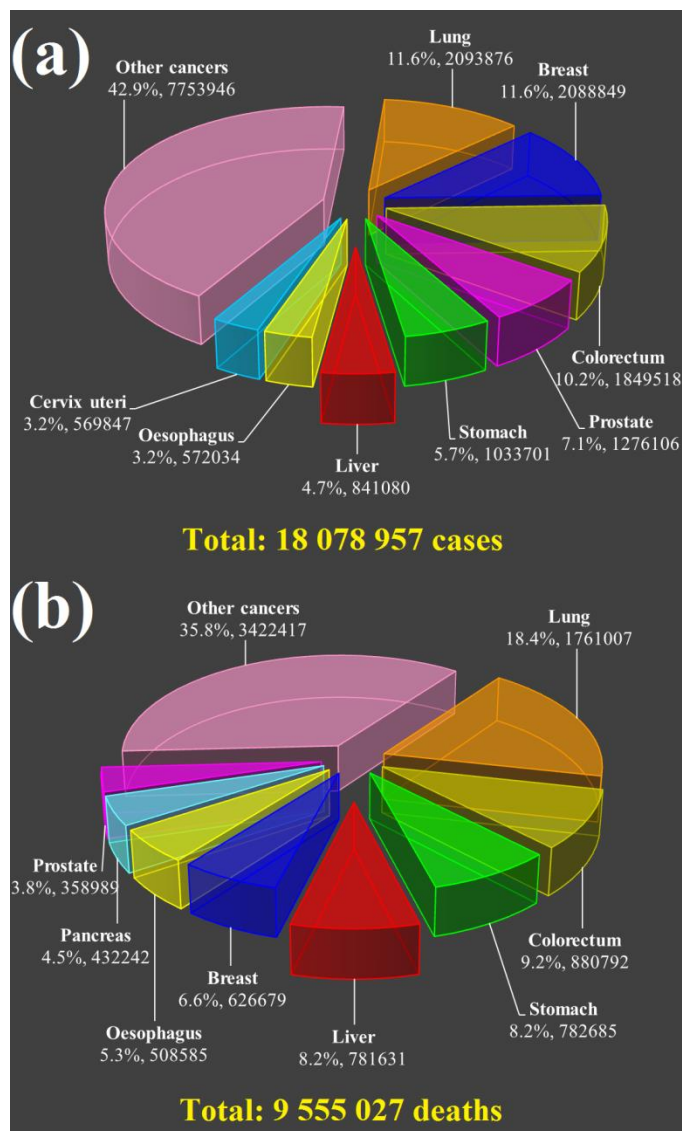


Figure 1.9. Cancer incidence and mortality statistics worldwide. Number of (a) new cases and (b) deaths in 2018, in 185 countries of the world, for 36 types of cancer, for both sexes and for all ages. These results are available at Global Cancer Observatory (GCO) web site of the International Agency for Research on Cancer (IARC)

1.5. Diamond substrate for printing

Diamond is a very well-known semiconductor having unique physical and mechanical properties such as high band gap, high thermal conductivity, chemical inertness, optical transparency from ultraviolet to infrared, high mechanical stability and corrosion resistance. Diamond can be used in different areas like field emitters in electronic industry, chemical and biological sensors, DNA and protein chips, and electrodes for electrocatalytic reactions. Diamond has recently been employed as transducer for designing of advanced electronic devices

[18]. Sensing technologies used for detection and identification of molecules, cells, and tissues could be divided to direct and indirect (lock-and-key) approaches. The direct method is based on interaction between the analyte and the sensing element that can be result in a change that can be transduced into a specific and recognizable signal. But, in indirect method, sensors are based on specific recognition events such as antibody-antigen interaction which in this case different methods like enzyme-linked immunosorbent assay (ELISA) and fluorescence-immunoassays (FIA) or radio-immunoassays (RIA) can be named. Different parameters including reaction between antigen and antibody, immobilization of antibodies on the surface and the choice of transducer and signal probes can affect sensor efficiency [18b, 19]. Optical sensors are another class of sensors which gives us chemical information from analyte concentration. First light is coupled into the microring resonators through the linear waveguides and in the following, the phase shift can be measured. After functionalization of microring surface with an analyte, refractive index is affected by the binding of the analyte. In other words, binding turn into changes in the local refractive index at the sensor surface [20].

Chapter 2

Thesis overview and research objectives

Design and fabrication of biosensors are of great importance. One of the newest applications of these sensors is the rapid and accurate detection of protein substances like avidin or cancer biomarkers. For this, the molecules which have affinity with the protein substances and known as bioreceptor should be immobilized on the functionalized surface. This immobilization can be performed via click chemistry reactions having unique characteristics such as mild reaction conditions, high yields, high reaction rate, compatibility with different kinds of solvents specially water and easy post-treatment. There are different kinds of click chemistry reactions which in this project we have used strain-promoted azide-alkyne cycloaddition (SPAAC), thiol-yne coupling (TYC), thiol-ene Michael addition (TEMA) and ring opening of epoxy click reactions for immobilization of bioreceptor. The obtained results from this project have been presented in chapters 3-7.

In chapter 3, two different catalyst-free click approaches, namely strain-promoted azide-alkyne cycloaddition (SPAAC) and thiol-yne coupling (TYC) click chemistry have been used for the immobilization of microarrays of azide or thiol inks on the DBCO-terminated glass surfaces. Although both routes work reliable for surface functionalization, the protein binding experiments revealed that using a thiol-alkyne route will obtain the highest surface density of molecular immobilization in such spotting approaches. The results of this chapter have been published in “Small” journal as a paper titled “Site-specific surface functionalization via microchannel cantilever spotting (μ CS): comparison between azide-alkyne and thiol-alkyne click chemistry reactions”.

In chapter 4, TYC and thiol-ene Michael addition (TEMA) click approaches have been used for the immobilization of microarrays of DBCO or maleimide inks on the thiol-terminated glass surfaces. Both routes could successfully couple functional moieties to the surface as became evident from experiments with different fluorophores. However, when comparing the intensities obtained by protein coupling, the TEMA reaction yielded most efficient surface immobilization. Considering the findings of chapter 3 and this chapter and present, it can be concluded that the surface density of molecular immobilization on the glass surface via click reaction is in order: TEMA > TYC > SPAAC. The results of this chapter have been published in “Advanced Material Interface” journal as a paper titled “Site-specific surface functionalization via microchannel

cantilever spotting (μ CS): comparison between azide-alkyne and thiol-alkyne click chemistry reactions”.

In chapter 5, ring opening click reaction has been used for the immobilization of microarrays of thiol, amine or azide inks on the epoxy-terminated glass surfaces. When comparing these immobilization routes, the biotin-amine on the epoxy-terminated glass surfaces yielded higher fluorescence intensity. The results of this chapter will be submitted in the form of a paper titled “Ring opening of epoxy by thiol, amine and azide” in the future work.

In chapter 6, considering the obtained results from chapters 3-5 and combining click chemistry, biotin-streptavidin-biotin sandwich-type strategy and antigen-antibody interaction techniques, novel sensitive fluorescent immunosensors have been designed and fabricated for alpha-fetoprotein (AFP) detection which is the most commonly biomarker for early screening and diagnosis of hepatocellular carcinoma (HCC). In the presented setup with different biotin compounds, a functionalization by thiol-silane with subsequent biotin immobilization by biotin-maleimide and functionalization by epoxy-silane and subsequent biotin immobilization by biotin-amine showed best performance. The results of this chapter have been submitted in the form of a paper titled “Evaluation of click chemistry microarrays for immunosensing of alpha-fetoprotein (AFP)”.

In chapter 7, the experiments performed on the glass surfaces were repeated on the DBCO-, thiol- and epoxy-terminated diamond surfaces. Diamond is used as an excellent transducer in optical sensors. The obtained results from this chapter can be used for manufacturing optical biosensor based on waveguides and rings in the future works.

Chapter 3

Functionalization of DBCO-terminated glass surface

3.1. Introduction

The most popular click method is copper-catalyzed azide-alkyne cycloaddition (CuAAC) which was independently developed by Meldal et al. and Sharpless et al. in 2002 (Fig. 3.1a) ^[21]. However, concerns about the toxicity of copper catalysts limit the utility of this fast and versatile process in applications involving living systems or biomolecules. Therefore, there has been a special interest in developing novel azide-alkyne click reactions that do not require any metal catalyst ^[22]. In 2004, Bertozzi and co-workers developed the first copper-free, strain-promoted azide-alkyne cycloaddition (SPAAC) click reaction which was based on the use of cycloalkynes instead of linear alkynes (Fig. 3.1b) ^[23]. Some commonly used activated cycloalkynes for SPAAC include Bicyclo[6.1.0]nonyne (BCN), dibenzocyclooctyne (DIBO), biarylazacyclooctynone (BARAC), monofluorinated cyclooctyne (MOFO), and difluorinated cyclooctyne (DIFO) (see Fig. 3.2 for structures). Additionally, azadibenzocyclooctyne (ADIBO) or dibenzoazacyclooctyne (DIBAC) is often known simply as DBCO in the literature, which we will also use as common abbreviation for these two. Depending on the chemical structure of cyclooctyne, reaction rates of SPAAC are different. Reaction rates of these reactants in SPAAC click reaction are in the order: MOFO < DIBO < DIFO < DBCO < BARAC ^[24].

The photoinitiated addition of thiols to alkynes is another important type of catalyst-free click reactions which was introduced by Fairbanks et al. in 2008 ^[25]. This radical-mediated click reaction has rapidly become an important tool for scientists in recent years, especially in the synthetic materials and polymer arenas. Addition of thiol to linear alkyne consists of a two-step reaction and two thiol molecules react with one alkyne group (Fig. 3.1c). In the first step, a thiyl radical generated from a parent thiol is added to an alkyne, resulting in a vinyl sulfide. In the second step, another thiyl radical is added to the vinyl sulfide, yielding the 1,2-bis-thioether product. Reaction between a thiol and a cycloalkyne is slightly different. In this click reaction, the resulting vinyl sulfide does not permit subsequent thiol addition (Fig. 3.1d). Addition of a single thiol to a cycloalkyne is relatively rapid and this reaction can be performed spontaneously even in the absence of light and photoinitiator in an unpurged atmosphere. Cycloalkynes used for SPAAC (shown in Fig. 3.2) can be usable for doing click reaction with thiol as well ^[26].

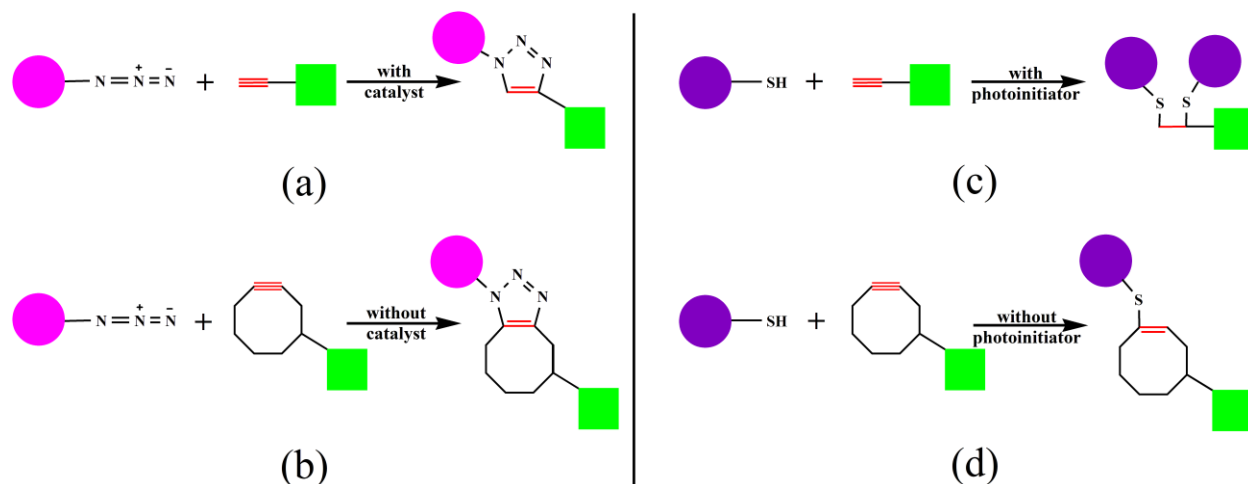


Figure 3.1. Different types of click chemistry reactions between (a) azide and linear alkyne (CuAAC); (b) azide and cycloalkyne (SPAAC); (c) thiol and linear alkyne and (d) thiol and cycloalkyne.

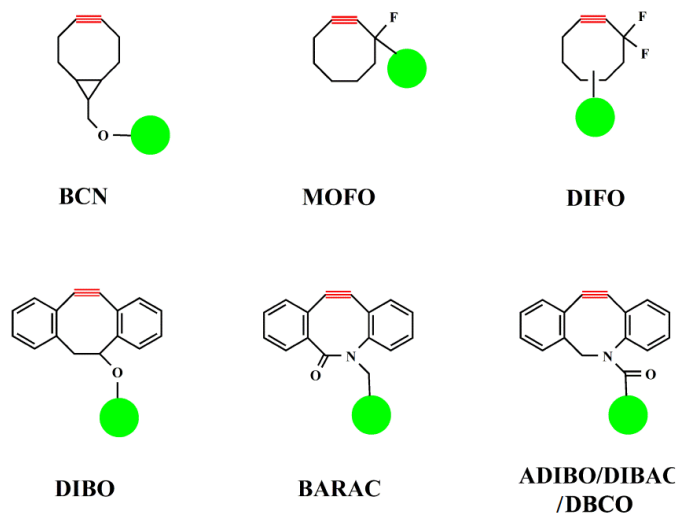


Figure 3.2. Some commonly used cyclooctynes for strain-promoted azide-alkyne cycloaddition (SPAAC)

Wijdeven et al. prepared a biotin-modified glass slide via the SPAAC reaction of azidocoumarin-functionalized glass surface and a biotin-linked BCN derivative [27]. Also, in a comparative study, two targeting peptides with azide-terminated groups were conjugated to BCN-functionalized porous silicon nanoparticles via copper-free azide-alkyne cycloaddition [28]. Similarly, Manova et al. described the metal-free functionalization of BCN-terminated Si_3N_4 surfaces with an azide-labeled dye [29]. Davydova et al. introduced a new route for the functionalization of nanocrystalline diamond films via catalyst-free click chemistry utilizing

spotting with microchannel cantilever spotting (μ CS) [5a]. Jung and Yi reported a strategy for protein immobilization onto a chitosan-PEG hybrid system activated with ADIBO [30]. Kuzmin et al. described a fast methodology for the immobilization of biotin onto ADIBO-coated glass substrates and subsequent avidin selective immobilization [31]. Pfeifer and co-workers used ADIBO-based SPAAC reaction to construct a diagnostic peptide microarray for tumor auto-antibody tests in cancer detection [32]. In continuation of previous works, Orski et al. functionalized the alkyne-derived polymer brushes through click-type cycloadditions with azido-containing compounds by two mechanisms: a SPAAC with DIBO and ADIBO or a CuAAC to a propargyl group [33]. Finally, Gobbo et al. reported the preparation of ADIBO-modified gold nanoparticles (Au NPs) which underwent a SPAAC reaction with azide-decorated polymersomes [34].

Guerrouache et al. immobilized Au NPs on a porous monolith surface with alkyne functionality through radical-mediated thiol-alkyne addition reaction [35]. Similarly, Escorihuela et al. used the same approach for site-specific immobilization of DNA on silicon surfaces [36]. Bhairamadgi et al. reported a comparative study of thiol-alkene and thiol-alkyne click chemistry reactions for modification of silicon surfaces [37]. A photoinitiated thiol-alkyne click reaction strategy was used by Sun et al. for fabrication of a novel responsive biomimetic nanochannel platform which was applicable to sensing in urine samples [38]. Feng and co-workers developed a fast and initiator-free approach for the fabrication of superhydrophilic-superhydrophobic micropatterns via UV-induced thiol-alkyne click chemistry [39]. Lastly, in an interesting study, Fairbanks et al. examined the photoinitiated addition of octanethiols to five terminal alkynes (1-octyne, propargyl acetate, methyl propargyl ether, methyl propargylamine, and ethyl propiolate) as well as two internal alkynes (2-octyne and cyclooctyne). The most rapid addition of thiols to alkynes was that to cyclooctyne, while ethyl propiolate and methyl propargylamine showed very small reaction rates with thiols. For other alkynes, the reaction rates with thiols were in order of 1-octyne > propargyl acetate > methyl propargyl ether > 2-octyne [26a].

In this chapter, we used two different catalyst-free click approaches for the highly localized and site-specific surface modification of glass and creating small-scale patterns suitable for different applications. For this purpose, we first functionalized the surface of hydroxyl-terminated glass with dibenzocyclooctyne-acid (DBCO-acid) which is a cyclooctyne with a

carboxyl group. Then, separately, the DBCO-terminated surfaces were functionalized via μ CS [40] with different azide and thiol inks in order to compare the efficiency of azide-alkyne and thiol-alkyne click reactions in the fabrication of micropatterns (Fig. 3.3). Lastly, the protein binding experiments were performed to study the feasibility of these micropatterns in biomedical and biological applications.

3.2. Results and discussion

3.2.1. XPS and contact angle measurements

To check the substrate preparation prior to the further experiments, the bare and functionalized glass surfaces were characterized by XPS and contact angle measurements. XPS confirms the presence of DBCO after functionalization (Fig. 3.4a and Table 3.1). The OH-terminated glass shows a nitrogen contamination of less than 0.3 at% whereas the DBCO-terminated glass shows two clear peaks: a first one at 400.2 eV attributed to the amide functionality and a second one at 402.7 eV which could stem from a positive charged nitrogen [41]. To be able to spot coupling reagents in high-resolution arrays, the contact angle of water droplets on the substrates should not be too low, as otherwise the spotted water-based inks will spread and destroy the ordered arrays. To elucidate the evolution of the contact angle over time, we compared a hydroxyl-terminated glass sample (plasma-treated) with a DBCO-terminated one (Fig. 3.4b). Freshly plasma-treated glass had a contact angle of 0° meaning complete spreading of applied droplets. DBCO-terminated glass directly after functionalization has a higher contact angle of 18° , as expected from the more hydrophobic terminal groups. Still both samples were in an activated state right after functionalization, as became obvious by a rise of contact angle on both surfaces when monitoring the contact angle over the course of several days. After oxygen plasma, the glass surface is completely covered with a layer of hydroxyl groups, rendering it very hydrophilic with a low contact angle. Over time, this plasma activation will decay due to exposure to the ambient air and the moisture and other contaminants it contains. This reaction is rapid in the beginning and then slows down, approaching the contact angle of untreated glass. A DBCO covered surface shows a higher contact angle as an OH-terminated glass surface, as expected from the chemical structure. Nevertheless, even in case of DBCO coating, one can still observe a rise in contact angle over time, probable by remaining OH-groups on the surface that decay in similar time scale as the solely plasma activated surface. After about 3 weeks, the

contact angles reached a plateau at about 60° for DBCO-terminated and 45° for hydroxyl-terminated glass (see Table 3.2).

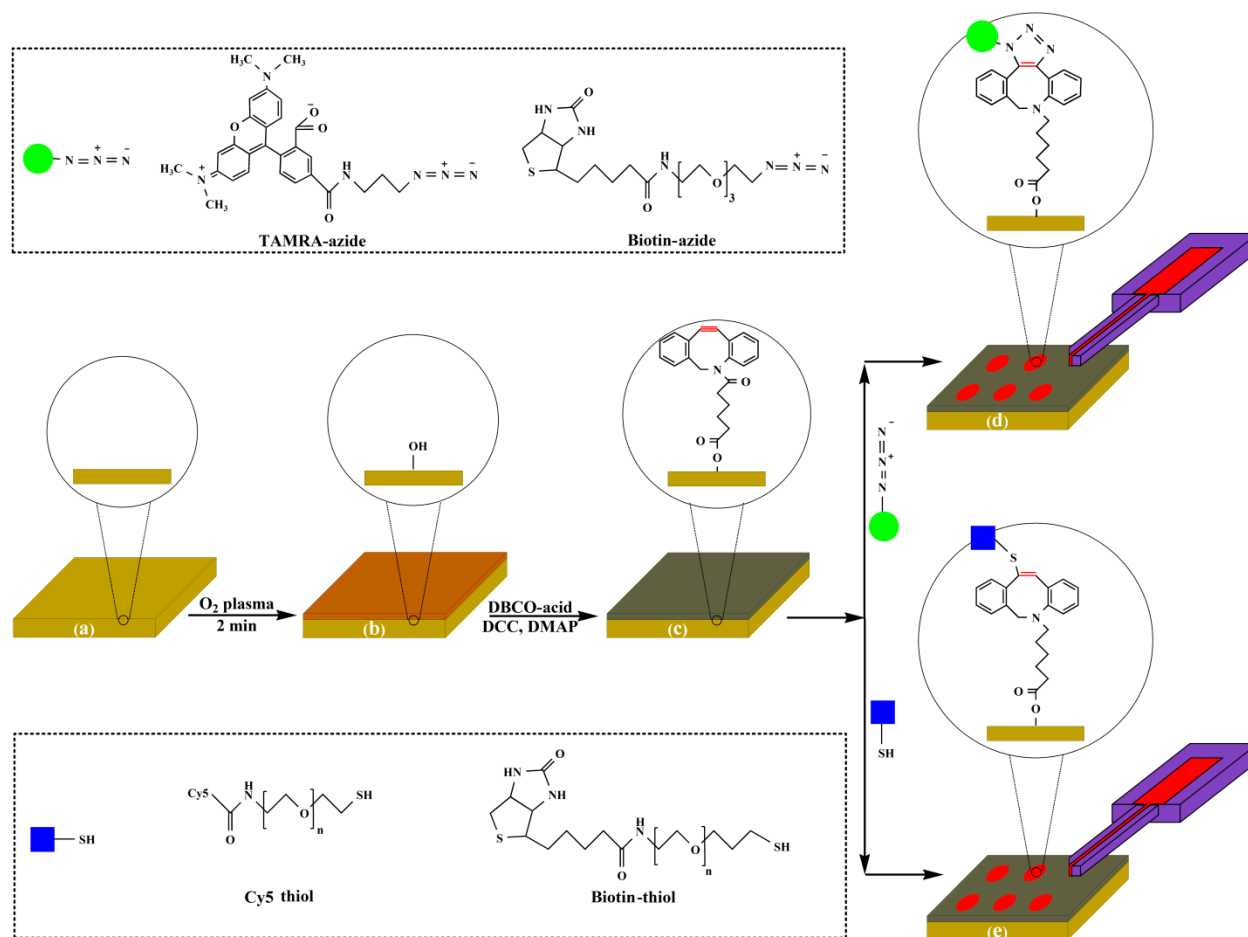


Figure 3.3. Comparison between azide-alkyne and thiol-alkyne click reactions: (a) bare glass; (b) hydroxyl-terminated glass; (c) DBCO-terminated glass; (d) treatment of the DBCO-terminated surface with TAMRA-azide and biotin-azide; (e) treatment of the DBCO-terminated surface with Cy5 thiol and biotin-thiol.

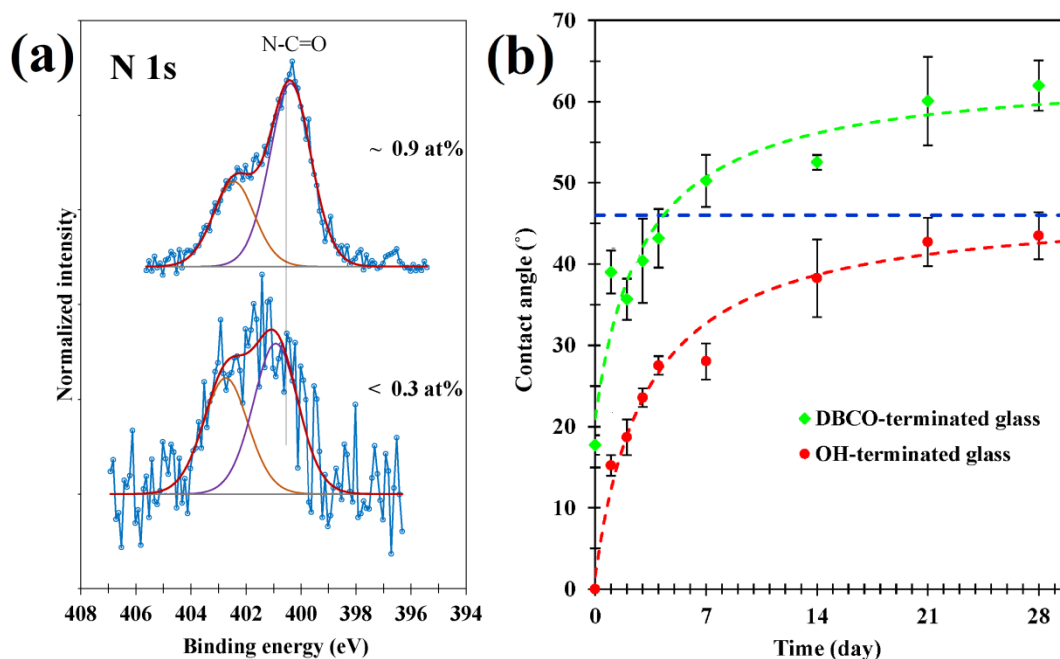


Figure 3.4. Characterization of OH-terminated and DBCO-terminated glasses by XPS and contact angle measurement. (a) N 1s XP spectra of OH-terminated (bottom) and DBCO-terminated (top) glasses; (b) Contact angle over time on DBCO- and OH-terminated glass. The experimental data was fitted using MATLAB software. The dashed horizontal line represents the contact angle of the bare glass which is about 46°. The red dashed line represents a curve of $y = (47.4x+5.1)/(x+3.3)$ and the green dashed curve $y = (63.9x+65.1)/(x+3.1)$, respectively.

Table 3.1. Elemental composition determined by XPS

| | | | a | b | c | d | e | f |
|----------------------|-------------------|---------------------|-----------------------------|------|------|------|------|------|
| | assignment | Binding energy (eV) | Elemental composition (at%) | | | | | |
| S 2p _{3/2} | S-C | 163.4 | – | – | – | – | 0.2 | 0.1 |
| | C-C, C-H | 285.0 | 5.9 | 4.7 | 38.3 | 9.1 | 15.8 | 29.2 |
| C 1s | C-N, C-O | 286.5 | 0.8 | 1.6 | 8.4 | 6.8 | 5.1 | 6.4 |
| | C=O, O=C-N | 288.1 | – | – | – | 2.6 | 1.0 | 1.1 |
| | O=C-O | 289.0 | 0.6 | 0.9 | 2.6 | – | 1.1 | 1.4 |
| N 1s | O=C-N, C-N, N-N=N | 400.2 | 0.2 | 0.6 | 1.5 | 2.5 | 1.6 | 1.3 |
| | N ⁺ | 402.7 | 0.1 | 0.3 | 0.2 | 0.4 | 0.3 | 0.3 |
| O 1s | O=C | 531.2 | 12.4 | 9.2 | 3.5 | 8.6 | 6.1 | 9.0 |
| | O-Si, O-C | 532.5 | 51.4 | 55.1 | 27.7 | 46.5 | 46.1 | 30.9 |
| Si 2p _{3/2} | SiO ₂ | 102.9 | 23.5 | 23.9 | 14.7 | 19.9 | 19.9 | 16.5 |
| K 2p _{3/2} | | 293.8 | 2.1 | 1.9 | 0.7 | 2.1 | 1.7 | 1.3 |
| Zn 2p _{3/2} | | 1022.6 | 0.8 | 0.5 | 0.1 | 0.4 | 0.3 | 0.2 |
| Na 1s | | 1072.6 | 2.0 | 1.3 | 0.3 | 1.5 | 0.9 | 0.7 |

^a OH-terminated glass

^b DBCO-terminated glass

^c DBCO-terminated glass after click reaction with TAMRA-azide at optimum time (20 min) and temperature (37 °C)

^d DBCO-terminated glass after click reaction with Cy5 thiol at optimum time (40 min) and temperature (37 °C)

^e DBCO-terminated glass after click reaction with biotin-azide at optimum time (20 min) and temperature (37 °C)

^f DBCO-terminated glass after click reaction with biotin-thiol at optimum time (40 min) and temperature (37 °C)

Table 3.2. Static contact angles of water droplets on the bare and functionalized glass surfaces

| Sample | After treatment (°) | After 4 weeks (°) |
|---------------------------|---------------------|-------------------|
| Bare glass (no treatment) | | 46.0 ± 1.9 |
| DBCO-terminated glass | 17.7 ± 1.2 | 62.0 ± 3.1 |
| OH-terminated glass | 0 | 43.5 ± 2.9 |

3.2.2. Array immobilization of TAMRA-azide and Cy5 thiol

To explore the potential of the azide-alkyne reaction to generate microarrays by μ CS, micropatterns of 10×10 spots with a pitch of 50 μ m were prepared. Different spotting humidities in the range of 20 to 70% were trialed to elucidate the influence of this parameter. Typical results at relative humidities of 20 and 70% can be seen in Fig. 3.5a. As shown in Fig. 3.5b, there is a sharp decrease in the observed fluorescence intensity and a slight rise in the radius with rising humidity. Based on these results, we chose to keep a spotting humidity of 20% for the rest of experiments. At this humidity, we can have spots with narrow size distribution, smaller radius, and higher fluorescence intensity.

After spotting in the optimum humidity of 20%, the spotted microarrays were left either at room temperature (25 °C) or physiological temperature (37 °C) for different times to study the influence of click reaction time and temperature. Fig. 3.6a shows the average fluorescence intensity of the TAMRA-azide spots immobilized on the DBCO-terminated glass after doing click reaction and rinsing with deionized water. At both temperatures, the observed fluorescence intensity (i.e. amount of linked azide) is rising with increasing binding time. This increase is gradually at 37 °C for all the times; while at 25 °C, a sudden rise in the intensity is observed when the time increases from 30 to 60 min. Furthermore, at physiological temperature, the binding process takes place more rapid and so, generally, the fluorescence intensity is higher for the 37 °C samples. It is worth mentioning that for both temperatures after about 4 h, it was observed no obvious increase in fluorescence intensity. In other words, the reaction between azide and cycloalkyne is completed within about 4 h and no more coupling will occur after this time.

Finally, by simultaneous consideration of both time and temperature parameters, the 37 °C and 20 min treatment - which had the best intensity at the lowest time - was chosen as the optimum one for further experiments. Fig. 3.6b illustrates an image of micropattern obtained at optimum time (20 min) and temperature (37 °C). As a first indication that coupling reaction worked as intended, spotting was repeated also on an unfunctionalized glass, where washing completely removes the array, while on DBCO terminated surfaces, only excess ink gets removed and a stable bound monolayer of fluorescent azide remains (Fig. 3.7). Also, characterization by XPS further proves the chemical reaction taking place (Fig. 3.6c and Table 3.1). The intensity of the peak at 400.2 eV stemming from N-C=O as well as from N-N=N present in the triazole ring formed after reaction of the azide increased [42]. A further peak at 402.7 eV is still present and can be attributed to N-N=N , which also refers to the triazole ring.

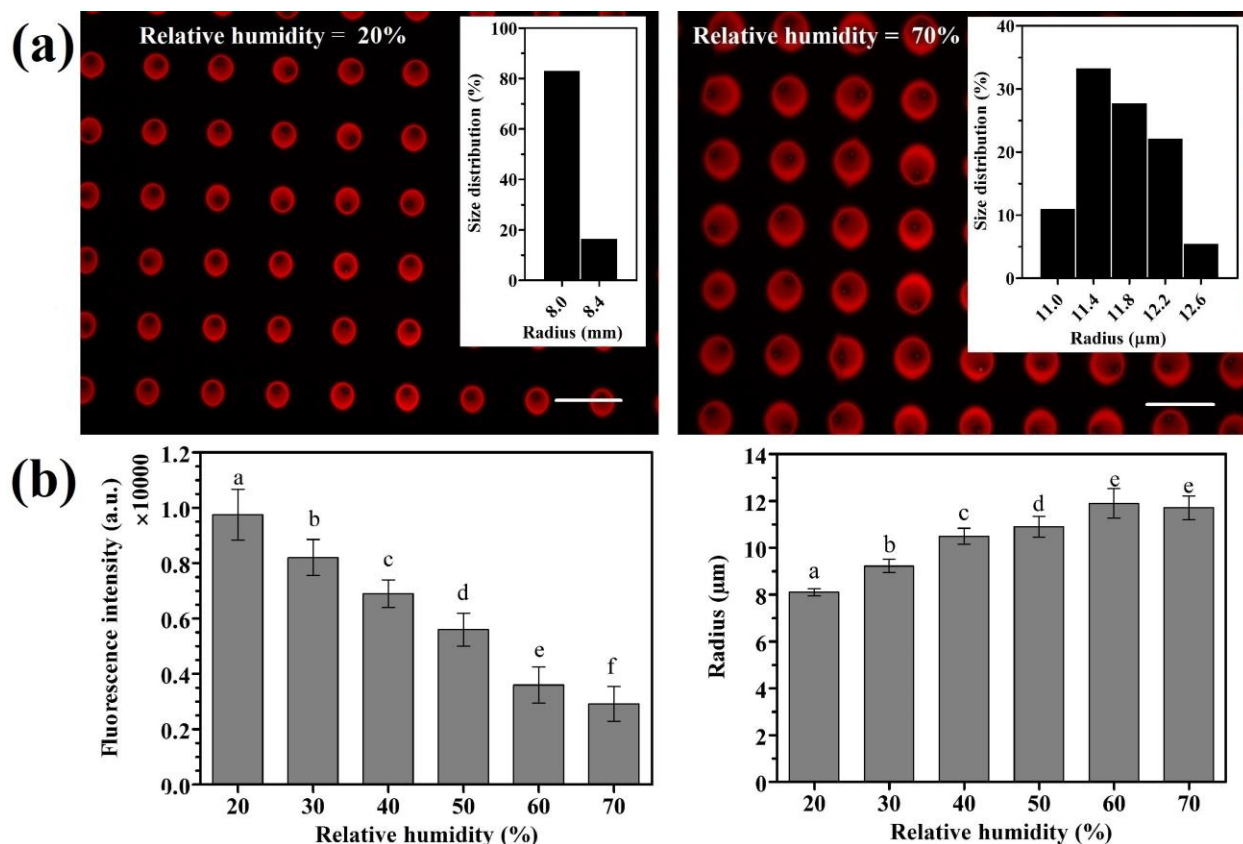


Figure 3.5. Array immobilization of TAMRA-azide on the DBCO-terminated glass: (a) fluorescence microscope images of two micropatterns at two different relative humidities. The inset shows the size distribution of the spots. Scale bars equal 50 μm. Dwell time was 0.1 s and exposure time for imaging 10 s; (b) effect of humidity on average radius and fluorescence intensity of the spots. Values with different letters differ significantly ($p < 0.05$), based on Duncan's test.

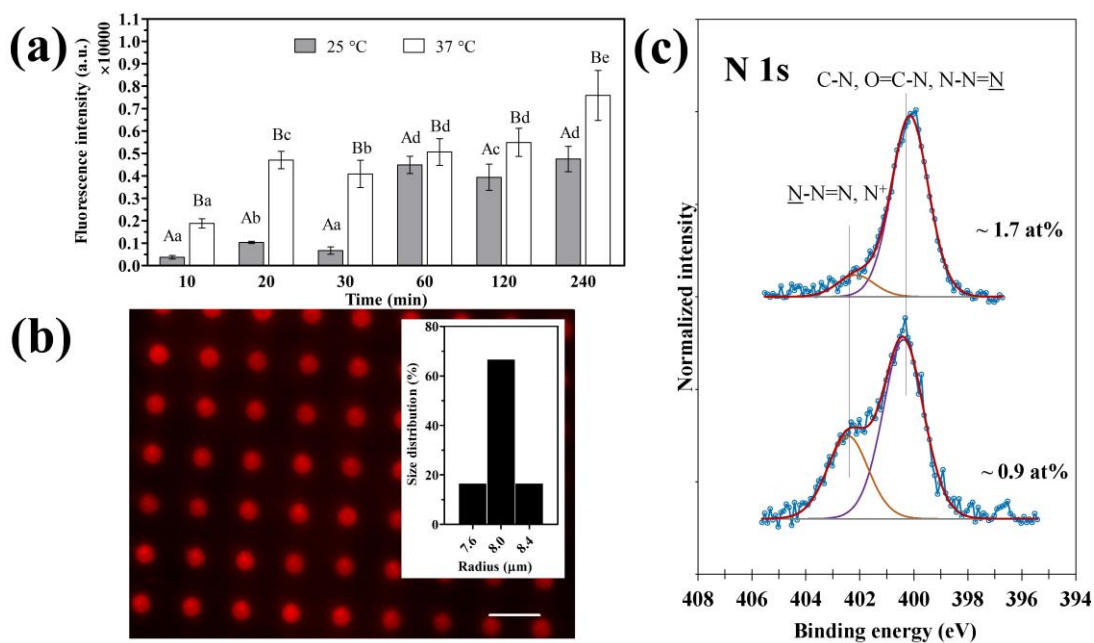


Figure 3.6. (a) Influence of reaction time and temperature on average fluorescence intensity of the TAMRA-azide spots immobilized on the DBCO-terminated glass through click reaction. For the same temperature, values with different lower case letters and for the same time, values with different capital letters are significantly different ($p < 0.05$), according to Duncan's test; (b) a fluorescence microscope image of micropattern obtained at optimum time (20 min) and temperature (37 °C) with a spotting humidity of 20% and dwell time of 0.1 s. The exposure time for the image was 10 s, the inset shows the size distribution of the spots, scale bar equals 50 μm ; (c) N 1s XP spectra of the DBCO-terminated glass after click reaction with TAMRA-azide at optimum time (20 min) and temperature (37 °C) (top) and of DBCO-terminated glass (bottom).

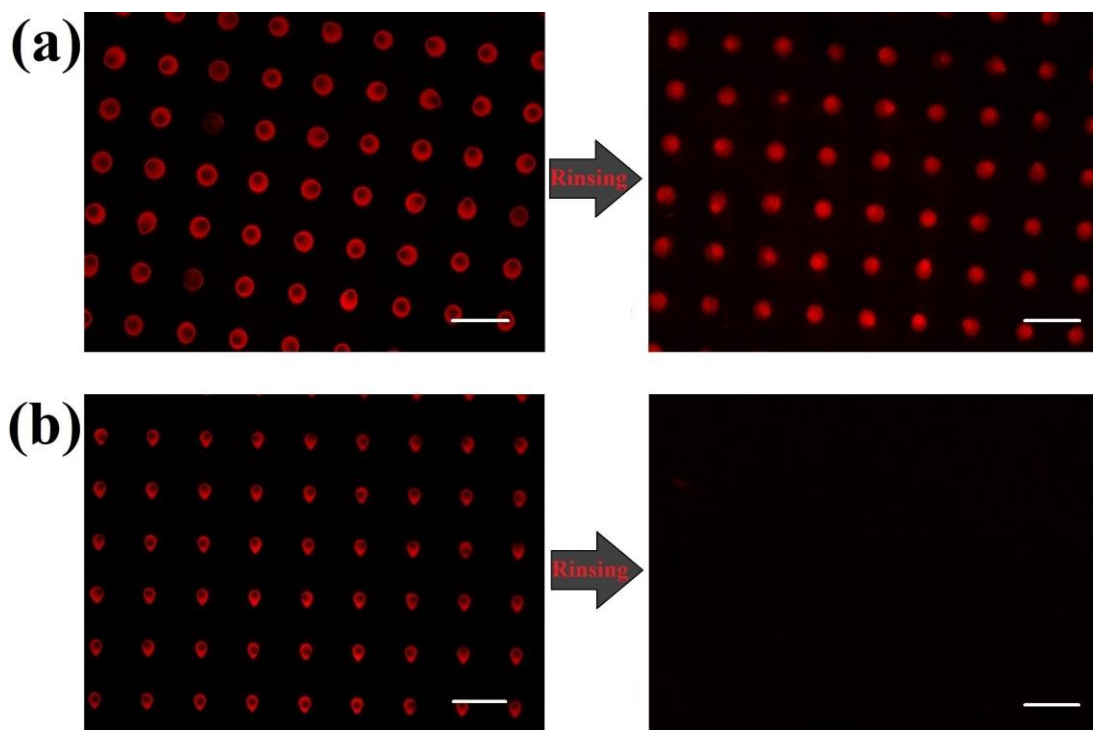


Figure 3.7. Lithography of (a) DBCO-terminated and (b) unfunctionalized glass with TAMRA-azide. Spotting humidity = 20%, dwell time = 0.1 s, reaction time = 4 h, reaction temperature = 37 °C, and exposure time = 10 s. Scale bars equal 50 μm .

As an alternative route for microarray formation, μCS utilizing the thiol-alkyne click reaction was implemented. Again, samples were spotted with an array of 10×10 spots with a pitch of 50 μm in the optimum humidity of 20%. After spotting, the microarrays were left either at room temperature (25 °C) or physiological temperature (37 °C) for different times to study the influence of click reaction time and temperature. Fig. 3.8a shows the average fluorescence intensity of the Cy5 thiol spots immobilized on the DBCO-terminated glass after lithography, click-reaction, and rinsing with deionized water. Similar to what was observed in the azide-alkyne route (Fig. 3.6a), at both temperatures, the observed fluorescence intensity (i.e. amount of linked thiol) is rising with increasing binding time. Compared to the azide-alkyne results, temperature seems to have a negligible influence on the speed of the thiol-alkyne coupling. At both temperatures, the observed fluorescence intensity is much closer together and generally rising with time. Only at the 40 min time point, the fluorescence intensity at physiological temperature is a little higher than for room temperature. It is important to note that for both temperatures, it was achieved no noticeable rise in fluorescence intensity after about 40 min and

the reaction between thiol and cycloalkyne was completed within this time. From Fig. 3.8a, it is evident that temperature of 37 °C and time of 40 min is the optimum one for the thiol-alkyne click reaction via μ CS. So, this treatment was chosen as the optimum one for further experiments (Fig. 3.8b). Likewise to the previous section, XPS measurements ensured that the reaction took place as intended (Fig. 3.8c and Table 3.1). The attachment of Cy5 thiol is clearly demonstrated by the significant increase of the C-O component at 286.5 eV [43], due to the long ethylene glycol chain present in the molecule (about 60 units). Furthermore, an increase of the nitrogen concentration from 0.9 at% up to 2.9 at% can be observed. Like expected, because of the weak sulfur concentration due to the size of the molecule, we can note the absence of S 2p signal.

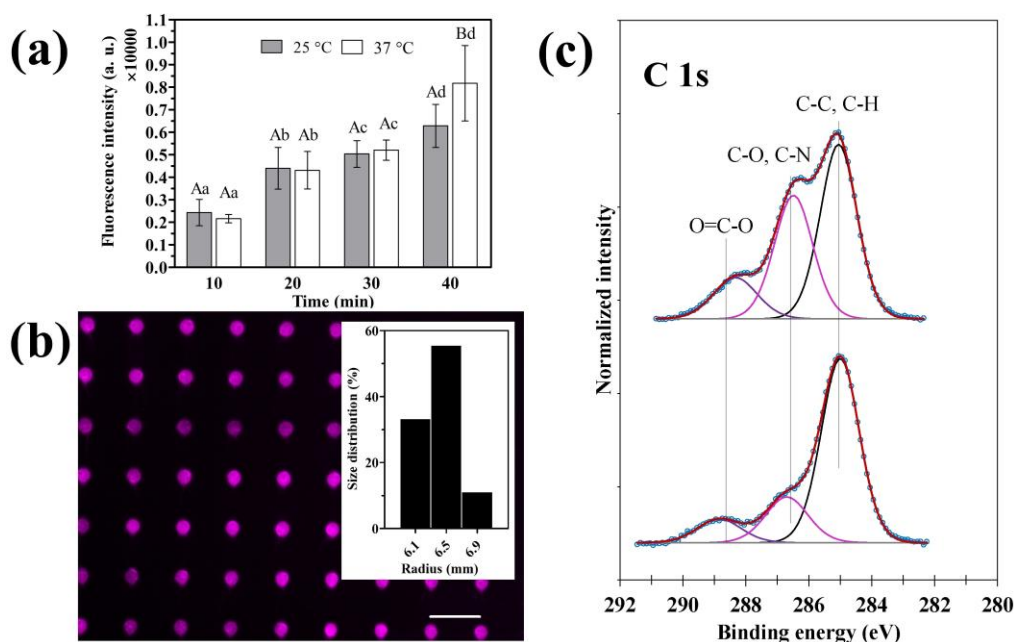


Figure 3.8. (a) Influence of reaction time and temperature on average fluorescence intensity of the Cy5 thiol spots immobilized on the DBCO-terminated glass. For the same temperature, values with different lower case letters and for the same time, values with different capital letters are significantly different ($p < 0.05$), according to Duncan's test; (b) fluorescence microscope image of micropattern obtained at optimum time (40 min) and temperature (37 °C) with a spotting humidity of 20% and dwell time of 0.1 s. The exposure time for the image was 5 s, the inset shows the size distribution of the spots, scale bar equals 50 μ m; (c) C 1s XP spectra of the DBCO-terminated glass after click reaction with Cy5 thiol at optimum time (40 min) and temperature (37 °C) (top) and DBCO terminated glass (bottom).

As an important result and with comparison of the results depicted in Fig. 3.6a and Fig. 3.8a, it can be concluded that the reaction between thiol and cycloalkyne is faster than the reaction

between azide and cycloalkyne and this reaction will be completed in lower time. As mentioned earlier, the azide-alkyne reaction continued until 4 h while the thiol-alkyne reaction was finished within about 40 min. To the best of our knowledge, there are no references in the literature comparing reaction rates of azide/alkyne and thiol/alkyne in the context of surface functionalization by spotting. In addition to required time for finishing the reaction which is a very significant parameter, other parameters like volume, structure, and number of reactant molecules (azide or thiol) as well as potential differences in the dye intensity of the fluorescent thiol and azide must be considered for comparison of reaction rates.

3.2.3. Protein coupling by biotin-azide and biotin-thiol

In the previous sections, we demonstrated the fruitful immobilization of arrays of fluorescent TAMRA-azide and fluorescent Cy5 thiol on DBCO-terminated glass through click reaction. To compare both coupling routes despite potential differences in the dye intensity of the fluorescent thiol and azide compound that make it unreliable to compare arbitrary intensities directly for judging binding efficiency, we utilized specific protein binding between biotin and streptavidin. This widely used binding motif ^[6] also underlines the potential for application of these arrays in protein presentation, as it builds a bridge to immobilizing a plethora of biotinylated proteins, antibodies and small molecules. Furthermore, this approach can demonstrate the feasibility of using the μ CS spotting for design and manufacturing of small-scale patterns suitable for biomedical and biological applications. For that, biotin-azide and biotin-thiol were immobilized separately on the surface of DBCO-terminated glass via μ CS. After grafting of fluorescent-labeled streptavidin, patterns were evaluated for fluorescence intensity. The study of the fluorescence intensity of streptavidin adsorbed on the surface provides a more reliable judgment of the amount of linked azide or thiol, and consequently reaction rates of azide-alkyne and thiol-alkyne. Fig. 3.9 compares two microarrays of biotin-azide and biotin-thiol (10×10 spots with a pitch of $50 \mu\text{m}$) that were immobilized on the DBCO-terminated glasses through click reaction, and subsequently incubated with fluorescent-labeled streptavidin. In the direct comparison, the fluorescence intensity of streptavidin coupled with biotin-thiol was approximately 3.9 times higher than that of streptavidin joined with biotin-azide ((5508 ± 538) a.u. vs. (1397 ± 142) a.u.). On the other hand, molecular weights of biotin-azide and biotin-thiol shows that the initial molecular concentration of the second compound has been about 4.5 times lower than that of the first one. Considering both initial molecular concentration and

fluorescence intensity of streptavidin coupled, we can confidently conclude that the reaction between thiol and cycloalkyne is more efficient than the reaction between azide and cycloalkyne for μ CS arraying. To exclude steric effects introduced by different linker length (hence possibly different accessibility of the biotin moiety for the streptavidin), control experiments with different linker length were implemented. These showed, that for the used length variations in the present study, no significant difference could be found (Fig. 3.10), hence all linkers were already long enough to allow free access to the biotin moiety. The attachment of biotin-thiol can here be proved by the apparition of a S 2p doublet with S 2p_{3/2} at 163.4 eV [44] whereas the immobilization of biotin-azide is again evidenced by an increase of the nitrogen concentration, with 2 peaks attributed to the formed triazole ring (Fig. 3.9c-d and Table 3.1).

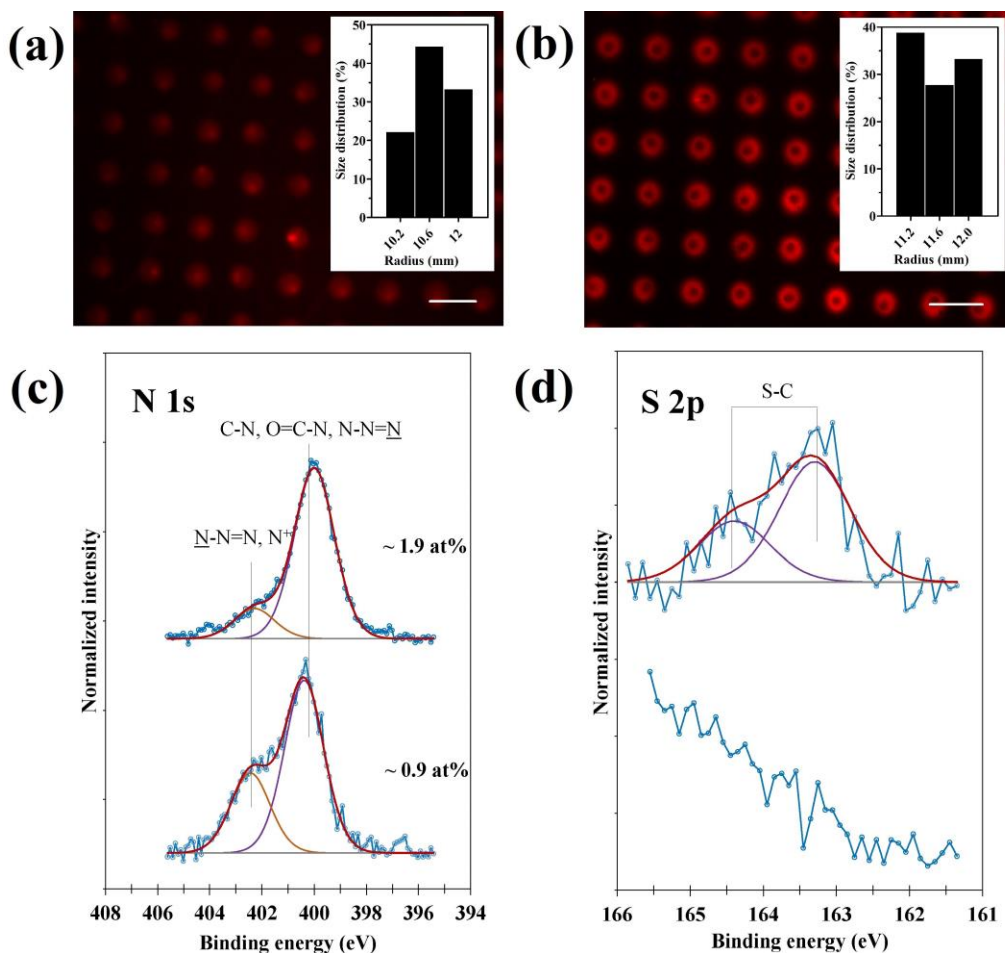


Figure 3.9. Fluorescence microscope images of microarrays of (a) biotin-azide immobilized on the DBCO-terminated glass after incubating with streptavidin-Cy3, click reaction time = 20 min, click reaction temperature = 37 °C; (b) biotin-thiol immobilized on the DBCO-terminated glass after incubating with streptavidin-Cy3, click

reaction time = 40 min, click reaction temperature = 37 °C. For both microarrays, spotting humidity was 20% and dwell time of 0.1 s was used. The exposure time of both images was 10 s, and the insets show the size distribution of the spots. Scale bars equal 50 μm ; (c) N 1s and (d) S 2p XP spectra of DBCO-terminated glass (bottom), biotin-azide immobilized on DBCO (c, top) and biotin-thiol immobilized on DBCO (d, top).

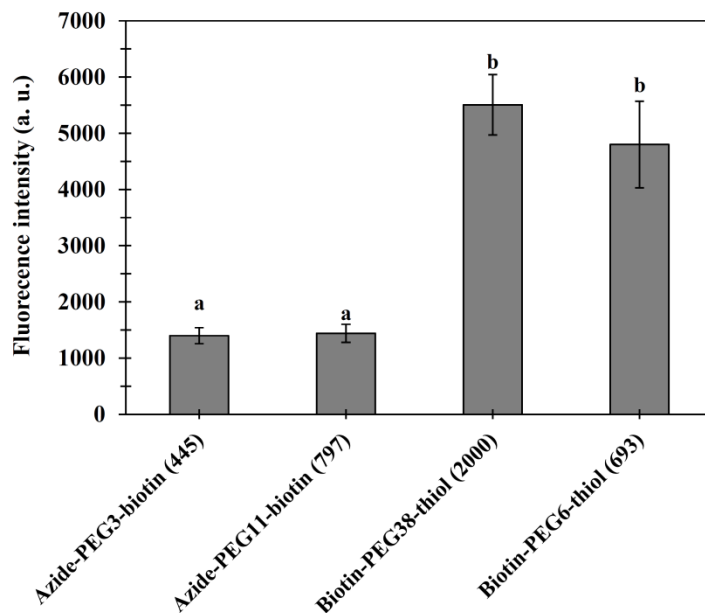


Figure 3.10. Effect of molecular weight / spacer length of biotin-azide or biotin-thiol on the intensity of spots after incubation with fluorescent-labeled streptavidin. Molar concentrations of biotin-azide and biotin-thiol solutions were about 2.2 and 0.5 mM, respectively. The numbers in the parentheses present the molecular weight of compounds. Values with the same letters do not differ significantly ($p < 0.05$), based on Duncan's test.

3.3. Summary

In summary, we presented and compared two catalyst-free immobilizing routes (azide-alkyne and thiol-alkyne) for the generation of covalently bound microarrays via μ CP. Click reactions were performed at different temperatures and times and the optimum conditions of 37 °C/20 min and 37 °C/40 min were found for azide-alkyne and thiol-alkyne reactions, respectively. While the thiol-alkyne reaction was completed within about 40 min, the azide-alkyne reaction continued until 4 h. Although due to lack of need for catalysts or additional additives, mild reaction conditions and high reaction rate both routes worked reliable for surface functionalization, the thiol-alkyne route showed much higher efficiency when compared with the azide-alkyne route over assessment by binding of a fluorescent-labeled protein. Therefore, in a free choice, our results recommend using a thiol-alkyne route to obtain the highest surface density of molecular immobilization. Furthermore, the protein binding experiments proved the potential for application of these microarrays in protein detection and other biomedical/biological applications.

Chapter 4

Functionalization of thiol-terminated glass surface

4.1. Introduction

Thiols can take part in the click reactions through three different routes including thiol-ene coupling (TEC), thiol-yne coupling (TYC) and thiol-ene Michael addition (TEMA) reactions [3a, 26b]. TEC reaction is initiated with the generation of a thiyl radical from the thiol by direct UV irradiation (often 365 nm) in the presence of a photoinitiator like 2,2-dimethoxy-2-phenylacetophenone (DMPA) [45]. The radical addition of thiols to linear alkynes, TYC, has shown to have the same attractive features of TEC, with the additional benefit of increased reactivity, as two thiol molecules can react with one alkyne group. Similar to the TEC reaction, this reaction is induced by photo-irradiation via a radical initiator. The reaction between thiol and cycloalkyne is a little different from the reaction of thiol with linear alkyne. In this type of TYC reaction, however only one thiol can be added to cycloalkyne, the reaction is relatively rapid and can be performed spontaneously even in the absence of light and photoinitiator in an unpurged atmosphere. In general, TYC reactions have recently become more favored over TEC ones [25-26, 46].

In 2012, Wu et al. coated alkene and alkyne-functionalized polymers on various substrates via chemical vapor deposition (CVD) polymerization process. Next, the coated surfaces were conjugated with thiol-terminated molecules via TEC and TYC reactions by UV activation using a photomask, allowing the selective preparation of patterns [47]. In another study of modification of polymer surfaces published in 2012, Norberg et al. produced lectin sensors by modification of alkene and alkyne-functionalized polystyrene with thiolated carbohydrates through TEC and TYC reactions [48]. In a valuable effort published in 2013, Bhairamadgi et al. reported a comparative study of TEC and TYC modification of oxide-free Si(111) surfaces which was the first study that obviously showed the TYC strategy yielded higher surface coverage than the TEC approach due to double addition of thiols to linear alkyne [37]. In addition to the mentioned examples, the TYC click reaction has been applied for the functionalization of another surfaces and particles including microporous membrane [49], porous monolith surface [35], boron-doped diamond electrodes [26d], superparamagnetic fluorescent nanoparticles [50], graphene oxide [51], oxide-free Si(111) [52], poly(ethylene terephthalate) (PET) nanochannel [38], gold [53], micropatterned hydrogel [54], poly hydroxyethyl methacrylate (pHEMA) hydrogel [55], polyurethanes [56], silica nanoparticle-graphene oxide composites [57] and degradable polylactides [58].

In addition to the radical-mediated TEC and TYC reactions, thiols can also react with alkenes having electron-withdrawing groups (EWG) such as maleimides, acrylates, vinyl sulfones, and acrylamides [3a, 45, 59]. However, this reaction was first reported by Komnenos [60], but it gained popularity by Arthur Michael [61]. So, this click reaction is known as thiol-ene Michael addition (TEMA). The reactivity of TEMA reaction can be accelerated by the addition of catalytic amounts of a weak base, such as an amine (base-initiated mechanism) or by a nucleophile, such as a phosphine compound (nucleophile-initiated mechanism). The most common catalysts used in this reaction are listed in Fig. 4.1. It is important to note that catalysis by a nucleophile gives considerably faster reaction and higher conversion than catalysis by a base, however, nucleophilic pathway results in the formation of some amount of by-product [62].

In 2007, Kimura et al. described the local attachment of maleimide-modified peptides onto thiol-modified surfaces through a thiol-maleimide Michael addition for its use in the fabrication of DNA microarrays [63]. In 2012, Tedja et al. reported the attachment of poly(oligo(ethylene glycol) methyl ether methacrylate) onto thiol-functionalized titanium oxide (TiO₂) nanoparticles using the thiol-acrylate Michael addition [64]. In the same year, Seto et al. functionalized the maleimide-terminated surface of siliceous materials using thiol-terminated polystyrene, poly(acrylic acid), poly(*N*-isopropylacrylamide), and poly(*p*-acrylamidophenyl- α -mannoside). Immobilization of poly(*p*-acrylamidophenyl- α -mannoside) onto the surface provided a microarray for the detection of FITC-Con A [65]. One year later, in 2013, this group fabricated streptavidin biosensor in an analogous manner using functionalization of maleimide-terminated silicon and nickel surfaces with thiolated biotin [66]. In 2013, another example of a surface modification strategy using a TEMA was described by Gobbo and co-workers. They synthesized the gold nanoparticle (AuNP)-carbon nanotube (CNT) hybrids through the click reaction between thiol-functionalized single-wall CNT and maleimide-functionalized AuNP [67]. In 2016, Fensterbank et al. combined the copper-catalyzed alkyne-azide cycloaddition (CuAAC) and thiol-maleimide Michael addition methods to functionalize a fullerene platform in a stepwise process [68]. In another study in 2016 by Xu et al., maleimide-containing tannic acid (TAMA) as a new surface anchor was developed to introduce the maleimide moieties onto the stainless steel (SS) surface. In this study, the surface conjugation efficiency of TAMA with the thiol-containing compounds via Michael addition was examined [69]. Also, in 2016, Gaitzsch et al. discussed and compared a variety of metal-free conjugation methods (such as thiol/maleimide conjugation) to

attach dyes to an amphiphilic block copolymer which can be used for imaging in optical microscopy or for tracing and marking macromolecules [70]. Recently, in an interesting study, Aktan et al. fabricated multifunctionalizable nanogels containing maleimide and thiol functional groups which can be easily conjugated with various appropriately functionalized molecules to tailor them for various applications in delivery and imaging [71]. Other studies in the field of modification using TEMA reaction have been reported for different surfaces and particles including glass and polymer surfaces [72], salmon calcitonin (sCT) [73], hydrogels [74], AuNPs [75], magnetic nanoparticles (Fe_3O_4) [76], porous cellulose nanocrystals (CNC)/poly(vinyl alcohol) (PVA) nanocomposite films on glass [77], porous polymeric monolith [78], and a mixed macrodiol polyurethane and tantalum [79].

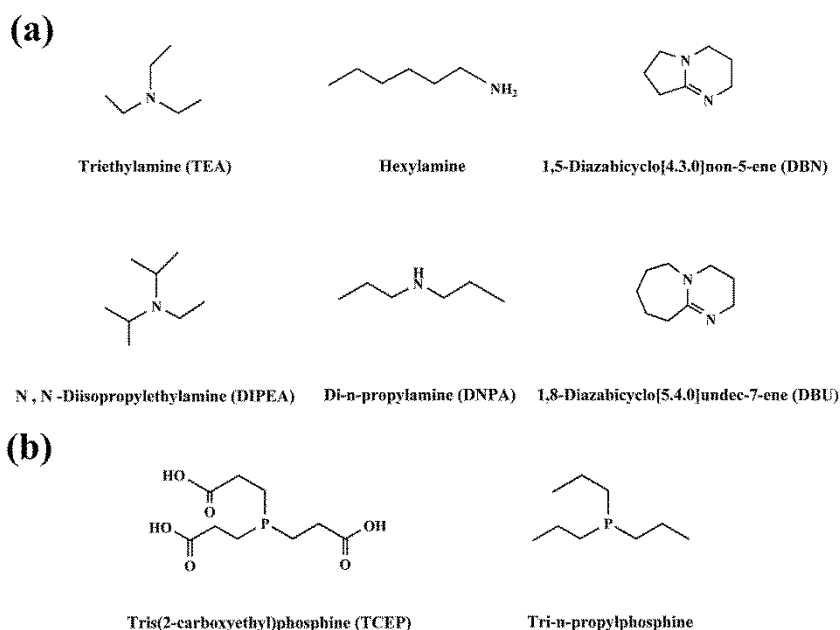


Figure 4.1. Examples of catalysts used in the (a) base-catalyzed and (b) nucleophile-catalyzed thiol-en Michael addition reaction.

As seen from the brief review, TYC and TEMA click reactions are frequently used in diverse modification applications. Nevertheless, a comparison of these approaches for immobilization purposes is still lacking. Our aim in this chapter is to compare the efficiency of TYC and TEMA click reactions in site-specific surface modification. It seems to be the first study that unequivocally compares these two approaches. For this purpose, the surface of hydroxyl-terminated glass was initially thiolated using (3-mercaptopropyl)trimethoxysilane

(MPTMS) which is a mercaptosilane. Subsequently, in the separate experiments, the thiol-terminated surface was reacted with different fluorescent and non-fluorescent inks containing cycloalkyne or maleimide groups via microchannel cantilever spotting (μ CS). Finally, the feasibility of these two routes and micropattern fabricated by them in biomedical and biological applications was examined through protein binding experiments (Fig. 4.2).

4.2. Results and discussion

4.2.1. Contact angle measurements

As preparation for the μ CS of arrays, substrates were functionalized with a mercaptosilane. This leaves the resulting surface terminated with thiol groups (SH) and reactive for the TYC and TEMA click reactions that will be evaluated for their efficiency in μ CS arraying. To achieve good silanization, the rinsed glass substrates were subjected to an oxygen plasma treatment to ensure high density of hydroxyl groups on the surface. After this activation procedure, the samples were treated with a solution of mercaptosilane in toluene, yielding a thiol-terminated surface. As a first check of successful functionalization, contact angle measurements were performed on the plasma-treated and thiol-terminated glasses, directly after treatment and over some following days (Fig. 4.3).

Plasma-treated glass directly after activation is highly hydrophilic (contact angle 0°). The hydrophilicity declines over the course of 3 to 4 weeks and is approaching that of a non-treated glass surface (contact angle $\sim 46^\circ$) again. The thiol-terminated surfaces are less hydrophilic with an initial contact angle of $57.8 \pm 1.0^\circ$ that quickly (compared to the OH-terminated glass surface) stabilizes at an angle around 68.1° (determined by the asymptotic approach of the fit function given in Fig. 4.3a). The initially lower contact angle for thiol-terminated surface might be induced by remaining OH groups from the plasma-treatment that decay until only the thiol surface groups remain.

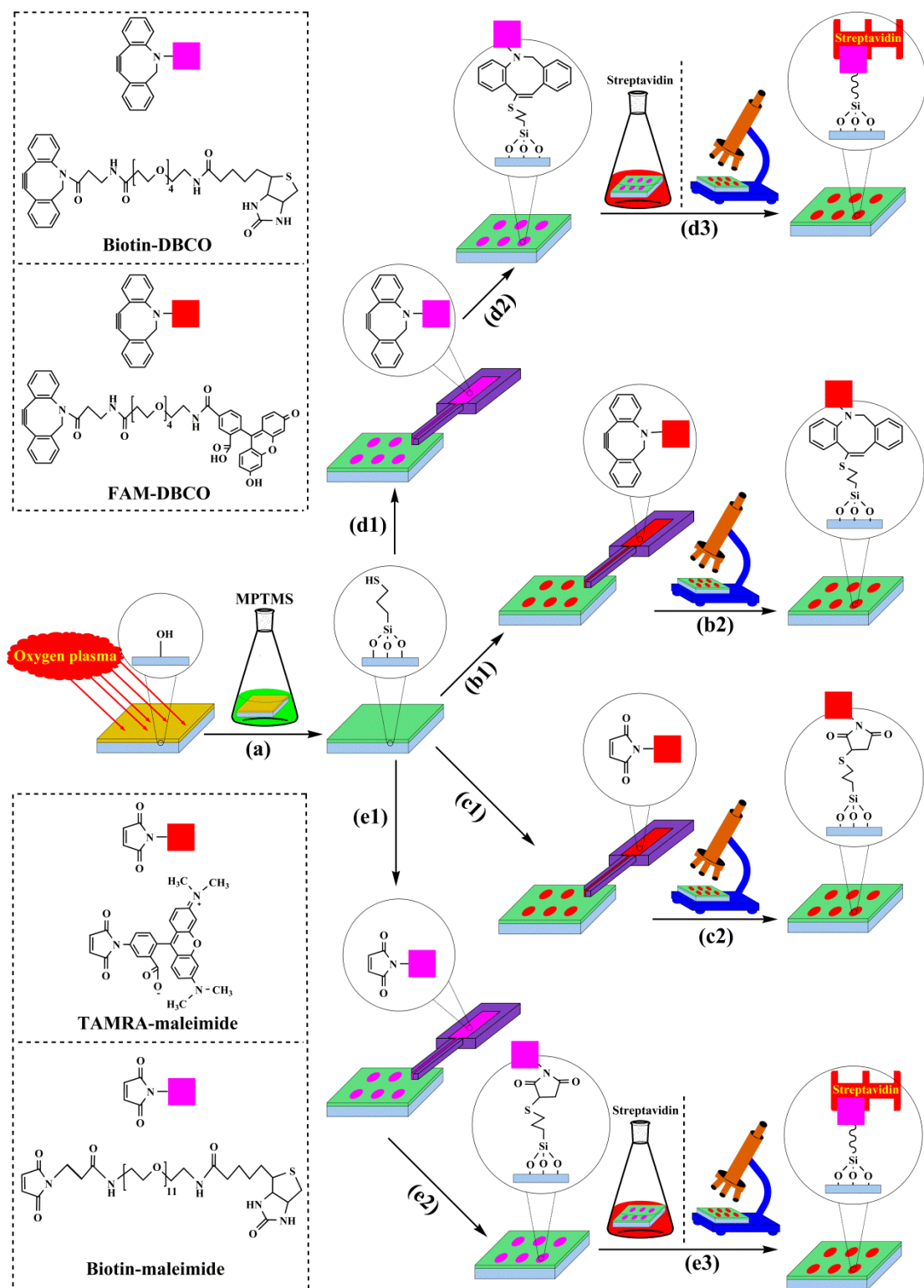


Figure 4.2. Schematic illustration for thiol-terminated surface modification by thiol-yne coupling and thiol-ene Michael addition click reactions. The pink and red squares symbolize non-fluorescent and fluorescent dyes, respectively.

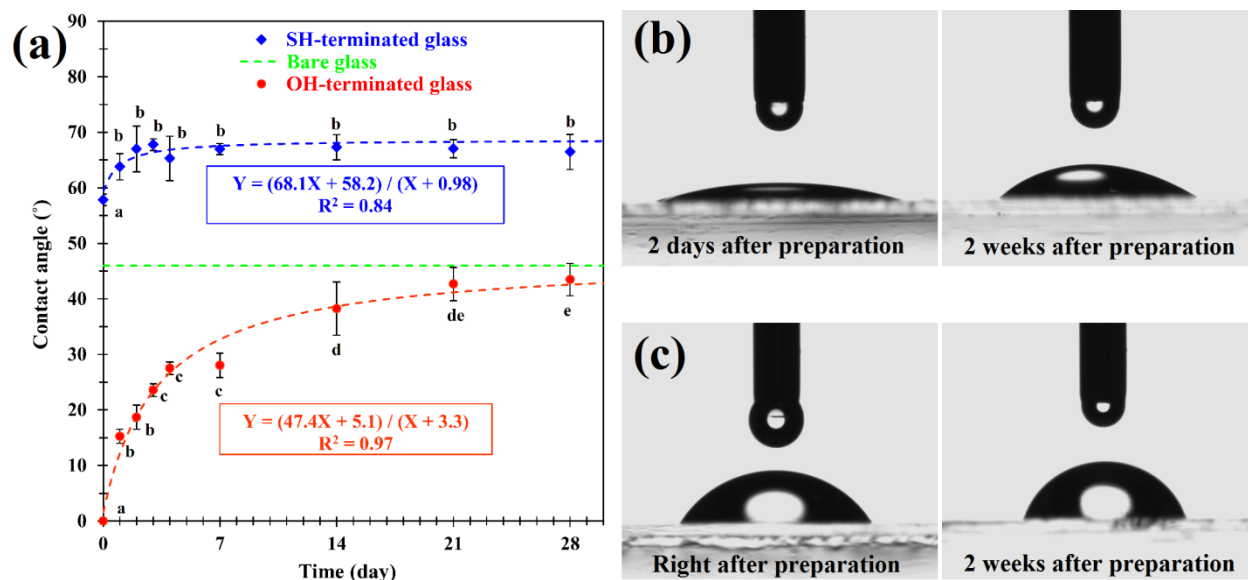


Figure 4.3. Characterization of hydroxyl-terminated and thiol-terminated glasses by contact angle measurement; (a) The experimental data of contact angle measurements which were fitted by rational functions using MATLAB software. The red and blue dashed curves are the best fitted curves related to OH-terminated and SH-terminated glasses, respectively. Also, the green horizontal dashed line denotes the contact angle of the bare glass which is about 46°. Values with different letters differ significantly ($p < 0.05$), based on Duncan's test; Images of water droplets on (b) OH-terminated and (c) SH-terminated glasses.

4.2.2. XPS measurements

For a better chemical characterization, the OH-terminated and SH-terminated as well as SH-terminated surfaces functionalized via the target reactions were subjected to XPS (Fig. 4.4). Whereas the OH-terminated surface doesn't show any sulfur, the SH-terminated surface shows clearly the presence of sulfur mainly as a thiol (S 2p_{3/2} at 163.5 eV) with a concentration of 1.5 at%, accompanied by an oxidized species at 168.0 eV (0.2 at%) and a further one, not clearly identified, at 162.5 eV (0.3 at%) which could be eventually attributed to a Si-S or S=C bond (Fig. 4.4a) [80]. The click reaction with TAMRA-maleimide is shown in Fig. 4.4b by the clear increase of the peak at quite low binding energy, namely 286.3 eV, due to the predominant presence of N-CH₃ groups in the molecule in comparison to C-O contribution, and the increase of the component at 288.6 eV proving the addition of maleimide and carboxyl groups. FAM-DBCO contains in contrary mainly C-O and few C-N so that the (C-O, C-N) peak appears at 286.7 eV. Its weak intensity is probably due to a smaller click density than the one of TAMRA-maleimide because of steric hindrance [81]. Further on the click reaction with biotin-DBCO and

biotin-maleimide (Fig. 4.4c) can be proven by considering the clear increase of intensity of the N 1s peak at 400.2 eV attributed to the introduced maleimide groups. A second component at 402.3 eV is attributed to a protonated species [82]. These measurements confirmed the presence of SH-groups after silanization, as well as the implementation of the TYC and TEMA reactions as expected.

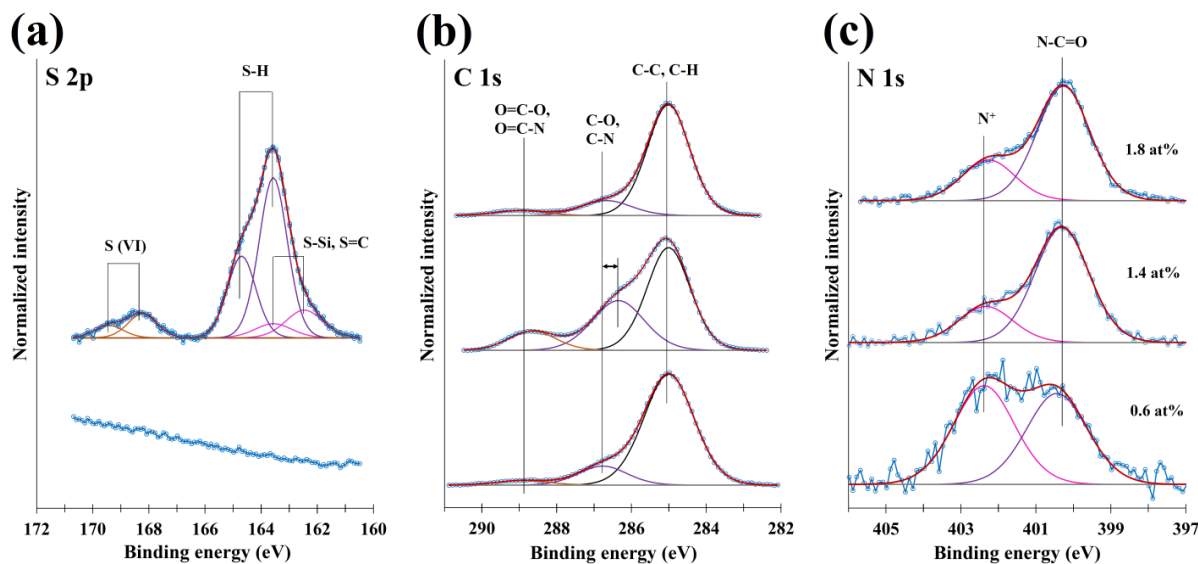


Figure 4.4. XP spectra of (a) OH-terminated (bottom) and SH-terminated (top) glasses; (b) SH-terminated (bottom) and SH-terminated glass after click reaction with TAMRA-maleimide (middle) and FAM-DBCO (top) at optimum time and temperature; (c) SH-terminated glass (bottom) and SH-terminated glass after click reaction with biotin-maleimide (middle) and biotin-DBCO (top) at optimum time and temperature.

4.2.3. Array immobilization of FAM-DBCO and TAMRA-maleimide

To establish the TYC/TEMA click reactions for μ CS and figure out optimal reaction parameters, respectively, arrays of fluorescently labeled DBCO (FAM-DBCO) and fluorescently labeled maleimide (TAMRA-maleimide) were spotted onto the prepared thiol-terminated substrates. For this, microchannel cantilevers were loaded with an ink solution of the respective compound dissolved in DMSO and admixed with some glycerol to prevent premature drying. Spotting was then achieved on a commercial DPN setup by bringing the cantilever into regular contact with the surface while controlling the x-y position to yield a 10×10 array of dot features. After the spotting, samples were allowed to react for different time durations (10, 20 and 40 min) and at two different temperatures (room temperature of 25°C and slightly elevated at 37°C). After the incubations times elapsed, samples were washed to remove excess ink and

stop the reactions. Then, samples were evaluated by fluorescence microscopy. A summary of results and micrographs of typical lithography outcomes are given in Fig 4.5.

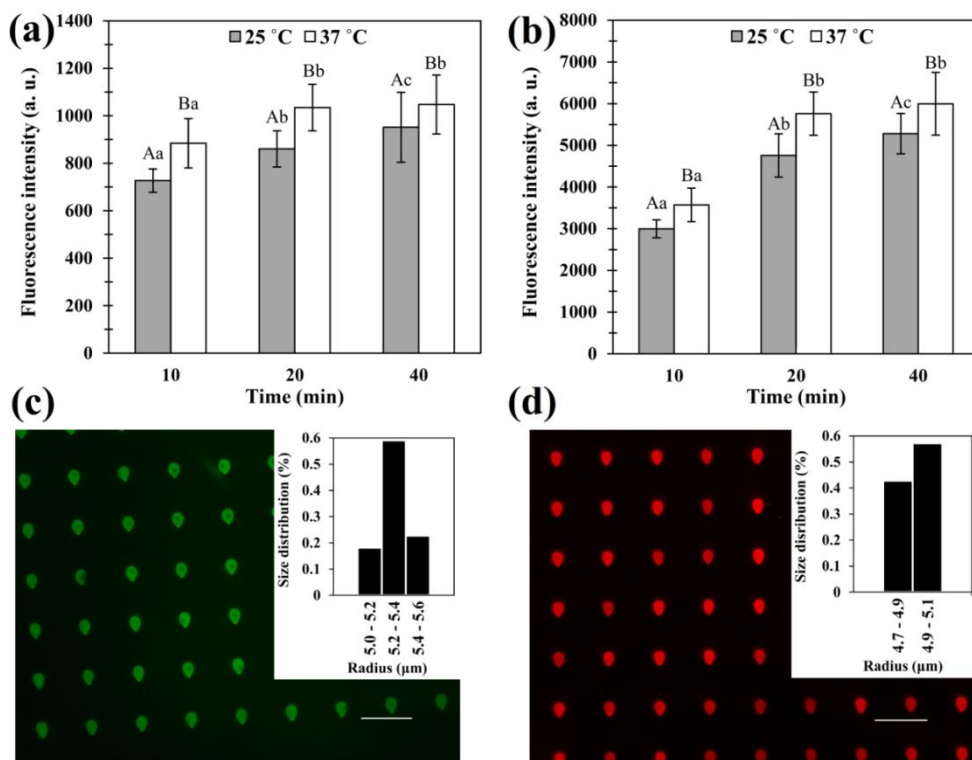


Figure 4.5. Influence of reaction time and temperature on average fluorescence intensity of the (a) FAM-DBCO and (b) TAMRA-maleimide spots immobilized on the thiol-terminated glass via click reaction. For the same temperature, values with different lower case letters and for the same time, values with different capital letters are significantly different ($p < 0.05$), according to Duncan's test; Fluorescence microscope images of micropatterns obtained at optimum reaction temperature and time (37 °C and 20 min) with a spotting humidity of 20% and dwell time (tip/surface contact time) of 0.1 s for (c) FAM-DBCO and (d) TAMRA-maleimide spots immobilized on the thiol-terminated glass. The exposure time for the images was 10 s, the insets show the size distribution of the spots and the scale bars equal 50 μm.

Both reactions obviously were able to take place and immobilize the respective fluorophore, as patterns remain stable and clearly visible after washing of the samples. For both reactions, a trend for increased intensity with elevation of temperature and with longer duration of incubation is visible. However, both reactions seem to be completed after 20 min, as there is no significant raise in fluorescence intensity for the 40 min time point in both cases. Consequently, by simultaneous consideration of both temperature and time, reaction temperature of 37 °C and reaction time of 20 min were chosen as the optimum ones for both TYC and TEMA click

reactions in further experiments. Fig. 4.5c-d shows the fluorescence microscope images of micropatterns obtained at optimum reaction conditions (37 °C and 20 min) for FAM-DBCO and TAMRA-maleimide spots immobilized on the thiol-terminated glass where obtained feature radius sizes were $5.3 \pm 0.12 \mu\text{m}$ for FAM-DBCO and $4.9 \pm 0.07 \mu\text{m}$ for TAMRA-maleimide, respectively.

4.2.4. Protein coupling by biotin-DBCO and biotin-maleimide

In the previous section, we fruitfully could immobilize either arrays of fluorescent FAM-DBCO and fluorescent TAMRA-maleimide on the thiol-terminated glass through TYC and TEMA click reaction, respectively. Also, we found the optimum reaction conditions for both routes. As the fluorophores with different functional groups for surface coupling are different from each other, with different spectra, and will therefore yield different intensities even for the same surface concentration of immobilized molecules, a different strategy was implemented for the direct comparison of the two reactions. For this, via both chemical routes, biotin bearing compounds, biotin-DBCO and biotin-maleimide, were spotted on thiol-terminated glass by μCS into 10×10 spot arrays. The biotin is a frequently used linker with strong affinity to streptavidin [30, 66, 83]. By utilizing a fluorescently labeled streptavidin as fluorophore to visualize the immobilized biotin patterns, the amount of immobilized biotin can be compared between the two coupling routes with exactly the same fluorophore and an influence of the different coupling linker on the fluorophore can be ruled out. Results for arrays fabricated at optimal conditions (37 °C and 20 min for both reactions) with different ink concentrations are summarized in Fig. 4.6. It is worth mentioning that as the molecular weights of inks were almost close to each other ($749.92 \text{ g}\cdot\text{mol}^{-1}$ for biotin-DBCO vs. $922.09 \text{ g}\cdot\text{mol}^{-1}$ for biotin-maleimide), similar mass concentrations of two inks resulted in their similar molar concentrations.

For both chemical routes, TYC and TEMA, immobilization of biotinylated compound was successful, as after staining the patterns with fluorescently labeled streptavidin, they all show up in the corresponding fluorescence channel. When comparing the two immobilization routes, it becomes obvious that the TEMA route is yielding a higher fluorescence intensity in the spots for every concentration: (1254 ± 158) a.u. to (1814 ± 169) a.u. for the biotin-DBCO spots versus (1662 ± 174) a.u. to (3953 ± 210) a.u. for the biotin-maleimide spots after binding with fluorescently labeled streptavidin (1.3-2.2 folds higher fluorescence intensities). This indicates a

more efficient biotin immobilization by the maleimide-based surface coupling. Fig. 4.6c-d shows the fluorescence microscope images of micropatterns obtained for biotin-DBCO and biotin-maleimide spots immobilized on the thiol-terminated glass after incubating with streptavidin. The feature radius is comparable with the results for the fluorophore spotting and ranges from $(5.4 \pm 0.24) \mu\text{m}$ for biotin-DBCO at a concentration of $400 \mu\text{g}\cdot\text{ml}^{-1}$ to $(6.7 \pm 0.25) \mu\text{m}$ for $2000 \mu\text{g}\cdot\text{ml}^{-1}$. For the biotin-maleimide, respectively, a range from $(5.1 \pm 0.29) \mu\text{m}$ with $400 \mu\text{g}\cdot\text{ml}^{-1}$ to $(6.4 \pm 0.19) \mu\text{m}$ with $2000 \mu\text{g}\cdot\text{ml}^{-1}$ was observed. In the previous chapter, we studied and compared two catalyst-free immobilizing routes including SPAAC and TYC for the generation of covalently bound microarrays on functionalized glass surfaces where the protein binding experiments revealed that the reaction between thiol and cycloalkyne showed much higher efficiency than the reaction between azide and cycloalkyne. Simultaneously considering of past and present findings, it can be concluded that the surface density of molecular immobilization on the glass surface via click reaction is in order: TEMA > TYC > SPAAC.

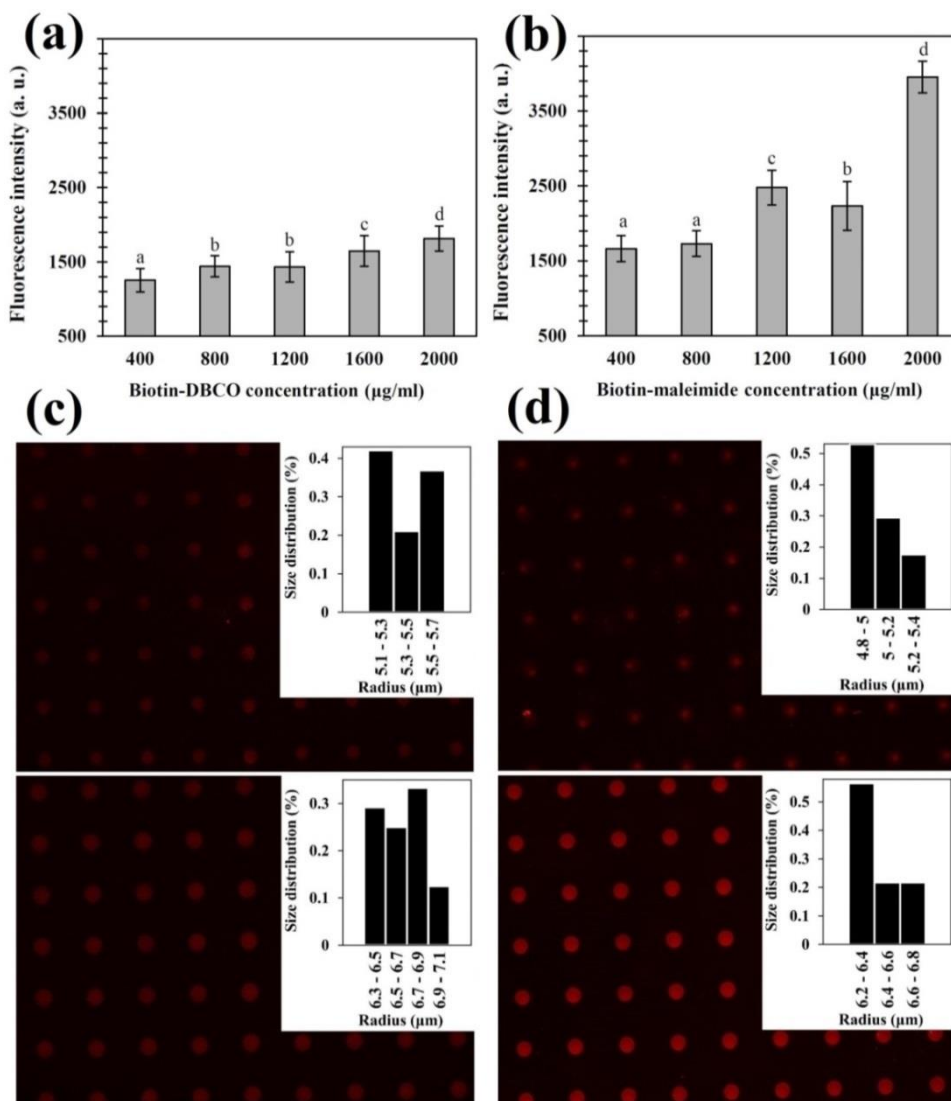


Figure 4.6. Influence of ink concentration on average fluorescence intensity of the (a) biotin-DBCO and (b) biotin-maleimide spots immobilized on the thiol-terminated glass through click reaction after incubating with fluorescently labeled streptavidin. Click reaction time and temperature were 20 min and 37 °C, respectively. Values with different letters differ significantly ($p < 0.05$), based on Duncan's test; Fluorescence microscope images of micropatterns for (c) biotin-DBCO and (d) biotin-maleimide spots immobilized on the thiol-terminated glass at ink concentrations 400 $\mu\text{g}\cdot\text{ml}^{-1}$ (c and d; tops) and 2000 $\mu\text{g}\cdot\text{ml}^{-1}$ (c and d; bottoms), after incubating with streptavidin. For all microarrays spotting humidity was 20% and dwell time of 0.1 s was used. Also, the exposure time of images was 20 s, the insets show the size distribution of the spots and scale bars equal 50 μm .

4.3. Summary

In this chapter, a systematic survey into the efficiency of TYC and TEMA click reactions for immobilization of functional compounds on thiol-terminated surfaces via μ CS was conducted. Both routes can successfully couple functional moieties to the surface as became evident from experiments with different fluorophores. When varying the incubation time and observing obtained fluorescence intensity in the arrays, we could determine that reaction time of 20 min before removing excess ink is sufficient in both routes, though the coupling over DBCO seems to react slightly faster compared to the maleimide. However, when comparing the intensities obtained by protein coupling to a biotin carrying spot array allowing for a direct comparison of immobilized biotin via two routes, we observed consistently higher amount of immobilized biotin via the TEMA route. In conclusion, when surface chemistry for μ CS can be chosen free of other concerns, the TEMA reaction will yield most efficient surface immobilization.

Chapter 5

Functionalization of epoxy-terminated glass surface

5.1. Introduction

Ring opening of epoxy via nucleophilic attack of thiols, amines, azides, alcohols, cyanides, carboxylic acids, phenols and hydrazides is of paramount significance in organic synthesis as it provides access to valuable products. Besides the clear significance of these reactions in traditional synthetic arenas and biological/pharmaceutical applications, they are significant industrially and the future of them in the preparation of reactive and functional materials appears bright. In a nucleophilic ring-opening reaction of asymmetric epoxies, depending on reaction conditions, two regio-isomers are possible (Fig. 5.1a) [84].

Catalyzed reaction between an epoxy and a thiol which leads to the formation of a β -hydroxythio-ether linkage is an efficient, robust and regio-selective reaction where if the appropriate kind of catalyst and reaction conditions is employed, high yield can rapidly achieved. This reaction can be carried out at room temperature and in the presence of air and moisture using a variety of solvents and a few minutes to a few hours is sufficient for completion of the reaction [26b, 84d, 85]. Formation of reactive hydroxyl groups is a significant aspect of the thiol-epoxy reaction opening up the opportunity to achieve a second reaction for modification. Polymerization process using monomers carrying thiol and epoxide functionalities can provide well-defined polymers with reactive hydroxyl groups. Subjecting the prepared reactive polymer to a subsequent post-polymerization modification is a valuable route toward the preparation of functional materials [86]. Surface modification via the thiol-epoxy reaction is a useful way for functionalization of different solid substrates. The substrates can be designed to carry polymers or immobilized small molecular species containing reactive thiol or epoxide sites. The surface functionalization can then be done either by using polymer or small molecules with complementary thiol or epoxide groups [87]. The thiol-epoxy reaction has also been extensively used in dual-curable systems with a controlled curing sequence in order to expand adhesives, composites and high-performance coatings [88].

β -Amino alcohols such as metoprolol, propranolol, atenolol, and dopamine which are versatile intermediates in the synthesis of various biologically active compounds have earned a valuable place in pharmaceutical and medicinal chemistry. These materials can be easily achieved via ring opening of epoxy by a diversified class of amines, but this approach has a slow reaction rate due to the poor nucleophilic character of amine. Therefore, researchers have

introduced a variety of homogeneous and heterogeneous catalysts that can enhance the electrophilic character of epoxies. Homogeneous catalytic processes have disadvantages like the use of toxic solvents, the difficulty of separation and poor reusability of the catalyst. Heterogeneous catalysts also have some limitations like the need for longer reaction times, difficult synthesis of the catalyst and non-ambient reaction conditions [89].

In contrast to amines and thiols, azides do not react with epoxies directly. Azido groups are greatly suitable for either the click reaction or the Staudinger ligation. The Staudinger reaction which was discovered by and named after Hermann Staudinger is a chemical reaction of an azide with a phosphine or phosphite. This reaction produces an iminophosphorane which subsequent hydrolysis of it results in an amine [90].

Design and fabrication of biosensors are of great importance. One of the newest applications of these sensors is the rapid and accurate detection of protein substances like avidin or cancer biomarkers. For this, molecules which have affinity with the protein substances (bioreceptor) should be immobilized on the surface known as transducer [91]. In chapters 3 and 4, we prepared microarrays of dyes containing azide or thiol groups on the DBCO-terminated glass surfaces [92] and dyes containing maleimide or DBCO groups on the thiol-terminated glass surfaces [93] using microchannel cantilevers spotting (μ CS). In this chapter, three other different routes for the surface functionalization of the epoxy-terminated glasses will be examined. Our purpose here is to study the fundamental aspects of thiol-epoxy, amine-epoxy and azide-epoxy reactions, and to document their utilities in the creating microarrays suitable for sensing applications (Fig. 5.2).

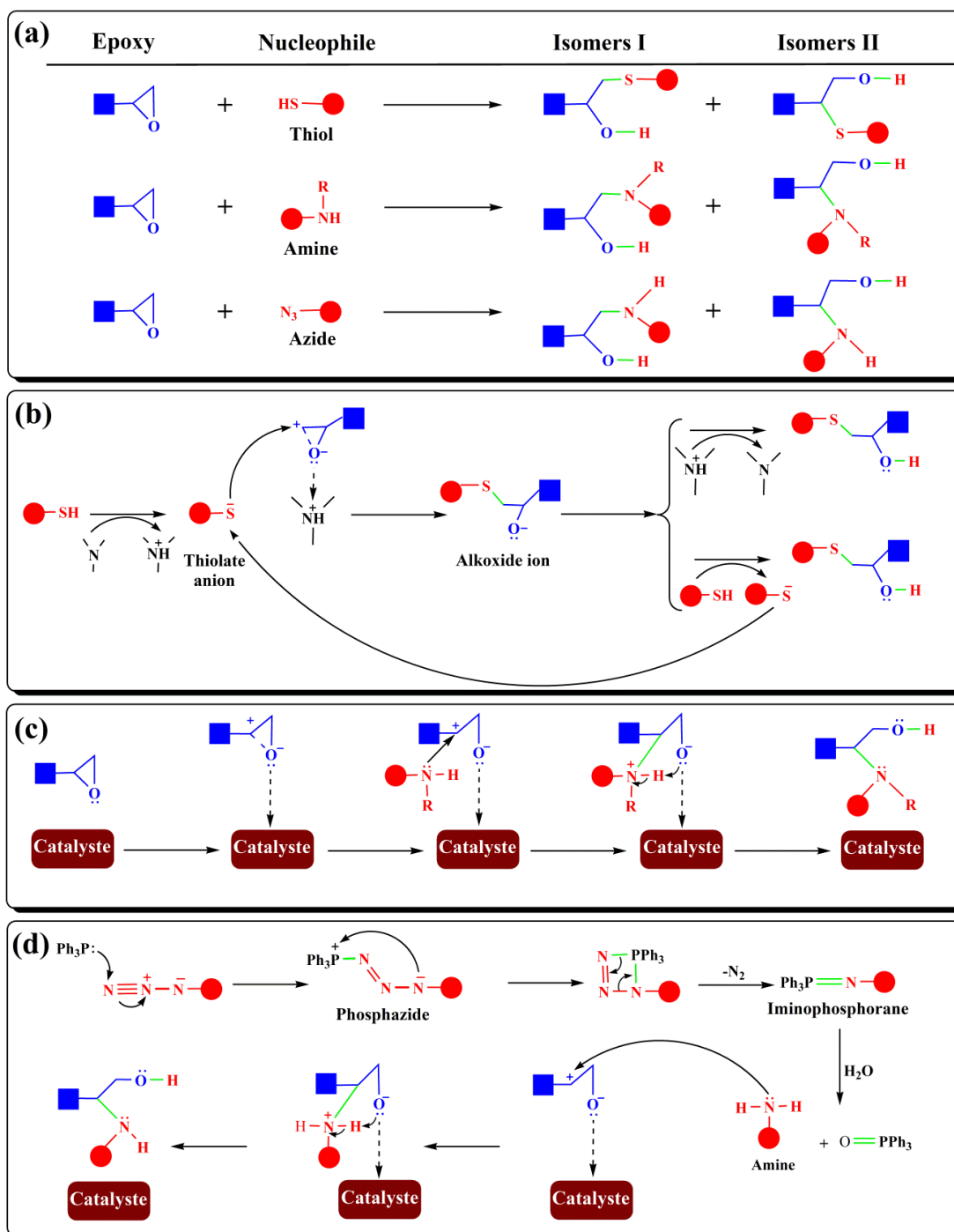


Figure 5.1. (a) Two possible regio-isomers expected from ring opening of epoxide by thiol, amine and azide; proposed literature mechanisms for (b) thiol-epoxy reaction initiated by base catalyst, (c) epoxy-amine reaction and (d) epoxy-azide reaction.

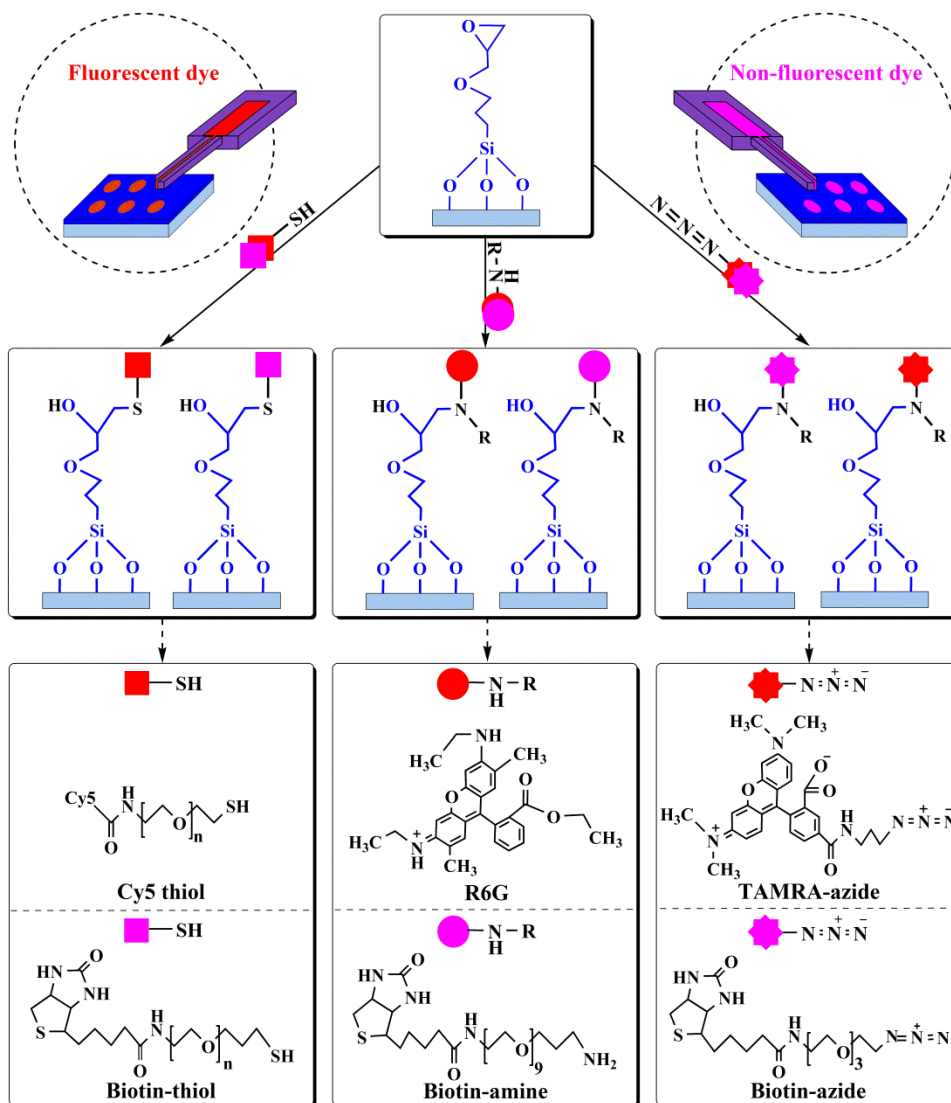


Figure 5.2. Schematic representation of the chemical strategies used for functionalization of epoxy-terminated glasses by different fluorescent and non-fluorescent dyes.

5.2. Results and discussion

5.2.1. Characterization of surfaces by contact angle and AFM

Functionalization of glass substrates with GPTMS results in surfaces terminated with epoxide groups and reactive for ring-opening reactions. But, before silanization with GPTMS, the rinsed substrates are subjected to an oxygen plasma treatment to ensure a high density of hydroxyl groups on their surfaces. As a first check of successful functionalization prior to the further experiments, contact angle measurements were done on the hydroxyl- and epoxy-terminated glasses over the course of four weeks. To have a successful spot coating and high-resolution arrays, the contact angle of water droplets on the surface

should not be too low, as otherwise the spotted inks will spread and destroy the ordered arrays (Fig. 5.3). Plasma-treated glass surface is highly hydrophilic right after activation, but its hydrophilicity declines during the course of 3 to 4 weeks and is approaching that of a non-treated glass surface again. The epoxy-terminated surface is less hydrophilic with an initial contact angle of $(54.4 \pm 1.5)^\circ$ that stabilizes at an angle around 84.3° (determined by the asymptotic approach of the fit function given in Fig. 5.3). The change in contact angle of epoxy-terminated surface over time might be induced by unmodified hydroxyl groups on the surface decaying until only the thiol groups remain. Comparing the obtained results for contact angle value of epoxy-terminated surface with those of DBCO- and thiol-terminated surfaces studied in chapters 3 and 4 expresses the hydrophilicity order as follows: DBCO-terminated surface > thiol-terminated surface > epoxy-terminated surface.

Roughness values of the hydroxyl- and epoxy-terminated glasses as well as of the epoxy-terminated glasses after coating with different fluorescent and non-fluorescent dyes were monitored by AFM, results are shown in Fig. 5.4. The hydroxyl-terminated glass features a roughness of (0.25 ± 0.02) nm. While the silanization leads to significantly higher roughness ((0.59 ± 0.16) nm). This difference in roughness can be due to the probability of crosslinking between silanes, leading to a less even surface. Functionalization with Cy5 thiol, TAMRA-azide, biotin-thiol, biotin-amine and biotin-azide only slightly increases roughness to (0.62 ± 0.06) nm, (0.60 ± 0.17) nm, (0.64 ± 0.12) nm, (0.64 ± 0.12) nm and (0.73 ± 0.10) nm, respectively. Immobilization of R6G on the epoxy-terminated glass leads to significantly higher roughness ((1.35 ± 0.12) nm). This roughness increase is probably caused by the possibility of crosslinking between secondary amine groups in R6G.

5.2.2. Array immobilization of Cy5 thiol, R6G and TAMRA-azide

To establish different reactions for μ CS and to find optimal reaction parameters, microarrays of fluorescent-labeled dyes including Cy5 thiol, R6G and TAMRA-azide were prepared on the epoxy-terminated glass surfaces using μ CS. After the spotting, ring-opening reactions were allowed to continue for different time durations (10, 20 and 40 min). Reaction between epoxy and Cy5 thiol was examined at temperatures of 25 and 37 °C in the presence of TEA catalyst. Reaction between epoxy and R6G was performed with four different catalysts, at 37 °C and for two different amounts of catalyst (1 and 3 mol%). Bi(OTf)₃, LiCl, Cl₂O₈Zn and ZnO were used as catalysts for the reaction between epoxy and amine. Immobilization of TAMRA-azide on the epoxy-terminated surface was done through different way. First, TAMRA-azide was converted into an amine via Staudinger reaction and in the presence of 3 mol% Ph₃P to azide. Then, the prepared amine ink was mixed with different amounts of Bi(OTf)₃ and was spotted on the epoxy-terminated surface. After the reaction time elapsed, the surfaces of microarrays were rinsed with deionized water, were dried by blowing with nitrogen and were evaluated by fluorescence

microscopy. A summary of results and micrographs of typical lithography outcomes are given in Fig. 5.5. Apparently, all ring-opening reactions were able to take place and immobilize the respective fluorophore, as after washing, the patterns remained stable and highly visible. For epoxy-thiol reaction (Fig. 5.5a), a trend for increased intensity with elevation of temperature and time is visible. However, it was observed no significant rise in fluorescence intensity after 40 min. Therefore, reaction time of 40 min and reaction temperature of 37 °C were the best for this reaction. Epoxy-amine reaction was studied at 37 °C and for two different amounts of catalyst (Fig. 5.5b-e). Consequently, by simultaneous consideration of reaction time and catalyst type and amount, 40 min/3 mol% Bi(OTf)₃, 40 min/1 mol% LiCl, 20 min/3 mol% Cl₂O₈Zn and 40 min/1 mol% ZnO nanopowder were chosen as the optimal conditions for this reaction in further experiments. Among different catalysts, Bi(OTf)₃ showed better results than others in providing clear microarrays with high fluorescent intensity. For reaction between epoxy and azide which is basically an epoxy-amine reaction, reaction time of 20 min and 3 mol% Bi(OTf)₃ were chosen as the optimal conditions (Fig. 5.5f). Fig. 5.5g-l shows the fluorescence microscope images of micropatterns obtained at optimum reaction conditions.

Although the reaction between epoxy and thiol can take place at elevated temperatures without the need for any catalyst, lower temperatures can be achieved by using catalysts. Base catalysts such as triethylamine (TEA), diazabicyclo[4.3.0]non-5-ene (DBN), 1,8-diazabicyclo[5.4.0]undec-7-ene (DBU), benzyldimethylamine (BDMA) and 1-methylimidazole (1MI), and LiOH are frequently used to catalyze thiol-epoxy reactions. As shown in Fig. 5.1b, the mostly accepted mechanism for the base-catalyzed thiol-epoxy reaction is a simple nucleophilic ring-opening coupling. First, the initial thiolate anions are formed via deprotonation of the thiols by the base catalyst. Then, the thiolate anions undergo a nucleophilic ring-opening reaction with the epoxide groups to form alkoxide ions. Lastly, the protonation of the alkoxide ions via either deprotonation of the base catalyst or the thiol results in thiol-epoxy reaction product. Other catalysts like photobase generators and Lewis acids which weaken the carbon oxygen bond in epoxide and stabilize the alkoxide ions upon direct attack by the nucleophilic thiol, have also exhibited effectiveness in catalyzing this reaction. If the thiol-epoxy reaction is considered under basic conditions isomer I is expected to form. In acidic conditions, the nucleophilic attack results in the predominant formation of regio-isomer II ^[84d, 85, 94].

Normally, the reaction between epoxy and amine is performed in the presence of catalysts, although there are some studies ^[5a, 95] for ring-opening of the epoxide groups without catalyst. Ionic liquids, tetrafluoroborates of metals (metal: Li, Zn, Co, Cu, Fe and Ag), trifluoroacetate of metals (metal: Fe and Ca), perchlorates of metals (metal: Li, Ni, Mg, Co, Zn and Fe), halides of metals (LiBr, LiCl, AlCl₃, MnCl₂, CoCl₂, BiCl₃, ZnCl₂ and ZnI₂), tungsten salts (WO₂Cl₂, WO₂(acac)₂ and W(OEt₆)), metal oxides

in the form of nanoparticles (TiO₂, ZrO₂, Al₂O₃, Fe₂O₃, SiO₂, ZnO and CuO), triflates of metals ((Bi(OTf)₃, (Zr(OTf)₃ and Cu(OTf)₂), activated heterogeneous mesoporous carbons, sulfated metals (metal: Zr and W), metal amides or triflamides and biocatalyst are examples of catalysts which have been successfully employed in aminolysis of various types of epoxies [89a-c, 96].

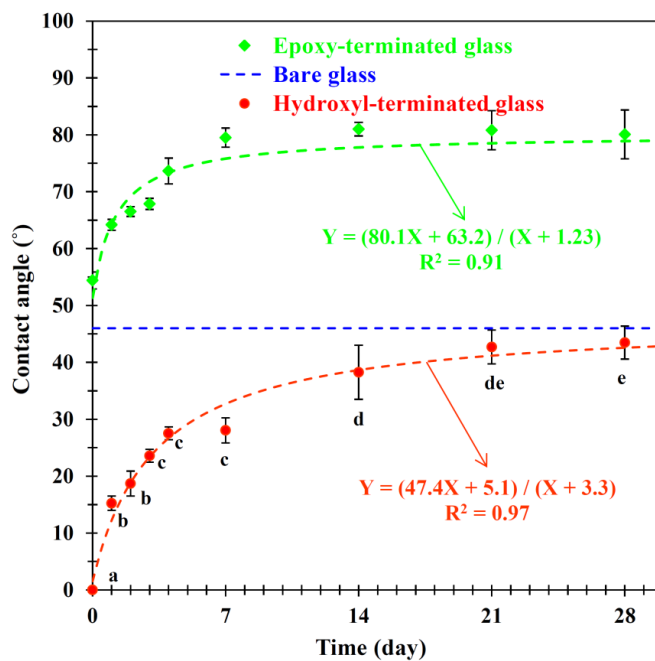


Figure 5.3. Water contact angles over time on hydroxyl- and epoxy-terminated glasses. Graphs of contact angle over time were fitted by rational functions utilizing MATLAB software to give a better guide to the eye. The red and green dashed curves are the best fit for OH-terminated (taken as comparison from [92]) and epoxy-terminated glasses, respectively. The blue horizontal dashed line represents the contact angle of the bare glass at about 46°. Significant changes in contact angle ($p < 0.05$) are marked by different letters.

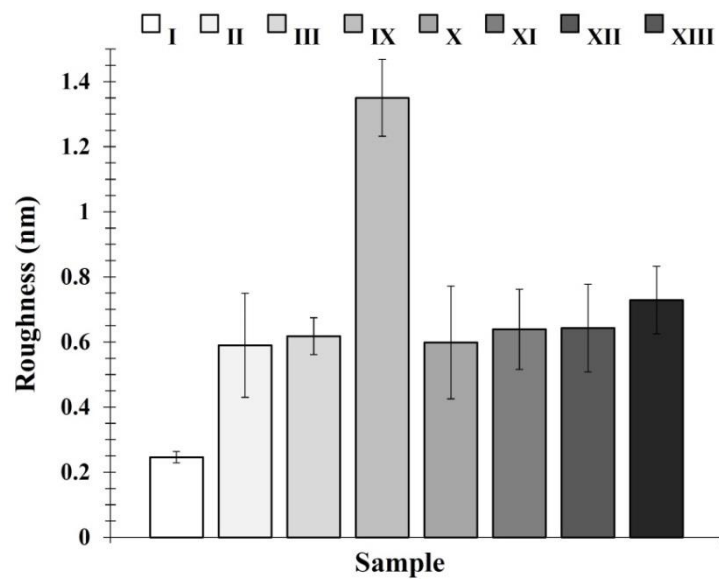


Figure 5.4. Roughness values determined by AFM test for the hydroxyl-terminated (I) and epoxy-terminated (II) glasses as well as for the epoxy-terminated glasses after coating with Cy5 thiol (III), TAMRA-azide (IX), R6G (X), biotin-thiol (XI), biotin-amine (XII) and biotin-azide (XIII).

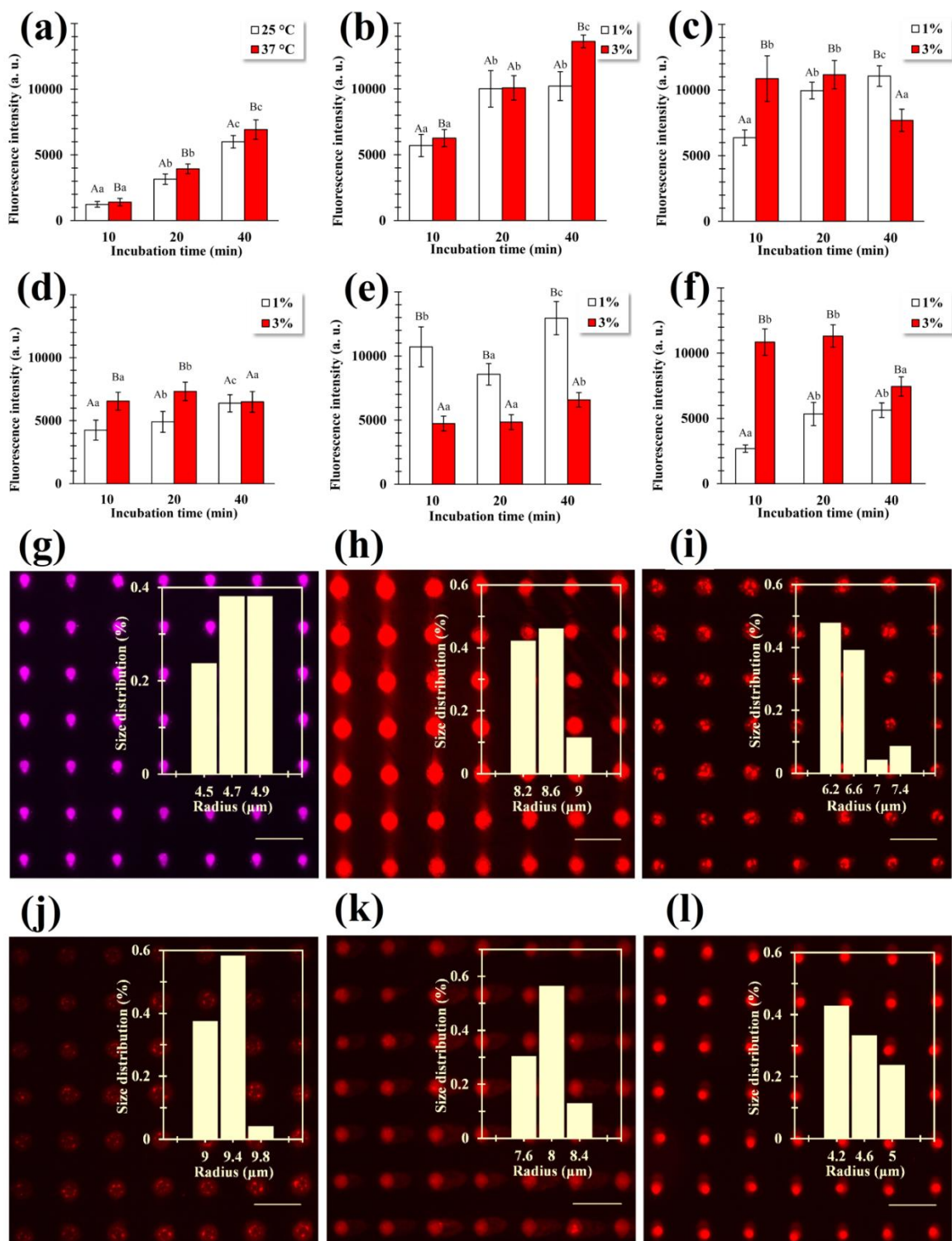


Figure 5.5. Arrays of fluorescently labeled dyes including Cy5 thiol, R6G and TAMRA-azide. For all microarrays spotting humidity was 20% and dwell time of 0.1 s was used. Also, the exposure time of images was 20 s, the insets show the size distribution of the spots and scale bars equal 50 μm.

5.2.3. Protein coupling by biotin-thiol, biotin-amine and biotin-azide

In the previous section, we demonstrated successful immobilization of fluorescent Cy5 thiol, R6G and TAMRA-azide arrays on epoxy-terminated glass through ring-opening reaction. Furthermore, considering the fluorescence intensity values of these microarrays, the optimum reaction conditions were identified. As, different fluorophores used for surface coupling have different functional groups, different emission spectra and different intensities even for the same surface concentration of immobilized molecules, another strategy should be employed for the direct comparison of these reactions. For this, via epoxide ring-opening routes, biotin-bearing compounds including biotin-thiol, biotin-amine and biotin-azide were spotted on the epoxy-terminated glasses by μ CS into 15×15 spot arrays. So, for visualizing the immobilized biotin patterns as well as determination of the amount of immobilized biotin, a fluorescent-labeled streptavidin can be used. Utilizing this technique along with using the same concentrations of a fluorescent-labeled streptavidin can provide a comparison between different coupling routes. Results for arrays spotted at optimal reaction conditions with the same mole concentrations of biotinylated inks ($2 \mu\text{mol}\cdot\text{ml}^{-1}$) and fluorescent-labeled streptavidin ($10 \mu\text{g}\cdot\text{ml}^{-1}$) are summarized in Fig. 5.6. As seen, immobilization of the biotinylated compounds for all chemical routes was successful, as following incubating the patterns with fluorescent-labeled streptavidin, they all showed up under the fluorescence microscope. When comparing the fluorescence intensity values of streptavidin bonded on the microarray prepared by these immobilization routes ((5257 ± 486) a.u. for the biotin-thiol spots, (13793 ± 407) a.u. for the biotin-amine spots and (6490 ± 742) a.u. for the biotin-azide spots), it becomes obvious that ring opening of epoxy with amine is yielding a higher fluorescence intensity.

In chapters 3 and 4, we studied and compared other immobilizing routes including strain-promoted azide-alkyne cycloaddition (SPAAC), thiol-yne coupling (TYC) and thiol-ene Michael addition (TEMA) for the generation of covalently bound microarrays on the functionalized glass surfaces where the protein binding experiments revealed that the surface density of molecular immobilization on the glass surface was in order: TEMA > TYC > SPAAC. Comparing the intensity of micropattern obtained for biotin-maleimide spots immobilized on the thiol-terminated glass via TEMA after binding with fluorescent-labeled streptavidin ((3953 ± 210) a.u.) with the results obtained in this chapter indicates a more efficient biotin immobilization by the ring opening of epoxy by thiol, amine and azide.

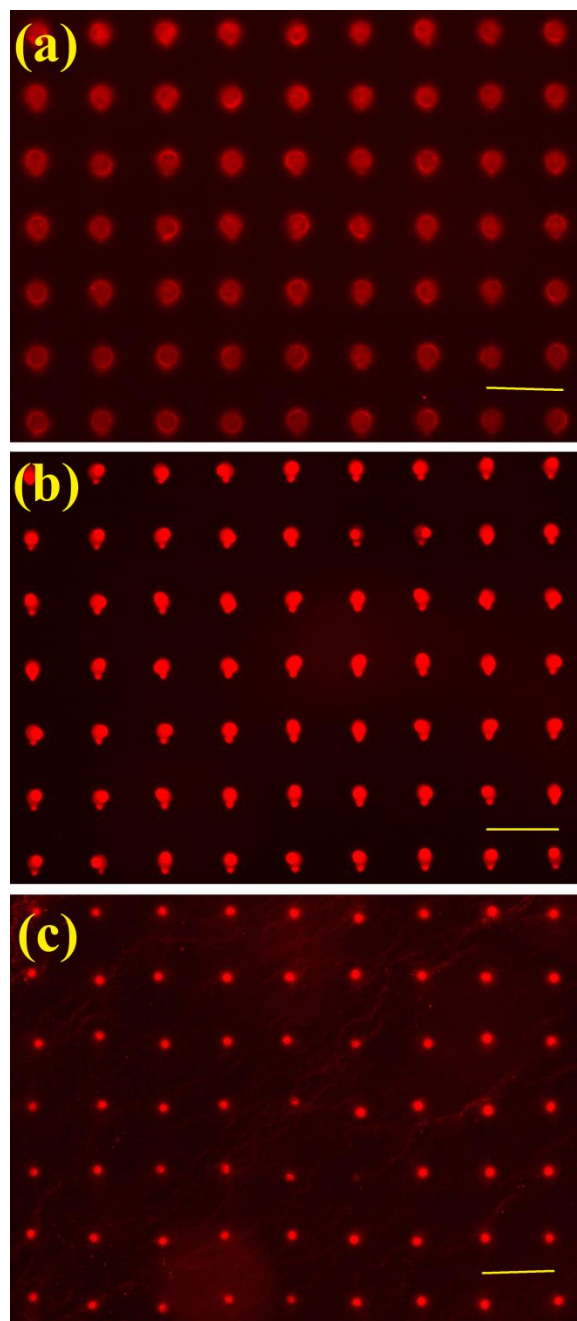


Figure 5.6. Arrays of biotin-thiol, biotin-amine and biotin-azide on epoxy-terminated glass after incubating with fluorescent-labeled streptavidin. For all microarrays spotting humidity was 20% and dwell time of 0.1 s was used. Also, the exposure time of images was 20 s and scale bars equal 50 μm .

5.3. Summary

Microarrays of different fluorescent and non-fluorescent dyes were created on the epoxy-terminated glass surfaces via μ CS. For this, different molecules containing thiol, amine and azide groups were used for immobilization of dyes and subsequently doing ring-opening reaction on the surface of epoxy-terminated glass. Ring opening by fluorescent Cy5 thiol was performed at different temperatures (25 and 37 °C) and times (10, 20 and 40 min) and the optimum condition of 37 °C/40 min was found for this type of ring opening. R6G was the second fluorescent molecule used as an amine for ring opening of epoxy. As the choice and amount of a catalyst have important effect on the outcome of the amine-epoxy reaction, the effect of four different catalysts ($\text{Bi}(\text{OTf})_3$, LiCl , $\text{Cl}_2\text{O}_8\text{Zn}$, and ZnO nanoparticles) in two different amounts (1 and 3 mol% to dye), at 37 °C was investigated. Screening of different reaction conditions concluded that 3 mol% $\text{Bi}(\text{OTf})_3$ afforded the maximum yield of product. TAMRA-azide was the third fluorescent molecule used for ring-opening purpose. First, TAMRA-azide turned into an amine via Staudinger reaction in the presence of 3 mol% Ph_3P . In the following, amine solution was mixed with different amounts of $\text{Bi}(\text{OTf})_3$ for spotting. For this reaction, reaction time of 10 min and 1 mol% $\text{Bi}(\text{OTf})_3$ were chosen as the optimal conditions for further experiments. Comparing between different intensities obtained by streptavidin coupling to a biotin compounds fixed on the surface of functionalized glass showed the highest amount of intensity value for biotin-amine spots incubated with streptavidin. So, the results of this study recommend the use of an epoxy-amine route to obtain the highest surface density of molecular immobilization.

Chapter 6

Fluorescent immunosensors for detection of alpha-fetoprotein (AFP)

6.1. Introduction

According to the five-phase program adopted by the Early Detection Research Network (EDRN) of the National Cancer Institute (NCI), most hepatocellular carcinoma (HCC) biomarkers have been evaluated in phase II and III studies and further investigations are needed to determine if they have utility for clinical purposes. Alpha-fetoprotein (AFP) is the only HCC biomarker that has been studied through all 5 phases of biomarker development. This biomarker has been the most commonly used one as an early screening and diagnosis tool of HCC [9b, 9c]. The average level of serum AFP in the healthy person is less than 20 ng.ml^{-1} , but high levels, sometimes exceeding $100 \text{ }\mu\text{g.ml}^{-1}$, can be found in the serum of patients suffering from HCC [97].

In this chapter, different approaches in binding chemistry for the construction of sensitive fluorescent immunosensors for AFP detection by combining the unique characteristics of click chemistry with the high sensitivity of biotin-streptavidin-biotin sandwich-type strategy as well as the high selectivity of antigen-antibody interaction are compared. Six different routes based on DBCO-, thiol- and epoxy-functionalization of glasses and click-chemistry attachment of biotinylated molecules (Fig. 6.1) were used to obtain biotinylated surfaces for construction of the AFP detection sandwich as compared for their efficiency as sensor platforms. Click chemistry reactions, which have been widely studied since their introduction by Kolb, Finn, and Sharpless in 2001 [4], own unique advantages such as high reaction rate, high yield, mild reaction conditions and easy post-treatment [3b, 5c, 92-93, 98]. Afterward, the biotinylated glasses which from now on, throughout the article referred as routes 1-6, were respectively incubated with solutions of streptavidin and biotinylated anti-AFP to obtain a biotin-streptavidin-biotin sandwich structure. Biotin-streptavidin-biotin strategy is used in immunosensors fabrication because of improvement in the sensitivity [99]. Lastly, in the respective experiments, micropatterns were fabricated using microchannel cantilever spotting (μCS) via writing with fluorescent-labeled AFP (as antigen) on the surfaces modified with anti-AFP (as antibody) (Fig. 6.2). In different studies, many selective biosensors have been developed based on antigen-antibody interaction [97, 99a, 99b, 100]. The technique used in this work can provide a new platform for fabrication of clinical immunosensor which is applicable in fast and effective diagnosis of HCC.

6.2. Results and discussion

6.2.1. Generation of biotinylated surfaces

To generate biotinylated surfaces as basis for the sensor antibody sandwich, overall six different routes were trialed (Fig. 6.1). First, the glass substrates were plasma treated for generating reactive hydroxyl groups on their surface and then functionalized with either acid (for obtaining DBCO-terminated surfaces) or silanes (for obtaining thiol- and epoxy-terminated surfaces). After base functionalization, biotin is immobilized on the DBCO-, thiol-, or epoxy-functionalized by incubation with the respective click-chemistry partner molecules, to obtain six different biotinylation routes: for DBCO-terminated glass, biotin-thiol (route 1) and biotin-azide (route 2) were used, for thiol-terminated glass biotin-maleimide (route 3) and biotin-DBCO (route 4), and for epoxy-terminated glass biotin-amine (route 5) and biotin-thiol (route 6), respectively. After the six different surfaces were obtained, they were characterized for successful implementation and comparison.

6.2.2. Characterization of surfaces by AFM

After each step of the functionalization experiments, samples roughness was monitored by atomic force microscopy (AFM), results are shown in Fig. 6.3. The bare glass features a roughness of (0.20 ± 0.01) nm. While DBCO functionalization by acid only slightly increases roughness to (0.22 ± 0.01) nm, the silanization for thiol- and epoxy-terminated leads to significantly higher roughness ((0.49 ± 0.04) nm and (0.60 ± 0.06) nm, respectively). This difference in roughness is probably caused by the possibility of crosslinking between silanes, leading to a less even surface. The next step in the different routes, the immobilization of biotin via a matching click-reaction, does increase roughness only slightly or even not significantly at all: on the DBCO-functionalized surfaces, adding of biotin-thiol (route 1) leads to a slightly increased roughness of (0.27 ± 0.04) nm, biotin-azide (route 2) yields (0.27 ± 0.02) nm. On the thiol-terminated glass, no significant further increase of roughness is observed for biotin-maleimide (route 3) with (0.50 ± 0.03) nm and biotin-DBCO (route 4) with (0.51 ± 0.02) nm. The epoxy-terminated glass shows slightly increase in roughness for biotin-amine (route 5) with (0.72 ± 0.09) nm and biotin-thiol (route 6) with (0.68 ± 0.10) nm.

6.2.3. Characterization of surfaces by XPS

All steps of the immobilization reactions were also characterized by XPS to validate the expected chemical reactions taking place (Fig. 6.4). The functionalization of glass with DBCO-OH is proven by the appearance of a peak at 400.4 eV attributed to the N-C=O groups present in DBCO (Fig. 6.4a). For route 2, the nitrogen concentration increases clearly after reaction with the biotin-azide (Fig. 6.4c) whereas for route 1, the attachment of the biotin-thiol is shown here by the presence of the S 2p doublet with S_{2p3/2} at 163.3 eV (Fig. 6.4b). The thiol-terminated glass presents on the same way a clear sulfur signal attributed to the thiol and a weak component at 168.0 eV due probably to the oxidation from some sulfur atoms (Fig. 6.4d). The further steps (route 3 and 4) can be followed with the increase of the nitrogen content at the surface (Fig. 6.4e and Fig. 6.4f). The C 1s peak (Fig. 6.4g) proves without doubt the functionalization with GPTMS especially with the pronounced increase of the intensity of the component at 286.6 eV attributed to C-O moiety. The following clear presence of nitrogen in the spectra (Fig. 6.4h) and (Fig. 6.4i) of the routes 5 and 6 also underlines the successful reactions.

6.2.4. Comparison of immobilization routes for sandwich application

After the different types of biotinylated surfaces were obtained, their performance for the sensing application was trialed by addition of a streptavidin/biotin sandwich structure for antibody immobilization (Fig. 6.2). For this, the surfaces were first incubated with streptavidin and subsequently with a biotinylated anti-AFP antibody, leading to a surface homogeneously covered by the antigen binding antibody. To evaluate the amount of antigen that surfaces established by the different routes can bind, fluorescently labeled AFP was then spotted onto the surfaces via microchannel cantilever spotting (μ CS). The microarrays were left for different incubation times (10 to 60 minutes) and at different temperatures (room temperature of 25 °C and elevated physiological temperature of 37 °C), then samples were washed and the fluorescence signal from the spot array was quantified (Fig. 6.5). As a general trend, it can be observed that at an elevated temperature of 37 °C for the same incubation time higher fluorescence intensity is obtained from the microarray. For room temperature incubation, the observed intensity increases with incubation time for all routes within the monitored time frame of 10 to 60 minutes. However, in case of incubation at elevated temperatures, some routes exhibit the same behavior (routes 2, 4, and 6) while the others (routes 1, 3, 5) peak after some time and then fluorescence intensity decreases again. This behavior is probably caused by drying

effect that gets more pronounced, as at elevated temperatures solvent evaporation is raised. When material is dried out and thus only physisorbs onto the surface, it is more easily removed in the subsequent washing step before observation of the fluorescence. Based on the results from the fluorescence measurements, incubation at 37 °C for 20 minutes with samples of either route 3 or 5 was determined to offer optimal performance.

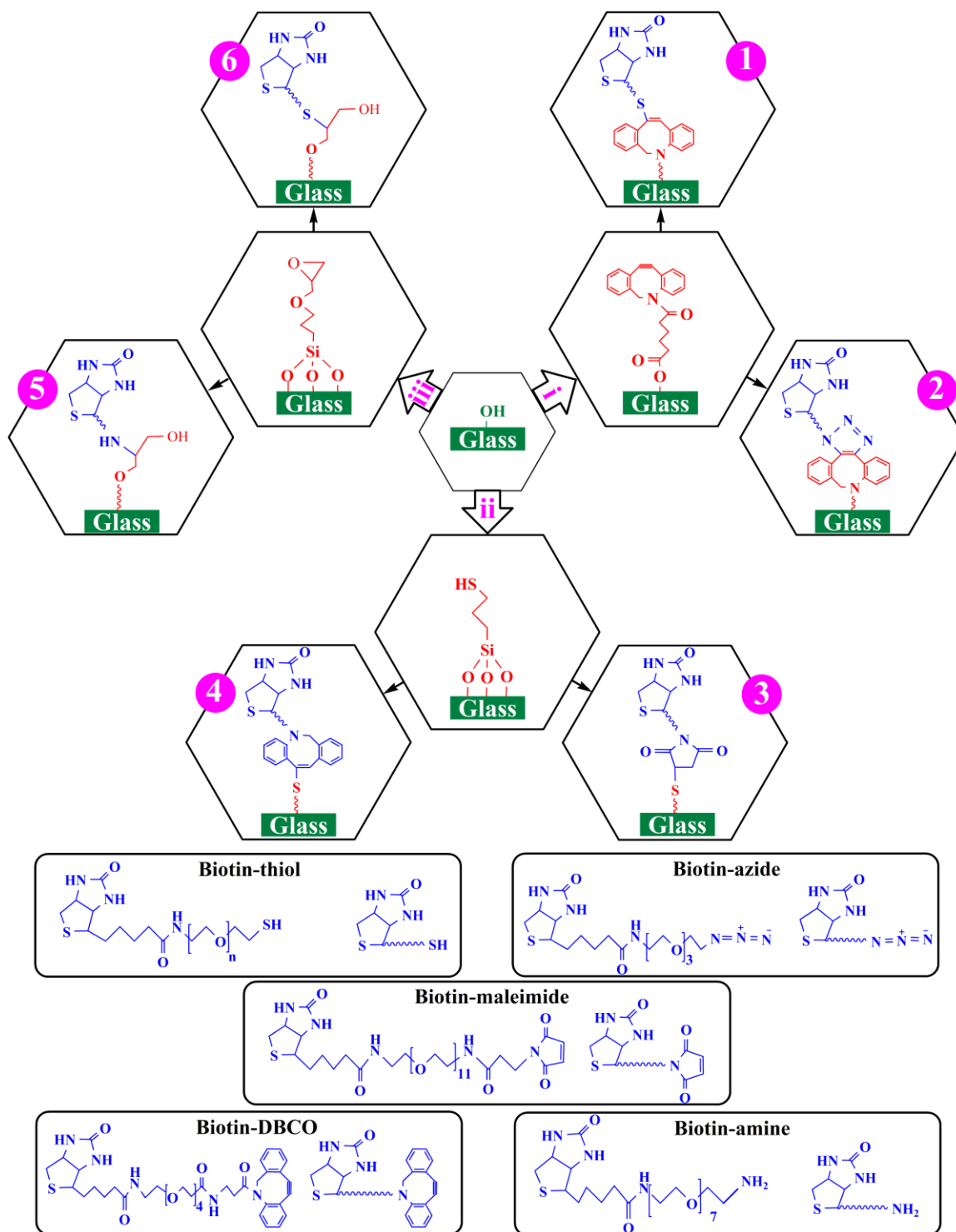


Figure 6.1. Biotin immobilization on the hydroxyl-terminated glasses via different click reactions. Hydroxyl-terminated glasses were first functionalized with DBCO-OH (path i), MPTMS (path ii), or GPTMS (path iii), subsequently biotinylated through different click reactions (routes 1-6)

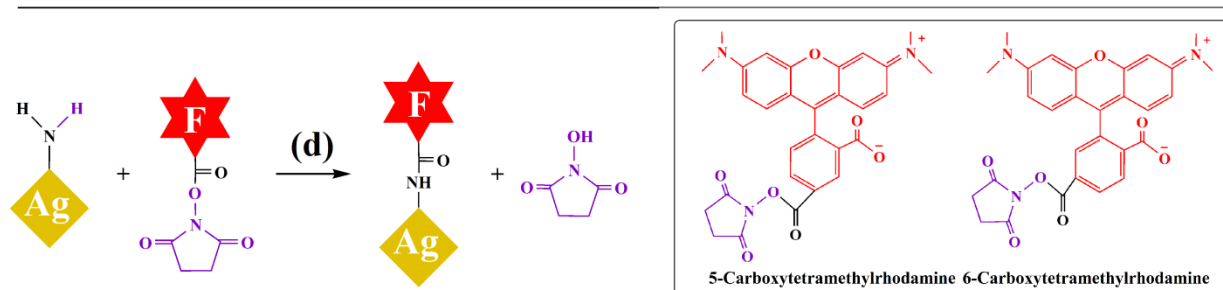
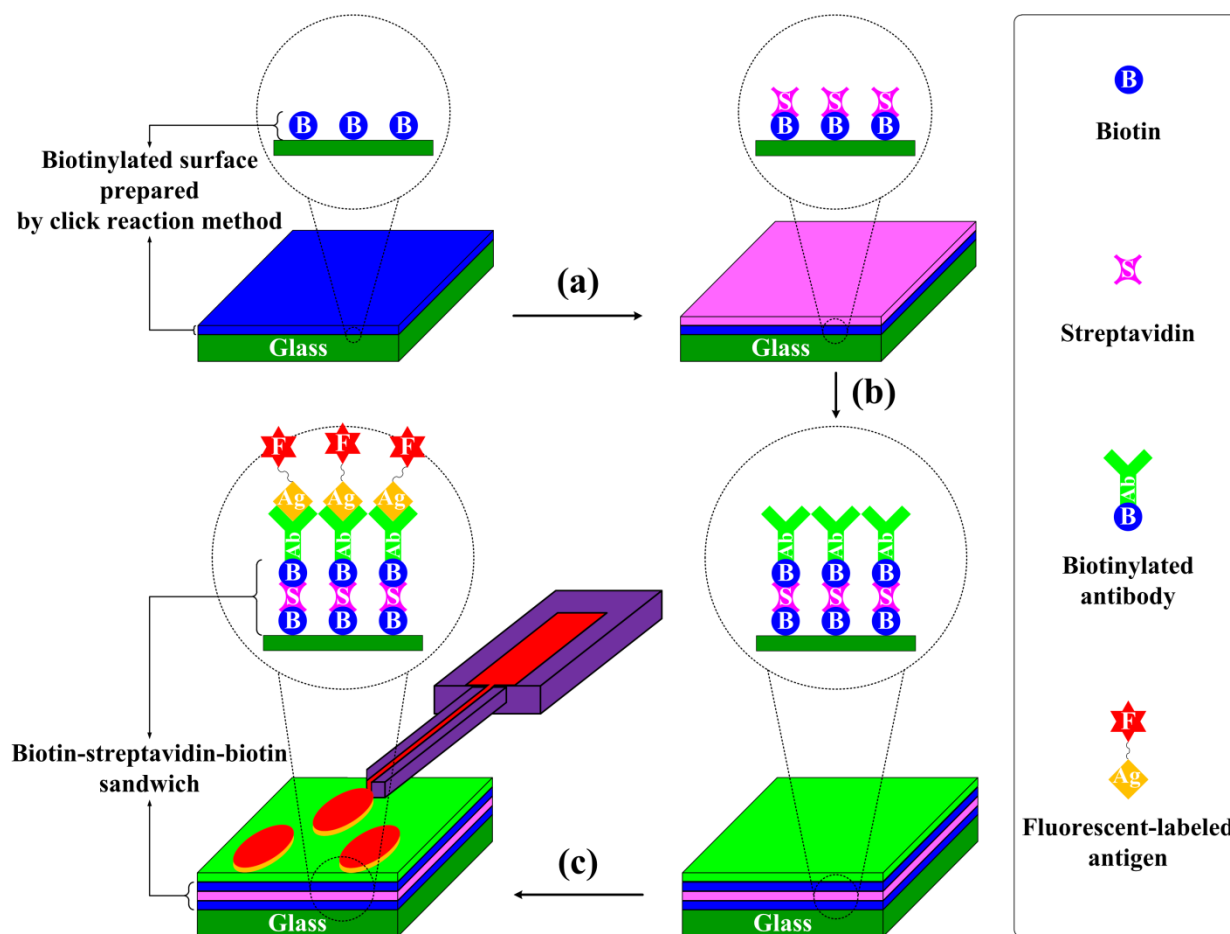


Figure 6.2. Schematic of microarrays prepared for AFP detection. (a) Incubating biotinylated surfaces with streptavidin solution, (b) reaction of the streptavidin on the surface with biotinylated anti-AFP (c) delivery of fluorescently labeled AFP via μ CS and (d) preparation of fluorescently labeled AFP through reaction between NHS-ester reagent (NHS-rhodamine) and primary amine of antigen (AFP).

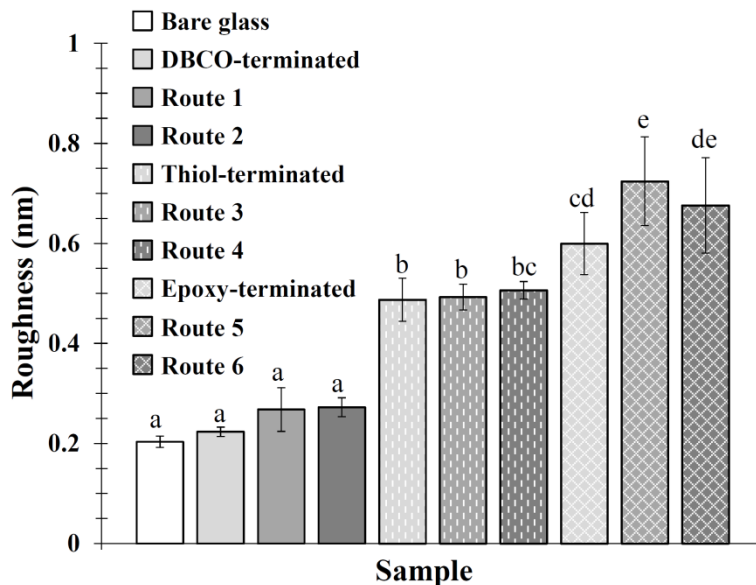


Figure 6.3. Roughness values determined by AFM test for the bare glass and hydroxyl-, DBCO-, thiol- and epoxy-terminated glasses as well as for samples of routes 1-6. Values with the same letters do not differ significantly ($p < 0.05$), based on Duncan's test.

6.2.5. Evaluation of sensitivity

To further elucidate the capability of the approach for sensing applications, a sensitivity curve for the optimal incubation process (route 5, 37 °C, 20 minutes) was obtained. Here, the optimal microarray was incubated with different concentrations of fluorescent-labeled AFP (ranging from 12.5 to 800 $\mu\text{g}\cdot\text{ml}^{-1}$), resulting fluorescence intensity curve and representative images are presented in Fig. 6.6. When extrapolating the low-concentration part in the linear regime of the curve ($y = 40.77x + 345.22$) and taking into account the fluorescence background in the different experiments (745.58 ± 118.32 in a.u.), a limit of detection of $(9.8 \pm 2.9) \mu\text{g}\cdot\text{ml}^{-1}$ is obtained for the given conditions of our setup. Finally, it should be noted that also unlabeled AFP could be detected in this approach. For demonstration, unlabeled AFP was spotted by μCS and stained via the same type of biotinylated antibody as immobilized on the surface, thus exhibiting biotin-binding sites at the sites where AFP was present that could be stained by fluorescently labeled streptavidin (Fig. 6.7). After implementation of the additional incubation steps, a fluorescent microarray pattern becomes visible again (Fig. 6.8).

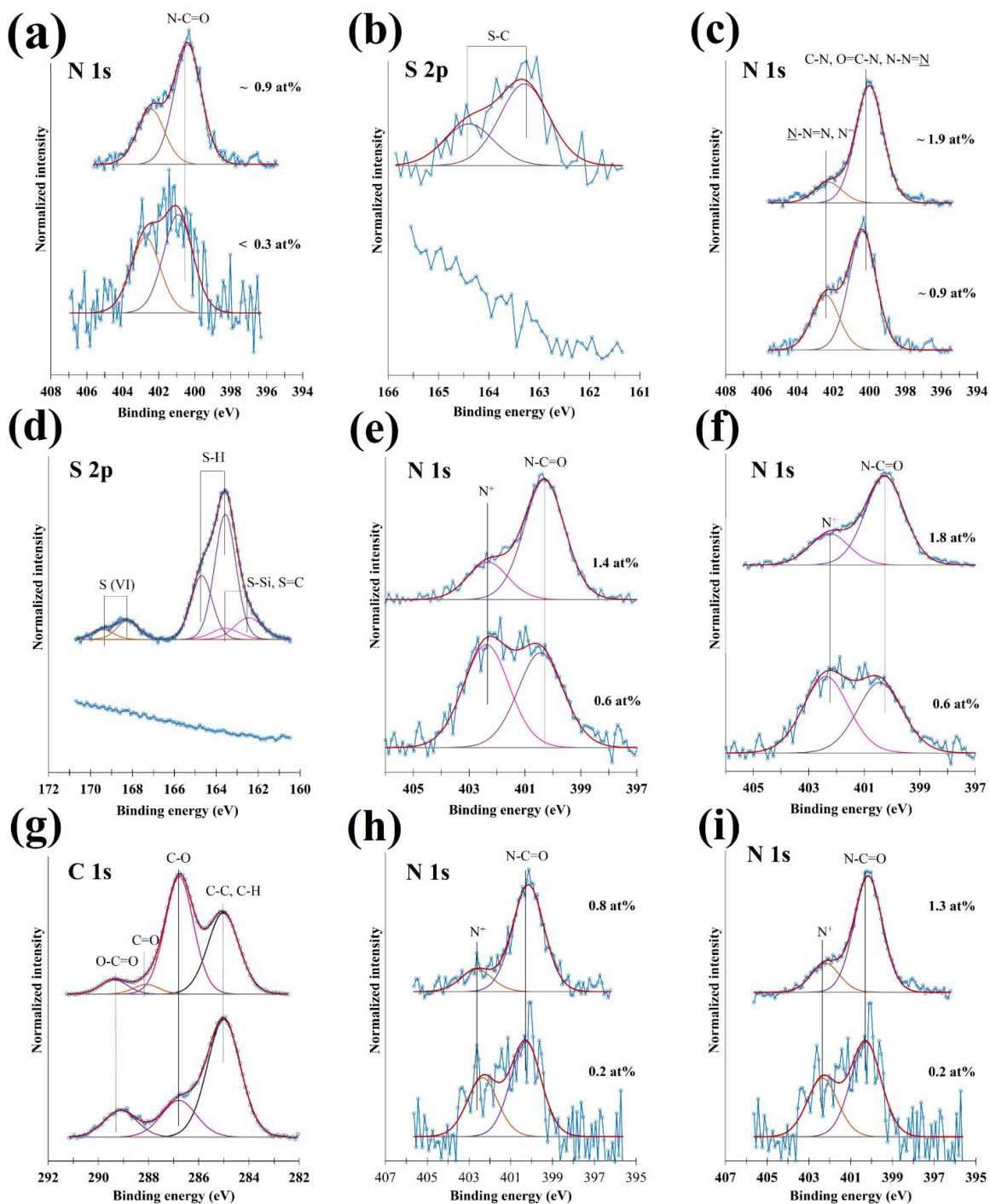


Figure 6.4. XPS characterization of (a) hydroxyl-terminated (bottom) and DBCO-terminated (top) glasses; (b) DBCO-terminated glass (bottom) and sample of route 1 (top); (c) DBCO-terminated glass (bottom) and sample of route 2 (top); (d) hydroxyl-terminated (bottom) and thiol-terminated (top) glasses; (e) thiol-terminated glass (bottom) and sample of route 3 (top); (f) thiol-terminated glass (bottom) and sample of route 4 (top); (g) hydroxyl-terminated (bottom) and epoxy-terminated (top) glasses; (h) epoxy-terminated glass (bottom) and sample of route 5 (top) and (i) epoxy-terminated glass (bottom) and sample of route 6 (top).

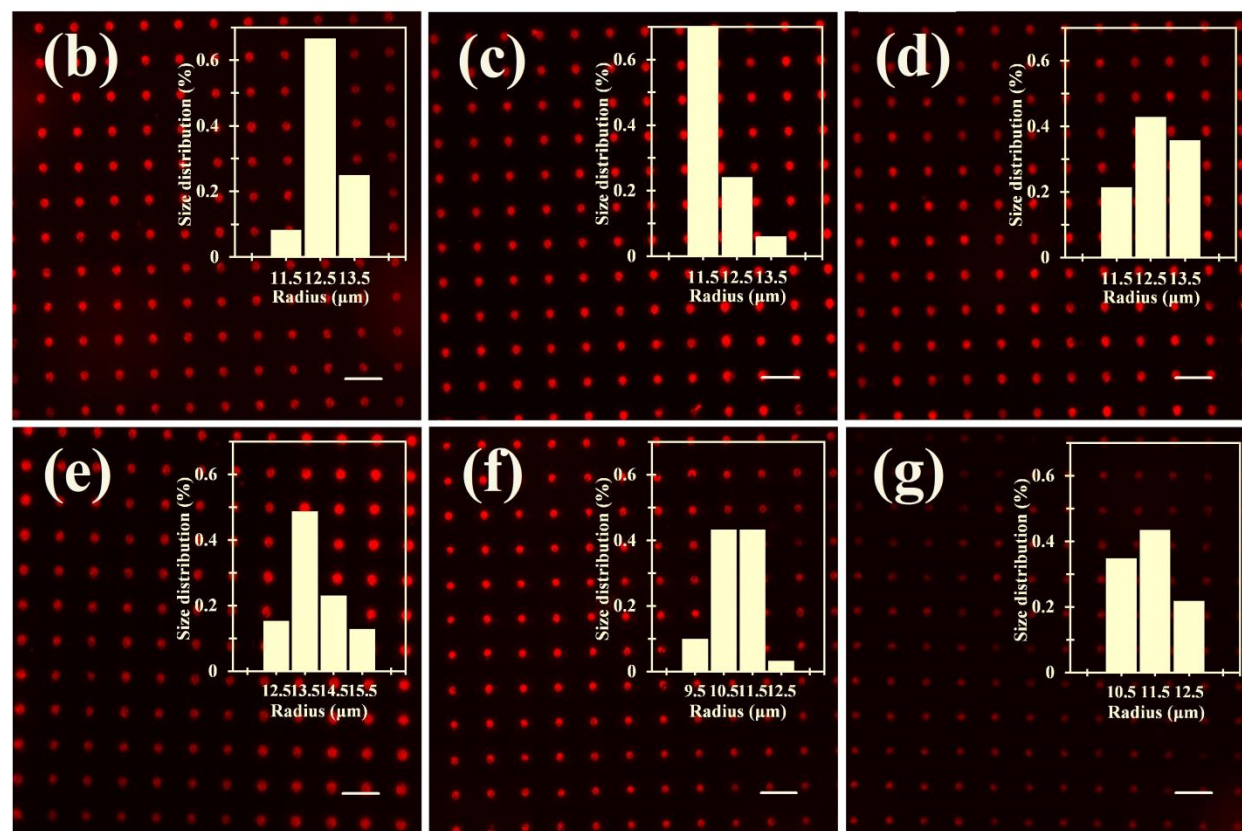
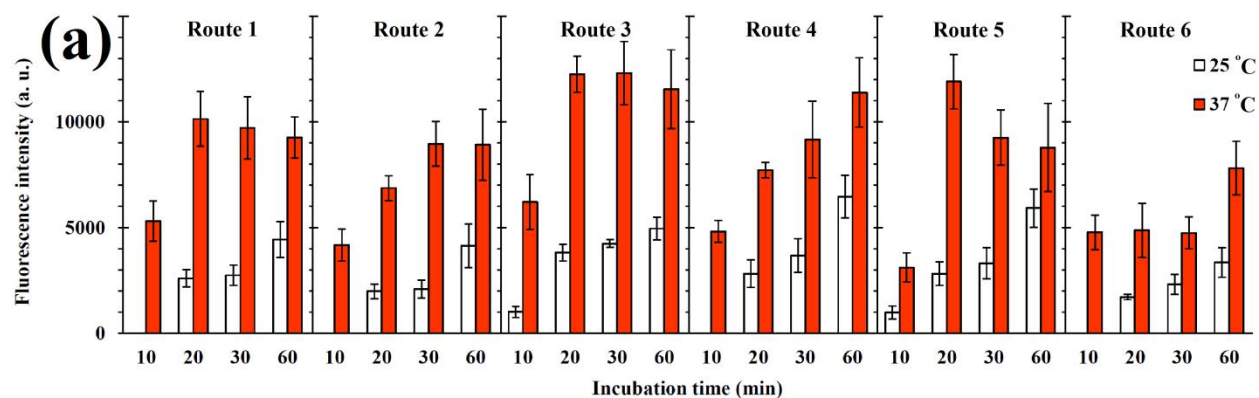


Figure 6.5. Detection of AFP antigen. (a) Fluorescence intensity of microarrays after incubating fluorescent-labeled AFP spots with anti-AFP on the surfaces at different times (10, 20, 30 and 60 min) and two temperatures (25 and 37 °C). Anti-AFP was immobilized via biotin-streptavidin-biotin sandwich technique on the different biotinylated surfaces (samples of routes 1-6) previously prepared via different click reaction methods. (b-g) fluorescence microscope images of micropatterns obtained at optimum incubation time and temperature. All microarrays were spotted at 20% relative humidity. Ink concentration was $800 \mu\text{g}\cdot\text{ml}^{-1}$. Dwell and exposure times of all images were 0.1 and 0.4 s, respectively. Spot size distribution is given in the insets. All scale bars equal 100 μm .

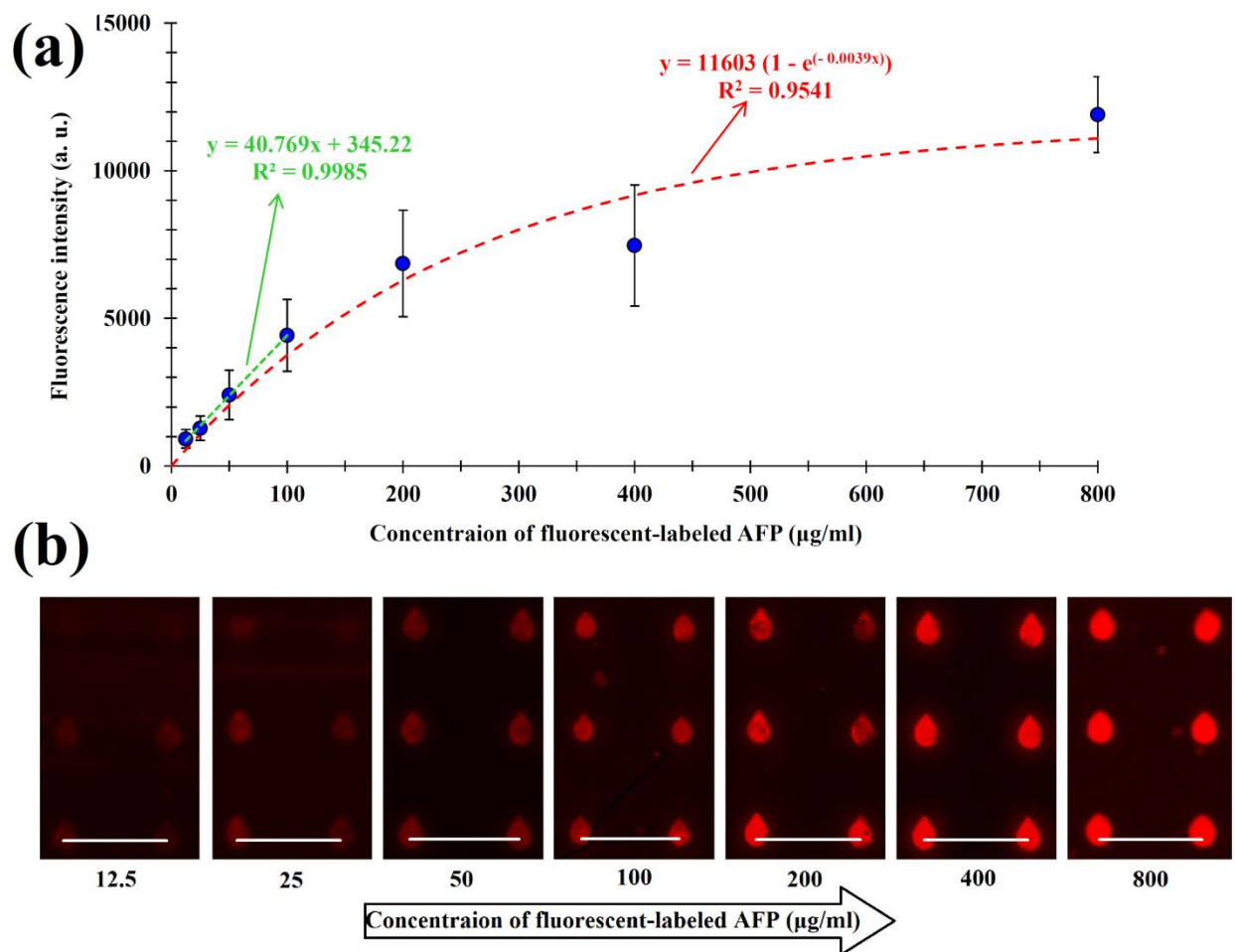


Figure 6.6. Evaluation of sensitivity of microarrays prepared from sample of route 5 after incubating anti-AFP spots with fluorescent-labeled AFP. (a) Fluorescence intensity of microarrays at different concentrations of fluorescent-labeled AFP (12.5, 25, 50, 100, 200, 400 and 800 $\mu\text{g}\cdot\text{ml}^{-1}$) and (b) fluorescence microscope images of micropatterns. All microarrays were spotted at 20% relative humidity. Dwell and exposure times of all images were 0.1 and 0.4 s, respectively. Incubation conditions were 37 °C and 20 min.

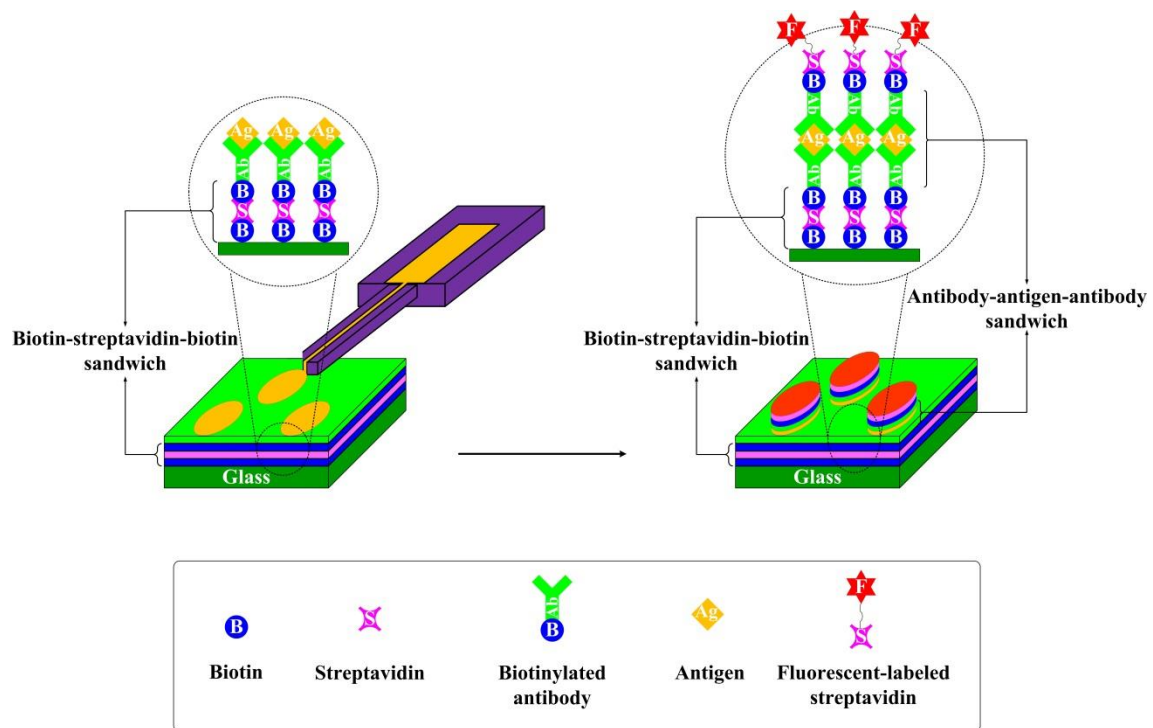


Figure 6.7. Detection of unlabeled AFP by additional sandwich approach via a second binding of biotinylated antibody and fluorescent-labeled streptavidin

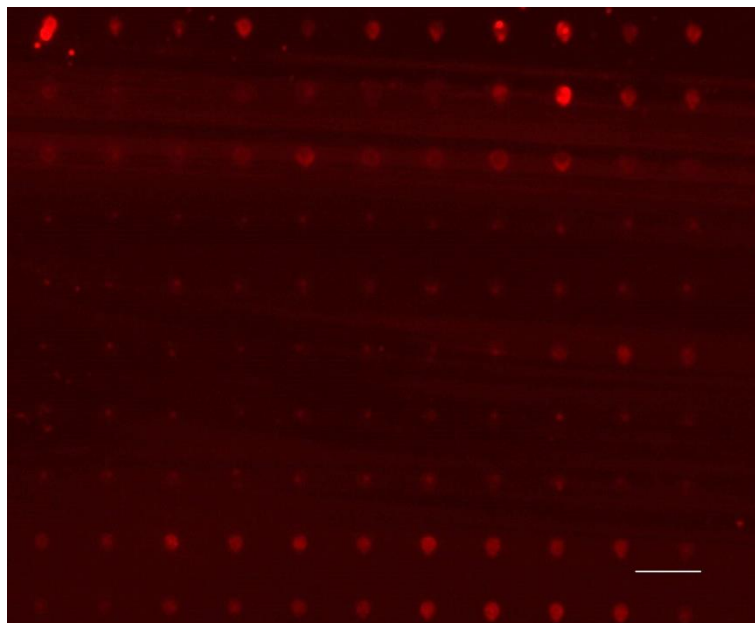


Figure 6.8. Fluorescence microscope image of micropattern obtained from unlabeled AFP after implementation of the incubation step with fluorescent-labeled streptavidin.

6.3. Summary

In this chapter, different functionalization (DBCO-, thiol-, and epoxy-termination) and subsequent click-chemistry immobilization of biotin resulting in six different routes for the detection of AFP (as cancer related model protein) in microchannel cantilever spotted microarrays were compared. In the present setup, a functionalization by thiol-silane with subsequent biotin immobilization by biotin-maleimide and functionalization by epoxy-silane and subsequent biotin immobilization by biotin-amine showed best performance. The sensitivity of an epoxy/amine based array was evaluated to be of $(9.8 \pm 2.9) \mu\text{g}\cdot\text{ml}^{-1}$, which already could offer a feasible rapid and inexpensive screening test (compared to more sensitive, but also much more elaborate detection approaches). The approach can be extended to label-free detection by additional sandwich approach as demonstrated with a second binding of biotinylated antibody and fluorescently labeled streptavidin. The results of this study can be used for rational choice of binding chemistry in the building of highly sensitive protein detection as e.g. needed in cancer biomarker detection.

Chapter 7

Functionalization of DBCO-, thiol- and epoxy terminated diamond surface

7.1. Introduction

In chapters 3, 4 and 5, different click approaches were used for the immobilization of microarrays of different fluorescent and non-fluorescent inks on the DBCO-, thiol- and epoxy-terminated glass surfaces, respectively. In this chapter, considering the optimal reaction conditions like temperature reaction, time reaction, catalyst type, catalyst amount obtained in chapters 3-5, immobilization of microarrays of fluorescent and non-fluorescent inks was performed on the DBCO-, thiol- and epoxy-terminated diamond surfaces. For this, two oxygen-terminated diamonds with average roughnesses of 4 and 14 nm were prepared (Fig. 7.1) and then, in the separate experiments, their surfaces were functionalized similar to the method used for functionalization of hydroxyl-terminated glasses. Then, for creating microarrays, writing on the DBCO-, thiol- and epoxy-terminated diamond surfaces was performed using microchannel cantilever spotting (μ CS).

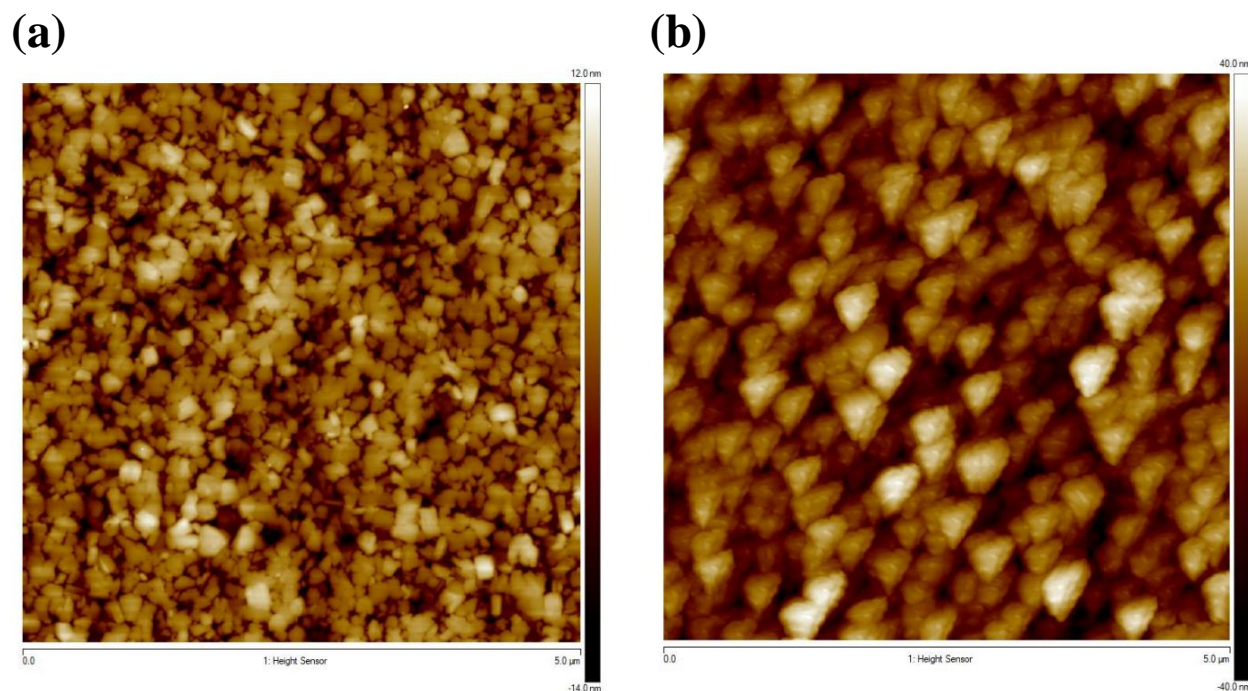


Figure 7.1. Diamond surfaces with average roughness of (a) 4 nm and (b) 14 nm

7.2. Results and discussion

7.2.1. Contact angle measurement

To have a successful spot coating and high-resolution arrays, the contact angle of water droplets on the surface should not be too low, as otherwise the spotted inks will spread and destroy the ordered arrays. Fig. 7.2 shows the contact angle for hydrogen-, oxygen-, DBCO-, thiol- and epoxy-terminated diamond surfaces. For all surfaces, evolution of the contact angle of water on the surface over time showed no change with the passage of time. Comparison of hydrogen-terminated sample with an oxygen-terminated one indicates that oxygen plasma creates a layer of hydroxyl groups, rendering it hydrophilic. But, after functionalization with MPTMS or GPTMS, a higher contact angle can be observed as expected from the more hydrophobic terminal groups.

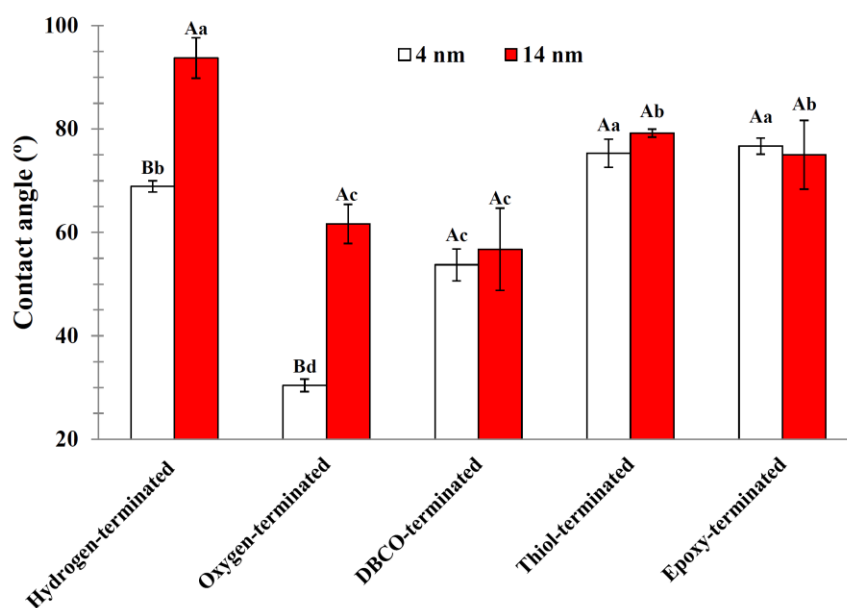
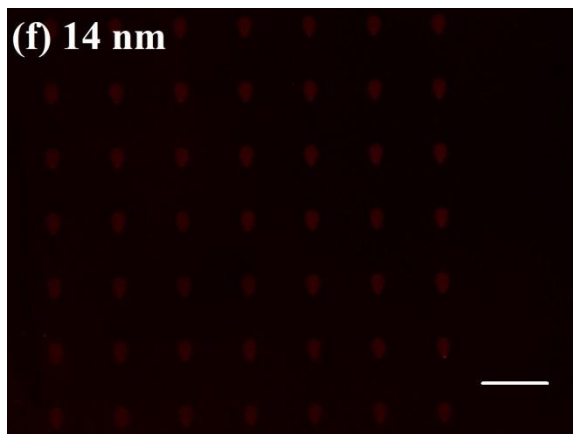
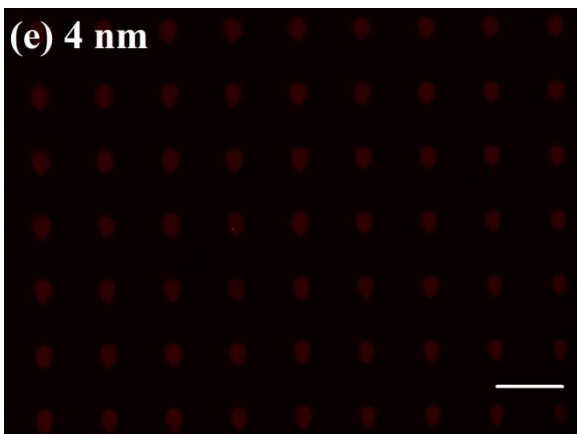
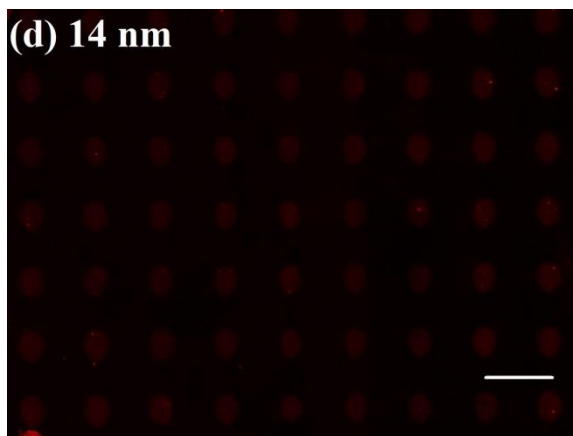
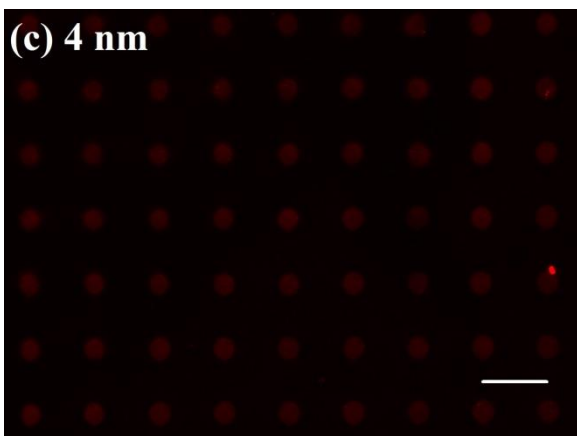
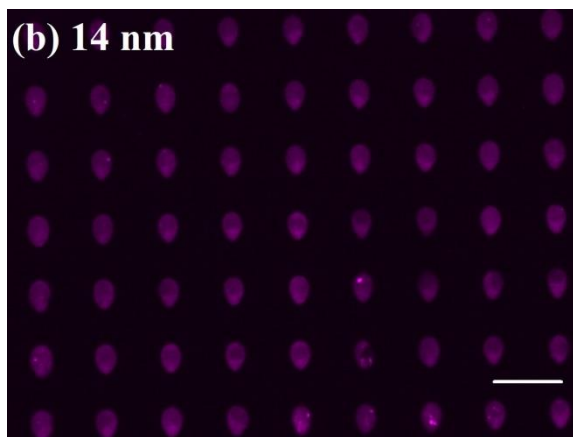
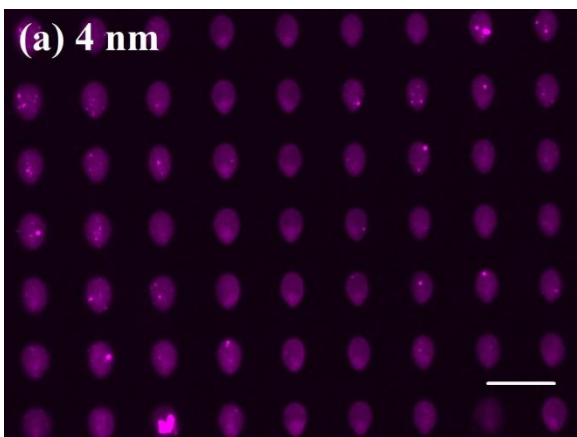


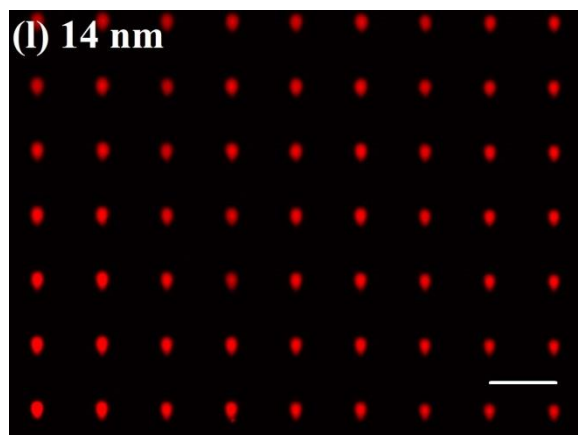
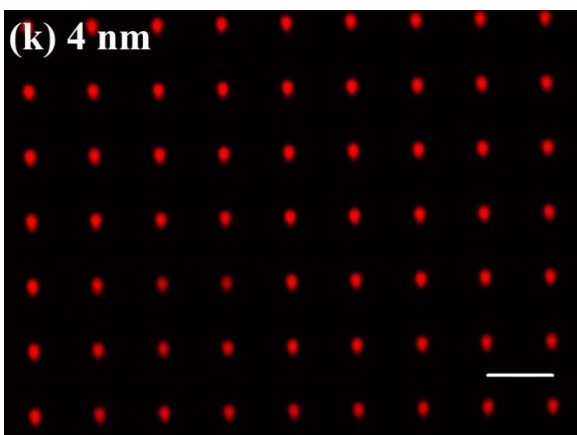
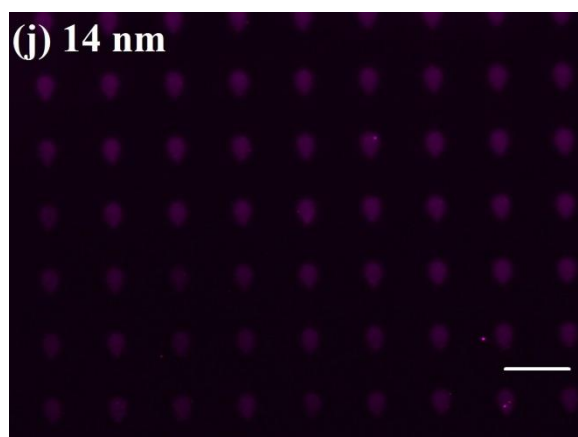
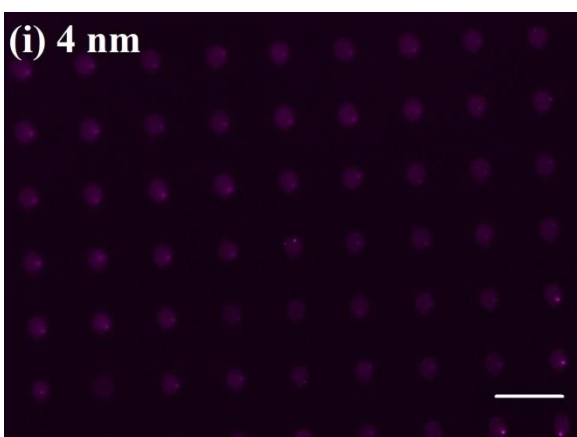
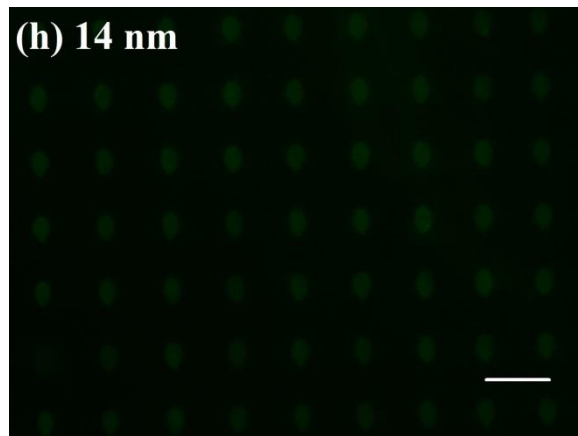
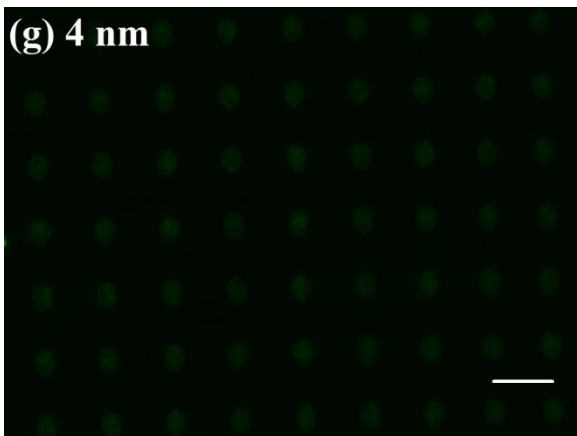
Figure 7.2. Contact angle measurement for different types of functionalized diamond

7.2.2. Array immobilization on the diamond surfaces

To explore the potential of different click reaction to generate microarrays by μ CS, micropatterns of 15×15 spots with a pitch of $50 \mu\text{m}$ were prepared from different fluorescent inks on the different functionalized surfaces: Cy5 thiol and TAMRA azide on the DBCO-terminated, TAMRA-maleimide and FAM-DBCO on the thiol-terminated and Cy5 thiol, R6G and TAMRA-azide on the epoxy-terminated diamonds. Reaction conditions were exactly the

same ones optimized for glass surfaces and reported in chapter 3-5. Fig. 7.3 and Table 7.1 show the fluorescence microscope images and average fluorescence intensity of micropatterns of fluorescent inks obtained at optimum reaction conditions. It seems that similar to glass, immobilization on the diamond has been successful.





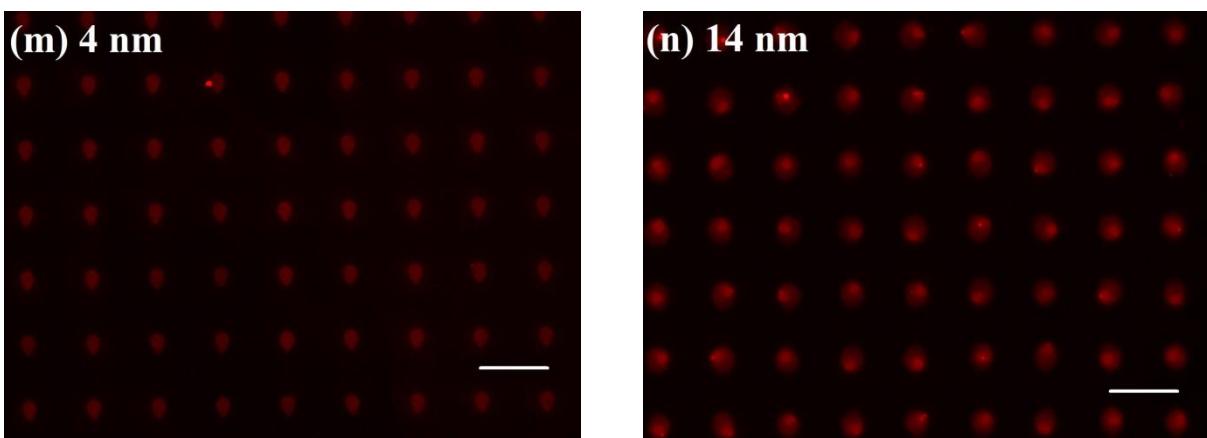


Figure 7.3. Fluorescence microscope images of micropatterns of fluorescent inks obtained at optimum reaction conditions with a spotting humidity of 20%, dwell time (tip/surface contact time) of 2 s and exposure time of 10 s. (a) and (b) Cy5 thiol on the DBCO-terminated surface, (c) and (d) TAMRA-azide on the DBCO-terminated surface, (e) and (f) TAMRA-maleimide on the thiol-terminated surface, (g) and (h) FAM-DBCO on the thiol-terminated surface, (i) and (j) Cy5 thiol on the epoxy-terminated surface, (k) and (l) R6G on the epoxy-terminated surface and (m) and (n) TAMRA-azide on the epoxy-terminated surface. The scale bars equal 50 μm .

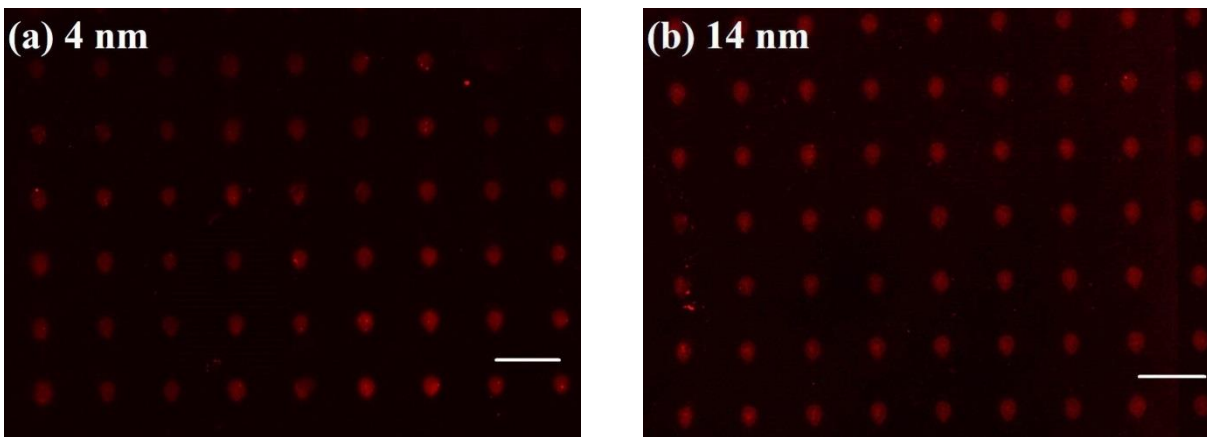
Table 7.1. Average fluorescence intensity of different fluorescent spots immobilized on the different functionalized diamond via click reaction

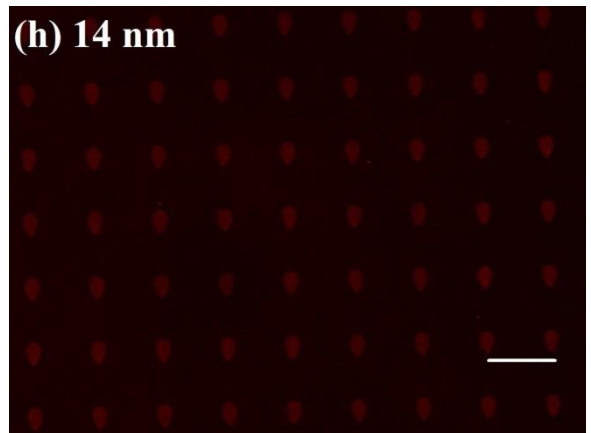
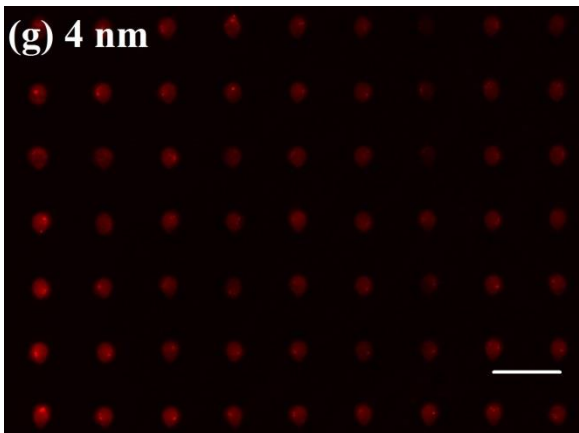
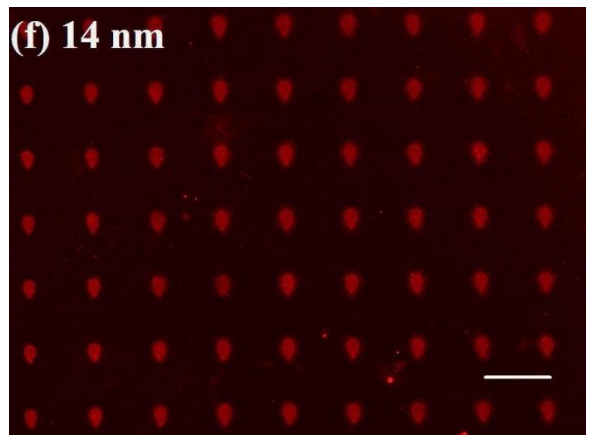
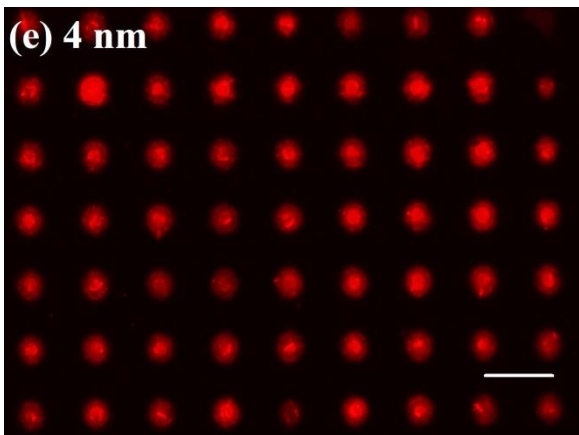
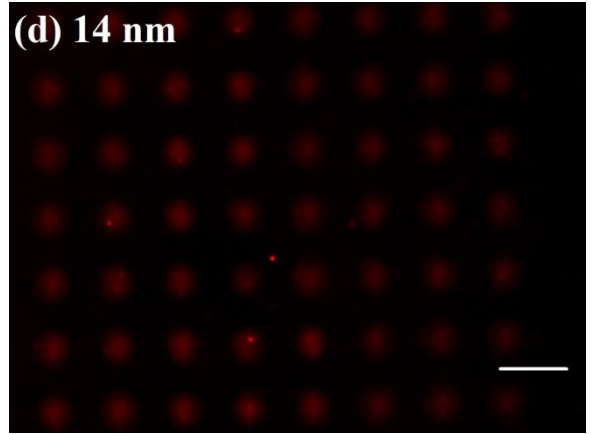
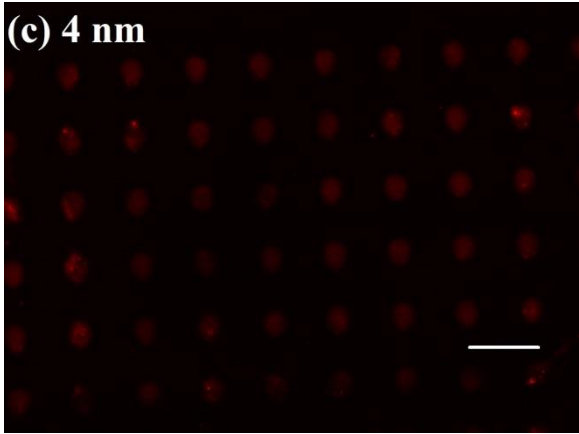
| Fluorescent ink | Diamond surface | Roughness (nm) | Fluorescence intensity (a. u.) |
|-----------------|------------------|----------------|--------------------------------|
| Cy5 thiol | DBCO-terminated | 4 | 4544 ± 389 |
| Cy5 thiol | DBCO-terminated | 14 | 3803 ± 354 |
| TAMRA azide | DBCO-terminated | 4 | 2277 ± 206 |
| TAMRA azide | DBCO-terminated | 14 | 1548 ± 195 |
| TAMRA-maleimide | Thiol-terminated | 4 | 5401 ± 106 |
| TAMRA-maleimide | Thiol-terminated | 14 | 5044 ± 180 |
| FAM-DBCO | Thiol-terminated | 4 | 2978 ± 107 |
| FAM-DBCO | Thiol-terminated | 14 | 2131 ± 164 |
| Cy5 thiol | Epoxy-terminated | 4 | 1400 ± 211 |
| Cy5 thiol | Epoxy-terminated | 14 | 1569 ± 237 |
| R6G | Epoxy-terminated | 4 | 11869 ± 985 |
| R6G | Epoxy-terminated | 14 | 10070 ± 780 |
| TAMRA-azide | Epoxy-terminated | 4 | 4715 ± 525 |
| TAMRA-azide | Epoxy-terminated | 14 | 3138 ± 478 |

7.2.3. Protein coupling on the diamond surfaces

In the previous section, we fruitfully could immobilize arrays of fluorescent inks on the DBCO-, thiol- and epoxy-terminated diamonds through different click reactions. Although the same mole concentration of fluorophores has been used for microarray fabrication but the comparison between different routes for finding the best one is impossible due to different

spectra of the fluorophores. So, a different strategy should be implemented for direct comparison of the routes. For this, biotin bearing compounds were spotted on the functionalized diamonds by μ CS into 15×15 spot arrays. The biotin is a commonly used linker with strong affinity to streptavidin as mentioned in chapter 3. By the use of a fluorescently labeled streptavidin as fluorophore to visualize the immobilized biotin patterns, the amount of immobilized biotin can be compared between different routes. The found results for arrays fabricated at optimal conditions are summarized in Fig. 7.4 and Table 7.2. For all chemical routes, immobilization of biotinylated compound was successful, as after staining the patterns with fluorescent-labeled streptavidin, they all show up in the corresponding fluorescence channel. When comparing the different immobilization routes, it becomes obvious that biotin-amine on the epoxy-terminated diamond (ring opening of epoxy by amine route) and biotin-maleimide on the thiol-terminated diamond (thiol-ene Michael addition (TEMA) route) are yielding higher fluorescence intensity. This very important result is in good agreement with the obtained ones for functionalization of glass in chapters 3-5.





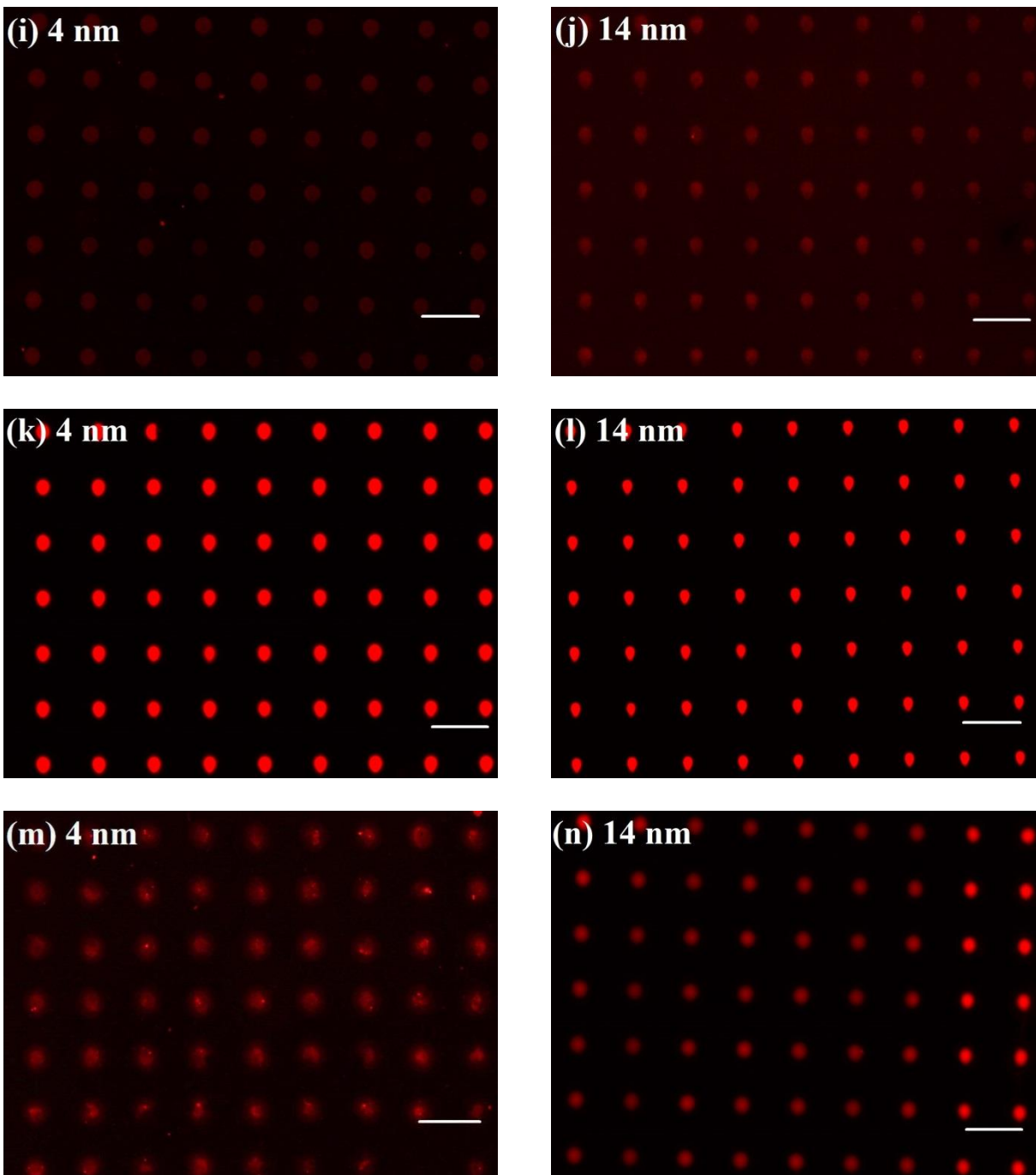


Figure 7.4. Fluorescence microscope images of micropatterns non-fluorescent inks after incubation with fluorescent-labeled streptavidin obtained at optimum reaction conditions with a spotting humidity of 20%, dwell time (tip/surface contact time) of 2 s and exposure time of 10 s. (a) and (b) biotin-thiol on the DBCO-terminated surface, (c) and (d) biotin-azide on the DBCO-terminated surface, (e) and (f) biotin-maleimide on the thiol-terminated surface, (g) and (h) biotin-DBCO on the thiol-terminated surface, (i) and (j) biotin-thiol on the epoxy-terminated surface, (k) and (l) biotin-amine on the epoxy-terminated surface and (m) and (n) biotin-azide on the epoxy-terminated surface. The scale bars equal 50 μm .

Table 7.2. Average fluorescence intensity of different non-fluorescent spots immobilized on the different functionalized diamond via click reaction

| Non-fluorescent ink | Diamond surface | Roughness (nm) | Fluorescence intensity (a. u.) |
|----------------------------|------------------------|-----------------------|---------------------------------------|
| Biotin-thiol | DBCO-terminated | 4 | 2001 ± 428 |
| Biotin-thiol | DBCO-terminated | 14 | 3031 ± 119 |
| Biotin-azide | DBCO-terminated | 4 | 1583 ± 335 |
| Biotin-azide | DBCO-terminated | 14 | 1549 ± 235 |
| Biotin-maleimide | Thiol-terminated | 4 | 7179 ± 815 |
| Biotin-maleimide | Thiol-terminated | 14 | 5827 ± 131 |
| Biotin-DBCO | Thiol-terminated | 4 | 4138 ± 660 |
| Biotin-DBCO | Thiol-terminated | 14 | 4261 ± 97 |
| Biotin-thiol | Epoxy-terminated | 4 | 3278 ± 163 |
| Biotin-thiol | Epoxy-terminated | 14 | 3935 ± 198 |
| Biotin-amine | Epoxy-terminated | 4 | 10421 ± 498 |
| Biotin-amine | Epoxy-terminated | 14 | 9121 ± 578 |
| Biotin-azide | Epoxy-terminated | 4 | 3265 ± 87 |
| Biotin-azide | Epoxy-terminated | 14 | 4087 ± 124 |

7.3. Summary

Diamond surfaces with average roughnesses of 4 and 14 nm were functionalized with different molecules including DBCO-acid, MPTMS and GPTMS for generating DBCO-, thiol- and epoxy-terminated surfaces, respectively. In the following, different types of click reactions were performed to immobilize fluorescent inks on the functionalized diamond via μ CS: Cy5 thiol and TAMRA azide on the DBCO-terminated, TAMRA-maleimide and FAM-DBCO on the thiol-terminated and Cy5 thiol, R6G and TAMRA-azide on the epoxy-terminated diamonds. In most cases, intensity for diamond with roughness of 4 nm was more than 14 nm. Moreover, to have a comparison between different types of click reactions and find the best one, biotin compounds as nonfluorescent inks were immobilized on the DBCO-, thiol- and epoxy-terminated diamond surfaces and binding of a fluorescently-labeled streptavidin to them was studied. Consequently, biotin-amine on the epoxy-terminated diamond (ring opening of epoxy by amine route) and biotin-maleimide on the thiol-terminated diamond (TEMA route) showed the highest amount of intensity or in other words the highest surface density of molecular immobilization.

Chapter 8

Summary

Functionalization of surfaces and materials through the covalent attachment of organic monolayers has many applications in chemical/biological sensing, drug delivery, selective gas separation, cancer detection, etc. In this regard, click chemistry reactions, especially those that require no metal catalyst, are powerful candidates. This project focuses on the functionalization of glass and diamond surfaces via different click reactions with the purpose of creating microscale patterns for sensing applications. Before functionalization, the surfaces were modified using attachment of suitable functional groups through esterification or silanization techniques. The glass surfaces were divided into three groups. First groups were modified with dibenzocyclooctyne-acid (DBCO-acid), a cyclooctyne with a carboxyl group (DBCO-terminated glasses). Second groups were modified with (3-mercaptopropyl)trimethoxysilane (MPTMS) which is a mercaptosilane (thiol-terminated glasses). And finally, third groups were modified with (3-glycidyloxypropyl)trimethoxysilane (GPTMS) which is a glycidoxysilane (epoxy-terminated glasses). Then, in the distinct experiments, all glass surfaces were functionalized via microchannel cantilevers spotting (μ CS) with different fluorescent and non-fluorescent inks: DBCO-terminated glass surfaces with inks containing azide or thiol groups, thiol-terminated glass surfaces with inks containing maleimide or DBCO groups and epoxy-terminated glass surfaces with inks containing thiol, amine or azide groups. Experiments with different fluorophores showed that all routes were successful in coupling functional moieties to the surface in a short time and low temperature. Also, from these experiments, optimal reaction conditions were determined. The feasibility of these routes and micropattern fabricated by them in biomedical and biological applications was examined through protein binding experiments. Comparing the streptavidin binding experiments for different biotin carrying spot arrays (biotin-azide and biotin-thiol on DBCO-terminated, biotin-maleimide and biotin-DBCO on thiol-terminated glass surfaces and biotin-thiol, biotin-amine and biotin-azide on epoxy-terminated glass surfaces) revealed the higher surface density of immobilized biotin for biotin-maleimide on the thiol-terminated surface and biotin-amine on the epoxy-terminated surface which the former is a thiol-ene Michael addition (TEMA) reaction and the latter is a ring opening of epoxy by amine. Considering the obtained results from functionalization of different glass surfaces with different fluorescent and non-fluorescent inks, sensitive fluorescent immunosensors for Alpha-fetoprotein (AFP) detection were designed and fabricate. AFP is the most commonly biomarker for early screening and diagnosis of hepatocellular carcinoma (HCC). In assembling these

immunosensors, three techniques including click chemistry, biotin-streptavidin-biotin sandwich-type strategy and antigen-antibody interaction were combined. Finally, the experiments performed on the glass surfaces were repeated on the DBCO-, thiol- and epoxy-terminated diamond surfaces as diamond is used as an excellent transducer in optical sensor. The obtained achievements and results from this study are applicable in design and fabricating of biosensors, appropriate for protein detection and other biomedical/biological applications.

Chapter 9

Experimental section

9.1. Materials

Table 9.1 lists the materials used in this study. All materials were used as received without further purification steps.

Table 9.1. List of the used materials

| Commercial name | Short name | Description | Role | Company |
|---|-----------------|---|---|---------------------------|
| 5-Carboxytetramethylrhodamine-azide | TAMRA-azide | Appearance: dark red solid Molecular formula: $C_{28}H_{28}N_6O_4$ Molecular weight: $881.32 \text{ g.mol}^{-1}$ Spectroscopic properties: $\lambda_{\text{abs}} = 546 \text{ nm}$ and $\lambda_{\text{em}} = 579 \text{ nm}$ Solubility: DMF, DMSO, methanol | Fluorescent dye | Jena Bioscience (Germany) |
| Cy5 labeled polyethylene glycol thiol | Cy5 thiol | Appearance: blue or dark blue solid Molecular weight: 3400 g.mol^{-1} Spectroscopic properties: $\lambda_{\text{abs}} = 650 \text{ nm}$ and $\lambda_{\text{em}} = 670 \text{ nm}$ Solubility: soluble in regular aqueous solution as well as most organic solvents | Fluorescent dye | Nanocs Company (USA) |
| Rhodamine 6G | R6G | Appearance: powder or crystals, red to brown Molecular formula: $C_{28}H_{31}N_2O_3Cl$ Molecular weight: $479.01 \text{ g.mol}^{-1}$ Spectroscopic properties: $\lambda_{\text{abs}} = 530 \text{ nm}$ and $\lambda_{\text{em}} = 556 \text{ nm}$ Solubility: water, methanol | Fluorescent dye | Sigma-Aldrich (Germany) |
| Dibenzylcyclooctyne-PEG ₄ -5/6-FAM | FAM-DBCO | Appearance: orange solid Molecular formula: $C_{50}H_{47}N_3O_{12}$ Molecular weight: $881.32 \text{ g.mol}^{-1}$ Spectroscopic properties: $\lambda_{\text{abs}} = 492 \text{ nm}$ and $\lambda_{\text{em}} = 517 \text{ nm}$ Solubility: DMF and DMSO | Fluorescent dye | Jena Bioscience (Germany) |
| Tetramethylrhodamine-5-maleimide | TAMRA-maleimide | Appearance: dark violet powder Molecular formula: $C_{28}H_{23}N_3O_5$ Molecular weight: $481.50 \text{ g.mol}^{-1}$ Spectroscopic properties: $\lambda_{\text{abs}} = 543 \text{ nm}$ and $\lambda_{\text{em}} = 575 \text{ nm}$ Solubility: DMSO and methanol | Fluorescent dye | Sigma-Aldrich (Germany) |
| 5-(and 6)-carboxytetramethylrhodamine, succinimidyl ester | NHS-rhodamine | Appearance: orange solid Molecular formula: $C_{29}H_{25}N_3O_7$ Molecular weight: 528 g.mol^{-1} Spectroscopic properties: $\lambda_{\text{abs}} = 552 \text{ nm}$ and $\lambda_{\text{em}} = 575 \text{ nm}$ Solubility: DMF and DMSO | Fluorescent reagent for labeling | Thermo Scientific (USA) |
| Azide-PEG ₃ -biotin conjugate | Biotin-azide | Appearance: Off-white to grey solid Molecular formula: $C_{18}H_{32}N_6O_5S$ Molecular weight: $444.54 \text{ g.mol}^{-1}$ Solubility: chloroform, DCM, DMF, DMSO and THF | Non-fluorescent dye (biotinylated molecule) | Jena Bioscience (Germany) |

| | | | | |
|--|------------------|---|--|------------------------------|
| Biotin PEG thiol, MW 2000 | Biotin-thiol | Appearance: Off-white/white solid Molecular formula: C ₁₈ H ₃₂ N ₆ O ₅ S Molecular weight: 2000 g.mol ⁻¹ Solubility: soluble in regular aqueous solution as well as most organic solvents | Non-fluorescent dye (biotinylated molecule) | Nanocs Company (USA) |
| Biotin-dPEG [®] ₇ -NH ₂ | Biotin-amine | Appearance: white to off-white solid Molecular formula: C ₂₆ H ₅₀ N ₄ O ₉ S Molecular weight: 594.8 g.mol ⁻¹ Solubility: water and DMSO | Non-fluorescent dye (biotinylated molecule) | Sigma-Aldrich (Germany) |
| Biotin-dPEG [®] ₁₁ -MAL | Biotin-maleimide | Appearance: powder Molecular formula: C ₄₁ H ₇₁ N ₅ O ₁₆ S Molecular weight: 922.09 g.mol ⁻¹ Solubility: DMF and DMSO | Non-fluorescent dye (biotinylated molecule) | Sigma-Aldrich (Germany) |
| Dibenzylcyclooctyne-PEG ₄ -biotin conjugate | Biotin-DBCO | Appearance: off-white to slightly grey solid Molecular formula: C ₃₉ H ₅₁ N ₅ O ₈ S Molecular weight: 749.92 g.mol ⁻¹ Solubility: DMF and DMSO | Non-fluorescent dye (biotinylated molecule) | Jena Bioscience (Germany) |
| Dibenzocyclooctyne-acid | DBCO-acid | - | Coupling agent in esterification | Jena Bioscience (Germany) |
| (3-Mercaptopropyl)trimethoxysilane | MPTMS | Appearance: liquid Molecular formula: C ₆ SiO ₃ H ₁₆ S Molecular weight: 196.34 g.mol ⁻¹ Boiling point: 213-215 °C Density: 1.057 Solubility: toluene | Silane coupling agent | Sigma-Aldrich (Germany) |
| (3-Glycidyloxypropyl)trimethoxysilane | GPTMS | Appearance: liquid Molecular formula: C ₉ H ₂₀ O ₅ Si Molecular weight: 236.34 g.mol ⁻¹ Boiling point: 120 °C Density: 1.07 Solubility: toluene | Silane coupling agent | Sigma-Aldrich (Germany) |
| Streptavidin | S | - | Conjugation with biotinylated molecules | Sigma-Aldrich (Germany) |
| Streptavidin-Cy3 (fluorescently labeled streptavidin) | F-S | Appearance: pink buffered aqueous solution containing 1% BSA and 15 mM sodium azide (pH = 7.4) Spectroscopic properties: λ _{abs, max} = 552 nm and λ _{em, max} = 565 nm | Conjugation with biotinylated molecules | Sigma-Aldrich (Germany) |
| Alpha fetoprotein | AFP or Ag | Molecular weight: 69 kDa Source: human cord serum Gene: AFP, FETA, HPAFP | Biomarker or antigen | Lee BioSolutions, Inc. (USA) |
| AFP antibody (C3) [biotin] | B-Ab | - | Biotinylated antibody or biotinylated anti-AFP | Novus Biologicals (USA) |
| Bovine serum albumin | BSA | Appearance: lyophilized powder Molecular weight: ~ 66000 Da pH of 1% solution: 7 Solubility: water | Blocker | Sigma-Aldrich (Germany) |

| | | | | |
|---|-----------------------------------|---|--------------------|----------------------------|
| Phosphate buffered saline | PBS | Appearance: white powder pH of 1% solution: 7.2-7.6 Solubility: water | Buffer | Sigma–Aldrich (Germany) |
| Triethylamine | TEA | Appearance: colorless liquid Molecular formula: C ₆ NH ₁₅ Molecular weight: 101.19 g.mol ⁻¹ pH: 12.7 at 15 °C | Catalyst | Sigma–Aldrich (Germany) |
| N,N'-Dicyclohexylcarbodiimide | DCC | - | Catalyst | Sigma-Aldrich (Germany) |
| 4-Dimethylaminopyridine | DMAP | - | Catalyst | Sigma-Aldrich (Germany) |
| Bismuth(III) trifluoromethanesulfonate | Bi(OTf) ₃ | - | Catalyst | Sigma-Aldrich (Germany) |
| Lithium chloride | LiCl | - | Catalyst | Sigma-Aldrich (Germany) |
| Zinc perchlorate | Cl ₂ O ₈ Zn | - | Catalyst | Sigma-Aldrich (Germany) |
| Zinc oxide nanoparticles | ZnO | - | Catalyst | Sigma-Aldrich (Germany) |
| Triphenylphosphine | Ph ₃ P | - | Catalyst | Sigma-Aldrich (Germany) |
| Dimethyl sulfoxide (DMSO), glycerol, toluene, chloroform, 2-propanol, acetone | - | - | Solvent or rinsing | Sigma–Aldrich (Germany) |

9.2. Methods

9.2.1. Functionalization of DBCO-terminated glass surface (chapter 3)

Functionalized glasses used in chapter 3 were prepared as follows:

9.2.1.1. Substrate preparation

Standard glass coverslips (VWR, Germany) were cleaned with chloroform, 2-propanol, and deionized water, dried by blowing with nitrogen, and exposed to oxygen plasma (10 sccm O₂, 0.2 mbar, 100 W, 2 min) for hydroxyl functionalization of the surface. DBCO-acid (0.02 mmol, 6.67 mg), DCC (0.022 mmol, 4.53 mg), and DMAP (0.0035 mmol, 0.43 mg) were dissolved in DMSO. The hydroxyl-terminated glasses were immersed in the resulting solution and left at room temperature for 24 h under nitrogen atmosphere for DBCO functionalization of the surface. The DBCO-terminated samples were then washed with DMSO (5 min, 2 times), ethanol (5 min, 2 times), and finally with deionized water and dried under a nitrogen stream (refer to Fig 3.3a-c in chapter 3 for a schematic pictures of bare, OH-terminated, and DBCO-terminated samples).

9.2.1.2. Ink solution preparation

The fluorescent dyes used for the μ CS were TAMRA-azide and Cy5 thiol which were dissolved in a mixture of DMSO/glycerol (7:3) at a concentration of 500 $\mu\text{g}\cdot\text{ml}^{-1}$. Also, biotin-azide and biotin-thiol as non-fluorescent functional compounds were dissolved in a mixture of DMSO/glycerol (7:3) at a concentration of 1000 $\mu\text{g}\cdot\text{ml}^{-1}$ and used for μ CS.

9.2.1.3. Pattern writing via μ CS

The spotting procedures were performed on a NLP 2000 system (NanoInk, USA) equipped with SPT pens (SPT-S-C10S, Bioforce Nanosciences) [2b, 101]. Prior to use, the pen was freshly plasma cleaned by oxygen (10 sccm O_2 , 0.2 mbar, 100 W, 2 min) and used immediately. The pen reservoir was filled with 0.2 μl of ink solution. The spotting procedures were implemented at different relative humidity in the range of 20 to 70%. For all patterns, a dwell time of 0.1 s was used. Fig. 3.3d-e illustrates the schematic pictures of the lithography process on the DBCO-functionalized glasses with different azide and thiol ink solutions.

9.2.1.4. Click reaction between azides and alkyne

After the lithography process on the DBCO-functionalized glasses, the click reaction between fluorescent TAMRA-azide and cycloalkyne was allowed to proceed for 10, 20, 30, 60, 120, and 240 min at two different temperatures of 25 and 37 $^{\circ}\text{C}$ in a temperature chamber (PU-1KP, ESEPC, Japan) to study the influence of reaction time and temperature. Subsequently, the samples were rinsed with deionized water to remove the excess dye solution, and were dried by blowing with nitrogen. The same procedure was employed for doing the reaction between biotin-azide and cycloalkyne. This reaction was done at 37 $^{\circ}\text{C}$ for 20 min.

9.2.1.5. Click reaction between thiols and alkyne

Similar to the azide case, after lithography, the click reactions between fluorescent Cy5 thiol and cycloalkyne were allowed to proceed for different times of 10, 20, 30, and 40 min at two different temperatures of 25 and 37 $^{\circ}\text{C}$ in a temperature chamber. Subsequently, the samples were rinsed with deionized water to remove the excess dye solution, and were dried by blowing with nitrogen. The same procedure was employed for doing the reaction between biotin-thiol and cycloalkyne. This reaction was done at 37 $^{\circ}\text{C}$ for 40 min.

9.2.1.6. Protein binding on microarrays

The affinity of biotin and fluorescent streptavidin was examined for arrays of biotin-azide and biotin-thiol immobilized on the DBCO-terminated glasses through click reaction. Prior to adding the streptavidin solution, the samples were blocked with 10% bovine serum albumin (BSA) in PBS for 30 min. Subsequently, the samples were washed three times by pipetting on and off 30 μl of PBS and then incubated for 1 h with a solution of 10 $\mu\text{g}\cdot\text{ml}^{-1}$ of streptavidin-Cy3 in a dark environment. After that, the samples were washed three times with PBS, rinsed with deionized water and blow-dried with nitrogen before inspection by fluorescence microscopy.

9.2.2. Functionalization of thiol-terminated glass surface (chapter 4)

Functionalized glasses used in chapter 4 were prepared as follows:

9.2.2.1. Preparation of substrate

Fig. 4.2 shows the schematic route for preparing a thiol-terminated glass surface by conventional silanization method. First, for hydroxyl functionalization of the surface, the standard glass coverslips (1 cm \times 1 cm, VWR, Germany) were washed with chloroform, 2-propanol, and deionized water, dried by blowing with nitrogen, and exposed to oxygen plasma (10 sccm O_2 , 0.2 mbar, and 100 W) for 2 min. Subsequently, to obtain thiolated surface, the hydroxyl-terminated glasses were immersed in a 2% v/v MPTMS solution in toluene for 5 h, at room temperature. Finally, the thiol-terminated glasses were washed sequentially with acetone, toluene and deionized water, and then dried under a nitrogen stream.

9.2.2.2. Preparation of ink solution

The fluorescent dyes used for the μCS , including FAM-DBCO and TAMRA-maleimide were separately dissolved in the mixture of DMSO/glycerol (7:3 v/v) at concentrations of 900 and 500 $\mu\text{g}\cdot\text{ml}^{-1}$, respectively. Also, biotin-DBCO and biotin-maleimide as non-fluorescent dyes were dissolved at concentration range from 400 to 2000 $\mu\text{g}\cdot\text{ml}^{-1}$ in the mixture of DMSO/glycerol (7:3) and used for μCS . For TAMRA-maleimide and biotin-maleimide solutions, 10 mol% TEA to dye was added as catalyst.

9.2.2.3. Microarray printing via μCS

The paths labeled b1, c1, d1 and e1 in Fig. 4.2 illustrate schematically the lithography process on the thiol-functionalized glasses with different ink solutions containing DBCO or

maleimide groups. The spotting process was performed as discussed in 9.2.1.3 section at optimized relative humidity of 20% obtained in chapter 3.

9.2.2.4. Microarray immobilization via click reaction

After the lithography process on the thiolated glass surfaces, the click reaction between thiol and either FAM-DBCO or TAMRA-maleimide was allowed to continue for 10, 20, and 40 min at two different temperatures of 25 and 37 °C to study the influence of reaction time and temperature (paths b2 and c2 in Fig. 4.2). To better control the environmental conditions, the reaction at 37 °C was done in a temperature chamber (PU-1KP, ESEPC, Japan). Subsequently, the samples were rinsed with deionized water to eliminate the excess dye solution, and were dried by blowing with nitrogen. The same procedure was employed for the reaction between thiol and non-fluorescent dyes including biotin-DBCO and biotin-maleimide (respectively, paths d2 and e2 in Fig. 4.2). These reactions were all done at 37 °C for 20 min.

9.2.2.5. Protein binding on biotinylated microarrays

As shown in the paths d3 and e3 in Fig. 4.2, the affinity of biotin and fluorescent streptavidin was examined for arrays of biotin-DBCO and biotin-maleimide immobilized on the thiolated surfaces through click reaction. Streptavidin binding was done as discussed in 9.2.1.6 section.

9.2.3. Functionalization of epoxy-terminated glass surface (chapter 5)

Functionalized glasses used in chapter 5 were prepared as follows:

9.2.3.1. Cleaning and activation of glass slide surfaces

Standard glass coverslips (1 cm × 1 cm, VWR, Germany) were rinsed with chloroform, 2-propanol and deionized water, and dried by blowing with nitrogen. In order to activate the glass surfaces, they were exposed to oxygen plasma (10 sccm O₂, 0.2 mbar and 100 W) for 2 min. The obtained hydroxyl-terminated glasses prepared in this fashion were immediately submitted to functionalization procedure with GPTMS.

9.2.3.2. Preparation of epoxy-coated glasses

Freshly activated glass slides were immersed at room temperature in a 2% (v/v) solution of GPTMS in dry toluene for 5 h. After this time, the epoxy-functionalized glasses were removed

from the solution, thoroughly rinsed with acetone, toluene and deionized water, and dried under a stream of nitrogen.

9.2.3.3. Ink solution preparation

The fluorescent dyes used for the μ CS, including Cy5 thiol, R6G and TAMRA-azide were separately dissolved in the mixture of DMSO/glycerol (7:3 v/v) at concentration of $1 \mu\text{mol.ml}^{-1}$. Also, biotin-thiol ($M_w = 2000 \text{ g.mol}^{-1}$), biotin-amine ($M_w = 595 \text{ g.mol}^{-1}$) and biotin-azide ($M_w = 445 \text{ g.mol}^{-1}$) as non-fluorescent functional compounds were dissolved in a mixture of DMSO/glycerol (7:3) at a concentration of $2 \mu\text{mol.ml}^{-1}$ and were used for μ CS.

9.2.3.4. Microarray immobilization via click reaction

Arrays of fluorescent-labeled dyes including Cy5 thiol, R6G and TAMRA-azide were spotted onto prepared epoxy-terminated substrates using μ CS as discussed in 9.2.1.3 section at optimized relative humidity of 20% obtained in chapter 3. After the spotting, the reaction between fluorescent dye and epoxy was allowed to proceed for different time durations (10, 20 and 40 min). Reaction between epoxy and Cy5 thiol was studied at two different temperatures (25 and 37 °C). Also, for this reaction, 10 mol% TEA to Cy5 thiol was added as catalyst to the solution. Reaction between epoxy and R6G was performed at 37 °C by adding catalyst into ink solution. Different amounts of four catalysts ($\text{Bi}(\text{OTf})_3$, LiCl, $\text{Cl}_2\text{O}_8\text{Zn}$ and ZnO nanoparticles) were examined for this reaction. For immobilization of TAMRA-azide on the epoxy-terminated surface, azide was first converted into an amine in the presence of 3 mol% Ph_3P to azide via Staudinger reaction. Then, the prepared amine dissolved in DMSO/glycerol was mixed with different amounts of $\text{Bi}(\text{OTf})_3$ and spotted on the epoxy-terminated surface at 37 °C. After the incubation time elapsed, the samples were washed with deionized water to remove excess ink and stop the reactions and then dried by blowing with nitrogen. For the non-fluorescent dyes (biotin-thiol, biotin-amine and biotin-azide), the same procedures as fluorescent dyes but with optimum reaction conditions were implemented (Fig. 5.2).

9.2.3.5. Protein binding on biotinylated microarrays

Arrays of Cy5 thiol, R6G and TAMRA-azide immobilized on the epoxy-terminated glasses were directly evaluated by fluorescence microscopy. But, microarrays of biotin-thiol, biotin-amine and biotin-azide immobilized on the epoxy-terminated glasses were first incubated with

fluorescent-labeled streptavidin before fluorescence imaging. Streptavidin binding was done as discussed in 9.2.1.6 section.

9.2.4. Fluorescent immunosensors for detection of AFP (chapter 6)

9.2.4.1. Preparation of biotinylated substrates

Standard glass coverslips (1 cm × 1 cm, VWR, Germany) were cleaned with chloroform, 2-propanol and deionized water, dried by blowing with nitrogen, and exposed to oxygen plasma (10 sccm O₂, 0.2 mbar and 100 W) for 2 min. The obtained hydroxyl-terminated glasses were first functionalized with DBCO-acid, MPTMS, or GPTMS, then biotinylated via different click reactions as follows.

To obtain DBCO-functionalized surfaces, hydroxyl-terminated glasses were immersed in solution of DBCO-acid, DCC and DMAP in DMSO for 24 h at room temperature (Fig. 6.1, path i). Thiol-functionalized surfaces were obtained through soaking hydroxyl-terminated glasses in a 2% v/v solution of MPTMS in toluene for 5 h, at room temperature (Fig. 6.1, path ii). For obtain epoxy-functionalized surfaces, hydroxyl-terminated glasses were immersed in a 2% v/v solution of GPTMS in toluene for 5 h, at room temperature (Fig. 6.1, path iii). All the functionalized glasses were washed sequentially with deionized water and suitable solvents to remove unreacted materials, and dried under a nitrogen stream.

9.2.4.2. Biotin immobilization

Different click reactions were used for immobilization of biotin on the DBCO-, thiol-, or epoxy-functionalized surfaces (Fig. 6.1, routes 1-6). At all reactions, the same mole concentrations of biotin solution (2 μmol.ml⁻¹) were selected and biotin compounds were dissolved in DMSO. Also, all reactions were allowed to proceed for 20 min at 37 °C. Samples in routes 1 and 2 were prepared by immersing the DBCO-functionalized glasses in biotin-thiol (4000 μg.ml⁻¹) and biotin-azide (890 μg.ml⁻¹) solutions, respectively. In routes 3 and 4, samples were provided by soaking the thiol-functionalized glasses in biotin-maleimide (1844 μg.ml⁻¹) and biotin-DBCO (1500 μg.ml⁻¹) solutions, respectively. For reaction between thiol and maleimide, 10 mol% TEA to biotin-maleimide was added as catalyst to the solution. Samples in routes 5 and 6 were obtained by putting epoxy-functionalized glasses into biotin-amine (1190 μg.ml⁻¹) and biotin-thiol (4000 μg.ml⁻¹) solutions. For reaction between epoxy and amine, 1 mol% Bi(OTf)₃ to

biotin-amine was added as catalyst to biotin-amine solution. Also, for reaction between epoxy and thiol, 10 mol% TEA to biotin-thiol was added as catalyst to biotin-thiol solution. For all biotinylated glasses, after the incubation time was completed, the excess ink solution was rinsed with deionized water and suitable solvents and samples were dried in a nitrogen stream.

9.2.4.3. Antibody attachment via sandwich

To detect AFP antigen, anti-AFP as an antibody (Ab) needs to be coated on the surface of glass. As shown in Fig. 6.2a-b, this was done in two steps: biotinylated surfaces were incubated for 1 h with a solution of 10 $\mu\text{g}\cdot\text{ml}^{-1}$ of streptavidin solution in PBS. The samples were washed with PBS and deionized water and were blow-dried with nitrogen. After that, 10 $\mu\text{g}\cdot\text{ml}^{-1}$ biotinylated antibody (B-Ab) was made to react with the streptavidin on the surface. Antibody-terminated surfaces were rinsed with PBS to remove the excess solution and were dried by blowing with nitrogen.

9.2.4.4. Microarray writing via μCS

To study the interaction between antibody and antigen, fluorescent-labeled AFP ink was spotted on antibody-terminated surfaces by μCS into 15×15 spot arrays. The spotting process was performed as discussed in 9.2.1.3 section at optimized relative humidity of 20% obtained in chapter 3. Fig. 6.2c illustrates a schematic picture of the lithography process on the antibody-terminated glasses. After the lithography process and to study the influence of time and temperature on coupling content, the reaction between fluorescent-labeled AFP and anti-AFP was allowed to proceed for 10, 20, 30 and 60 min at two different temperatures of 25 and 37 °C in a temperature chamber (PU-1KP, ESEPC, Japan). After the incubation time was allotted, the excess ink solution was rinsed with deionized water and the surface was dried in a nitrogen stream.

9.2.4.5. Preparation of fluorescently labeled AFP ink

Succinimidyl-ester labeling reagents are the simplest and most frequently used reagents for labeling proteins like antibodies. Succinimidyl-ester reacts efficiently with primary amino groups ($-\text{NH}_2$) in the side chain of lysine (K) residues of proteins in pH 7-9 to form stable amide bonds. This reaction results in the release of N-hydroxysuccinimide (NHS). We used NHS-rhodamine - a succinimidyl-ester functional group attached to the rhodamine core - for labeling AFP (Fig.

2d). This fluorescent labeling reagent absorbs green visible light (552 nm) and emits orange-red visible light (575 nm). Since, AFP is in tris buffer solution and (-NH₂) is found in the structure of tris buffer, dialysis bag was used to replace tris buffer with PBS. In the following for AFP labeling, 10- to 15-fold molar excess of NHS-rhodamine was added to the prepared solution and dialyzed again for removing the extra NHS-rhodamine (Fig. 6.2d).

9.2.5. Functionalization of DBCO-, thiol- and epoxy-terminated diamond surfaces (chapter 7)

9.2.5.1. Preparation of hydrogen- and oxygen-terminated diamonds

Hydrogen- and oxygen-terminated diamonds were prepared by hydrogen and oxygen plasma and CVD method.

9.2.5.2. Functionalization of diamonds

Functionalized diamonds used in chapter 7 were prepared exactly in the same way used for functionalization of glasses in chapters 3-5.

9.3. Characterization techniques

9.3.1. Contact angle measurement

The static contact angles of water droplets on the bare and functionalized glass surfaces were recorded at room temperature using an OCA-20 contact angle analyzer from DataPhysics Instruments GmbH. For each measurement, five water droplets with same volume and rate (2 μl and 2 $\mu\text{l}\cdot\text{s}^{-1}$, respectively) were dropped on the surface and the average value of contact angle was reported.

9.3.2. X-ray photoelectron spectroscopy (XPS)

XPS measurements were performed using a K-Alpha+ XPS spectrometer (ThermoFisher Scientific, East Grinstead, UK). Data acquisition and processing using the Thermo Avantage software is described elsewhere [\[102\]](#). All samples were analyzed using a microfocused, monochromated Al K α X-ray source (400 μm spot size). The kinetic energy of the electrons was measured by a 180° hemispherical energy analyzer operated in the constant analyzer energy mode (CAE) at 50 eV pass energy for elemental spectra. The K-Alpha+ charge compensation system was employed during analysis, using electrons of 8 eV energy, and low-energy argon

ions to prevent any localized charge build-up. The spectra were fitted with one or more Voigt profiles (BE uncertainty: +0.2 eV) and Scofield sensitivity factors were applied for quantification. All spectra were referenced to the C 1s peak (C-C, C-H) at 285.0 eV binding energy controlled by means of the well-known photoelectron peaks of metallic Cu, Ag, and Au, respectively.

9.3.3. Atomic force microscopy (AFM)

AFM for mapping of roughness was conducted on a Dimension Icon (Bruker, Germany) in tapping mode with HQ:NSC15/Al BS cantilevers (MikroMasch, USA). All measurements were done in air and under ambient conditions. As measure for roughness, the root-mean-square (RMS) average of height deviations with regard to the mean image data plane (R_q in the software) was sampled from $5 \times 5 \mu\text{m}^2$ images with the AFM system onboard software (NanoScope 8.10, Bruker, Germany).

9.3.4. Fluorescence microscopy

The fluorescence imaging was performed on a Nikon Eclipse 80i upright fluorescence microscope (Nikon, Japan) equipped with an Intensilight illumination (Nikon, Japan), a CoolSNAP HQ2 camera (Photometrics, USA) and a Texas Red, FITC and Cy5 filters set (Nikon Y-2E/C).

9.3.5. Statistical analysis

All data are expressed as the means plus standard deviations. The significant differences between treatments were analyzed by one-way analysis of variance (ANOVA) and the Duncan tests at $P < 0.05$ using statistical package for the social sciences (SPSS, version 19.0.0 Abacus Concepts, Berkeley, California, USA).

References:

- [1] a) R. D. Piner, J. Zhu, F. Xu, S. Hong, C. A. Mirkin, *science* **1999**, 283, 661-663; b) K.-B. Lee, S.-J. Park, C. A. Mirkin, J. C. Smith, M. Mrksich, *Science* **2002**, 295, 1702-1705; c) C. C. Wu, D. N. Reinhoudt, C. Otto, V. Subramaniam, A. H. Velders, *Small* **2011**, 7, 989-1002; d) K. Salaita, Y. Wang, C. A. Mirkin, *Nature nanotechnology* **2007**, 2, 145; e) K.-B. Lee, J.-H. Lim, C. A. Mirkin, *Journal of the American Chemical Society* **2003**, 125, 5588-5589; f) M. Jaschke, H.-J. Butt, *Langmuir* **1995**, 11, 1061-1064; g) D. S. Ginger, H. Zhang, C. A. Mirkin, *Angewandte Chemie International Edition* **2004**, 43, 30-45; h) A. Pimpin, W. Srituravanich, *Engineering Journal* **2012**, 16, 37-56.
- [2] a) M. Hirtz, M. Lyon, W. Feng, A. E. Holmes, H. Fuchs, P. A. Levkin, *Beilstein journal of nanotechnology* **2013**, 4, 377-384; b) J. Xu, M. Lynch, J. L. Huff, C. Mosher, S. Vengasandra, G. Ding, E. Henderson, *Biomedical microdevices* **2004**, 6, 117-123.
- [3] a) J. Escorihuela, A. T. Marcelis, H. Zuilhof, *Advanced Materials Interfaces* **2015**, 2, 1500135; b) R. Kumar, A. Bonicelli, S. Sekula-Neuner, A. C. Cato, M. Hirtz, H. Fuchs, *small* **2016**, 12, 5330-5338; c) A. Tăbăcaru, B. Furdui, I. O. Ghinea, G. Carac, R. M. Dinică, *Inorganica Chimica Acta* **2017**, 455, 329-349.
- [4] H. C. Kolb, M. Finn, K. B. Sharpless, *Angewandte Chemie International Edition* **2001**, 40, 2004-2021.
- [5] a) M. Davydova, A. de los Santos Pereira, M. Bruns, A. Kromka, E. Ukraintsev, M. Hirtz, C. Rodriguez-Emmenegger, *Rsc Advances* **2016**, 6, 57820-57827; b) E. Mauri, F. Rossi, in *Bioresorbable Polymers for Biomedical Applications*, Elsevier, **2017**, pp. 303-329; c) N. Ji, L. Jian-Ping, D. Huan, P. Hong-Cheng, *Chinese Journal of analytical chemistry* **2015**, 43, 609-617; d) G. K. Such, A. P. Johnston, K. Liang, F. Caruso, *Progress in Polymer Science* **2012**, 37, 985-1003; e) Y. Zhou, Z. Xie, K. A. Brown, D. J. Park, X. Zhou, P. C. Chen, M. Hirtz, Q. Y. Lin, V. P. Dravid, G. C. Schatz, *Small* **2015**, 11, 913-918; f) J. Li, L. Li, X. Du, W. Feng, A. Welle, O. Trapp, M. Grunze, M. Hirtz, P. A. Levkin, *Nano letters* **2014**, 15, 675-681.
- [6] E. A. Bayer, M. Wilchek, *Journal of Chromatography A* **1990**, 510, 3-11.
- [7] a) M. F. Chedid, C. R. Krueel, M. A. Pinto, T. J. Grezzana-Filho, I. Leipnitz, C. D. Krueel, L. A. Scaffaro, A. D. Chedid, *ABCD. Arquivos Brasileiros de Cirurgia Digestiva (São Paulo)* **2017**, 30, 272-278; b) S. Daher, M. Massarwa, A. A. Benson, T. Khoury, *Journal of clinical and translational hepatology* **2018**, 6, 69; c) S. K. Olsen, R. S. Brown Jr, A. B. Siegel, *Therapeutic advances in gastroenterology* **2010**, 3, 55-66.
- [8] N. M. Tunissiolli, M. M. U. Castanhole-Nunes, P. M. Biselli-Chicote, É. C. Pavarino, R. F. da Silva, *Asian Pacific journal of cancer prevention: APJCP* **2017**, 18, 863.
- [9] a) J. Lou, L. Zhang, S. Lv, C. Zhang, S. Jiang, *Biomarkers in cancer* **2017**, 9, 1179299X16684640; b) R. Chaiteerakij, B. D. Addissie, L. R. Roberts, *Clinical Gastroenterology and Hepatology* **2015**, 13, 237-245; c) N. Tsuchiya, Y. Sawada, I. Endo, K. Saito, Y. Uemura, T. Nakatsura, *World journal of gastroenterology: WJG* **2015**, 21, 10573.

- [10] a) A. S. Lok, R. K. Sterling, J. E. Everhart, E. C. Wright, J. C. Hoefs, A. M. Di Bisceglie, T. R. Morgan, H. Y. Kim, W. M. Lee, H. L. Bonkovsky, *Gastroenterology* **2010**, *138*, 493-502; b) J. A. Marrero, Z. Feng, Y. Wang, M. H. Nguyen, A. S. Befeler, L. R. Roberts, K. R. Reddy, D. Harnois, J. M. Llovet, D. Normolle, *Gastroenterology* **2009**, *137*, 110-118; c) H.-G. Wan, H. Xu, Y.-M. Gu, H. Wang, W. Xu, M.-H. Zu, *Clinics and research in hepatology and gastroenterology* **2014**, *38*, 706-714.
- [11] a) T. Kumada, H. Toyoda, T. Tada, S. Kiriya, M. Tanikawa, Y. Hisanaga, A. Kanamori, J. Tanaka, C. Kagebayashi, S. Satomura, *Journal of gastroenterology* **2014**, *49*, 555-563; b) R. K. Sterling, L. Jeffers, F. Gordon, A. P. Venook, K. R. Reddy, S. Satomura, F. Kanke, M. E. Schwartz, M. Sherman, *Clinical gastroenterology and hepatology* **2009**, *7*, 104-113.
- [12] a) P. Tangkijvanich, T. Chanmee, S. Komtong, V. Mahachai, N. Wisedopas, P. Pothacharoen, P. Kongtawelert, *Journal of gastroenterology and hepatology* **2010**, *25*, 129-137; b) J. P. Yu, X. G. Xu, R. J. Ma, S. N. Qin, C. R. Wang, X. B. Wang, M. Li, M. S. Li, Q. Ma, W. W. Xu, *Journal of clinical laboratory analysis* **2015**, *29*, 85-93.
- [13] J. A. Marrero, P. R. Romano, O. Nikolaeva, L. Steel, A. Mehta, C. J. Fimmel, M. A. Comunale, A. D'Amelio, A. S. Lok, T. M. Block, *Journal of hepatology* **2005**, *43*, 1007-1012.
- [14] a) Y. Tomimaru, H. Eguchi, H. Nagano, H. Wada, S. Kobayashi, S. Marubashi, M. Tanemura, A. Tomokuni, I. Takemasa, K. Umeshita, *Journal of hepatology* **2012**, *56*, 167-175; b) X. Chen, Y. Ba, L. Ma, X. Cai, Y. Yin, K. Wang, J. Guo, Y. Zhang, J. Chen, X. Guo, *Cell research* **2008**, *18*, 997.
- [15] S. A. Fouad, N. A. G. Mohamed, M. W. Fawzy, D. A. Moustafa, *Hepatitis monthly* **2015**, *15*.
- [16] H. Zhang, M. Yao, W. Wu, L. Qiu, W. Sai, J. Yang, W. Zheng, J. Huang, D. Yao, *Tumor Biology* **2015**, *36*, 9373-9383.
- [17] W.-W. Zhu, J. Guo, L. Guo, H. Jia, M. Zhu, J.-B. Zhang, C. Loffredo, M. Forgues, X. Xing, N. Ren, *Clinical Cancer Research* **2013**, clincanres. 3363.2012.
- [18] a) C. E. Nebel, B. Rezek, D. Shin, H. Uetsuka, N. Yang, *Journal of Physics D: Applied Physics* **2007**, *40*, 6443; b) V. Vermeeren, S. Wenmackers, P. Wagner, L. Michiels, *Sensors* **2009**, *9*, 5600-5636; c) Y. Gurbuz, W. P. Kang, J. L. Davidson, D. V. Kerns, *Sensors and Actuators B: Chemical* **2004**, *99*, 207-215; d) N. Chaniotakis, N. Sofikiti, *Analytica chimica acta* **2008**, *615*, 1-9; e) C. Nebel, N. Yang, H. Uetsuka, E. Osawa, N. Tokuda, O. Williams, *Diamond and Related Materials* **2009**, *18*, 910-917.
- [19] a) J.-I. Kim, A. Bordeanu, J.-C. Pyun, *Biosensors and Bioelectronics* **2009**, *24*, 1394-1398; b) V. Vermeeren, L. Grieten, N. V. Bon, N. Bijmens, S. Wenmackers, S. Janssens, K. Haenen, P. Wagner, L. Michiels, *Sensors and Actuators B: Chemical* **2011**, *157*, 130-138; c) S. Wenmackers, V. Vermeeren, M. Vandeven, M. Ameloot, N. Bijmens, K. Haenen, L. Michiels, P. Wagner, *physica status solidi (a)* **2009**, *206*, 391-408.
- [20] a) X. Wang, M. Karlsson, P. Forsberg, M. Sieger, F. Nikolajeff, L. Österlund, B. Mizaikoff, *Analytical chemistry* **2014**, *86*, 8136-8141; b) B. J. Hausmann, I. Bulu, P. Deotare, M.

- McCutcheon, V. Venkataraman, M. Markham, D. Twitchen, M. Loncar, *Nano letters* **2013**, *13*, 1898-1902.
- [21] V. V. Rostovtsev, L. G. Green, V. V. Fokin, K. B. Sharpless, *Angewandte Chemie International Edition* **2002**, *41*, 2596-2599.
- [22] W. B. Chaderjian, E. T. Chin, R. J. Harris, T. M. Etcheverry, *Biotechnology progress* **2005**, *21*, 550-553.
- [23] N. J. Agard, J. A. Prescher, C. R. Bertozzi, *Journal of the American Chemical Society* **2004**, *126*, 15046-15047.
- [24] a) Y. Chu, Y. H. Oum, I. S. Carrico, *Virology* **2016**, *487*, 95-103; b) B. Gold, G. B. Dudley, I. V. Alabugin, *Journal of the American Chemical Society* **2013**, *135*, 1558-1569; c) C. G. Gordon, J. L. Mackey, J. C. Jewett, E. M. Sletten, K. Houk, C. R. Bertozzi, *Journal of the American Chemical Society* **2012**, *134*, 9199-9208; d) C.-F. Wang, M. P. Sarparanta, E. M. Mäkilä, M. L. Hyvönen, P. M. Laakkonen, J. J. Salonen, J. T. Hirvonen, A. J. Airaksinen, H. A. Santos, *Biomaterials* **2015**, *48*, 108-118; e) M. V. Bharathi, M. Chhabra, P. Paira, *Bioorganic & medicinal chemistry letters* **2015**, *25*, 5737-5742.
- [25] B. D. Fairbanks, T. F. Scott, C. J. Kloxin, K. S. Anseth, C. N. Bowman, *Macromolecules* **2008**, *42*, 211-217.
- [26] a) B. D. Fairbanks, E. A. Sims, K. S. Anseth, C. N. Bowman, *Macromolecules* **2010**, *43*, 4113-4119; b) C. E. Hoyle, A. B. Lowe, C. N. Bowman, *Chemical Society Reviews* **2010**, *39*, 1355-1387; c) F. Alimohammadi, C. Wang, O. Z. Durham, H. R. Norton, C. N. Bowman, D. A. Shipp, *Polymer* **2016**, *105*, 180-186; d) D. Meziane, A. Barras, A. Kromka, J. Houdkova, R. Boukherroub, S. Szunerits, *Analytical chemistry* **2011**, *84*, 194-200; e) C. Zhou, Y.-H. Li, Z.-H. Jiang, K.-D. Ahn, T.-J. Hu, Q.-H. Wang, C.-H. Wang, *Chinese Chemical Letters* **2016**, *27*, 681-684.
- [27] M. Wijdeven, C. Nicosia, A. Borrmann, J. Huskens, F. van Delft, *RSC advances* **2014**, *4*, 10549-10552.
- [28] C.-F. Wang, E. M. Mäkilä, M. H. Kaasalainen, D. Liu, M. P. Sarparanta, A. J. Airaksinen, J. J. Salonen, J. T. Hirvonen, H. A. Santos, *Biomaterials* **2014**, *35*, 1257-1266.
- [29] R. K. Manova, S. P. Pujari, C. A. Weijers, H. Zuilhof, T. A. van Beek, *Langmuir* **2012**, *28*, 8651-8663.
- [30] S. Jung, H. Yi, *Biomacromolecules* **2013**, *14*, 3892-3902.
- [31] A. Kuzmin, A. Poloukhine, M. A. Wolfert, V. V. Popik, *Bioconjugate chemistry* **2010**, *21*, 2076-2085.
- [32] a) D. Prim, F. Rebeaud, V. Cosandey, R. Marti, P. Passeraub, M. Pfeifer, *Molecules* **2013**, *18*, 9833-9849; b) V. Cosandey, F. Debrot, J. Kaeser, R. Marti, P. Passeraub, J. Pétremand, D. Prim, M. E. Pfeifer, *CHIMIA International Journal for Chemistry* **2012**, *66*, 803-806.

- [33] S. V. Orski, G. R. Sheppard, S. Arumugam, R. M. Arnold, V. V. Popik, J. Locklin, *Langmuir* **2012**, *28*, 14693-14702.
- [34] P. Gobbo, Z. Mossman, A. Nazemi, A. Niaux, M. C. Biesinger, E. R. Gillies, M. S. Workentin, *Journal of Materials Chemistry B* **2014**, *2*, 1764-1769.
- [35] M. Guerrouache, S. Mahouche-Chergui, M. M. Chehimi, B. Carbonnier, *Chemical Communications* **2012**, *48*, 7486-7488.
- [36] J. Escorihuela, M.-J. Bañuls, R. Puchades, Á. Maquieira, *Journal of Materials Chemistry B* **2014**, *2*, 8510-8517.
- [37] N. S. Bhairamadgi, S. Gangarapu, M. A. Caipa Campos, J. M. Paulusse, C. J. van Rijn, H. Zuilhof, *Langmuir* **2013**, *29*, 4535-4542.
- [38] Z. Sun, C. Han, M. Song, L. Wen, D. Tian, H. Li, L. Jiang, *Advanced Materials* **2014**, *26*, 455-460.
- [39] W. Feng, L. Li, E. Ueda, J. Li, S. Heißler, A. Welle, O. Trapp, P. A. Levkin, *Advanced Materials Interfaces* **2014**, *1*, 1400269.
- [40] M. Hirtz, A. M. Greiner, T. Landmann, M. Bastmeyer, H. Fuchs, *Advanced Materials Interfaces* **2014**, *1*, 1300129.
- [41] A.-L. Winkler, M. Koenig, A. Welle, V. Trouillet, D. Kratzer, C. Hussal, J. Lahann, C. Lee-Thedieck, *Biomacromolecules* **2017**, *18*, 3089-3098.
- [42] J. Eisenblaetter, M. Bruns, U. Fehrenbacher, L. Barner, C. Barner-Kowollik, *Polymer Chemistry* **2013**, *4*, 2406-2413.
- [43] S. Hansson, V. Trouillet, T. Tischer, A. S. Goldmann, A. Carlmark, C. Barner-Kowollik, E. Malmström, *Biomacromolecules* **2012**, *14*, 64-74.
- [44] a) D. G. Castner, K. Hinds, D. W. Grainger, *Langmuir* **1996**, *12*, 5083-5086; b) T. Tischer, A. S. Goldmann, K. Linkert, V. Trouillet, H. G. Börner, C. Barner-Kowollik, *Advanced Functional Materials* **2012**, *22*, 3853-3864.
- [45] a) C. E. Hoyle, C. N. Bowman, *Angewandte Chemie International Edition* **2010**, *49*, 1540-1573; b) A. B. Lowe, *Polymer Chemistry* **2014**, *5*, 4820-4870.
- [46] A. B. Lowe, *Polymer* **2014**, *55*, 5517-5549.
- [47] J. T. Wu, C. H. Huang, W. C. Liang, Y. L. Wu, J. Yu, H. Y. Chen, *Macromolecular rapid communications* **2012**, *33*, 922-927.
- [48] O. Norberg, I. H. Lee, T. Aastrup, M. Yan, O. Ramström, *Biosensors and Bioelectronics* **2012**, *34*, 51-56.
- [49] C. Wang, P.-F. Ren, X.-J. Huang, J. Wu, Z.-K. Xu, *Chemical Communications* **2011**, *47*, 3930-3932.
- [50] J. Bolley, E. Guenin, N. Lievre, M. Lecouvey, M. Soussan, Y. Lalatonne, L. Motte, *Langmuir* **2013**, *29*, 14639-14647.

- [51] I. Kaminska, W. Qi, A. Barras, J. Sobczak, J. Niedziolka-Jonsson, P. Woisel, J. Lyskawa, W. Laure, M. Opallo, M. Li, *Chemistry-A European Journal* **2013**, *19*, 8673-8678.
- [52] N. S. Bhairamadgi, S. P. Pujari, F. A. Leermakers, C. J. van Rijn, H. Zuilhof, *Langmuir* **2014**, *30*, 2068-2076.
- [53] C. A. Stevens, L. Safazadeh, B. J. Berron, *Langmuir* **2014**, *30*, 1949-1956.
- [54] Y. Xu, H. Xu, X. Jiang, J. Yin, *Advanced Functional Materials* **2014**, *24*, 1679-1686.
- [55] X. Hu, H. Tan, X. Wang, P. Chen, *Colloids and Surfaces A: Physicochemical and Engineering Aspects* **2016**, *489*, 297-304.
- [56] M. Comí, G. Lligadas, J. C. Ronda, M. Galià, V. Cádiz, *Polymer* **2016**, *103*, 163-170.
- [57] X. He, L. Chen, Y. Zhang, *Journal of Chromatography A* **2017**, *1513*, 118-125.
- [58] A. Concellón, L. Asín, S. González-Lana, M. Jesús, C. Sánchez-Somolinos, M. Pinol, L. Oriol, *Polymer* **2017**, *117*, 259-267.
- [59] D. P. Nair, M. Podgórski, S. Chatani, T. Gong, W. Xi, C. R. Fenoli, C. N. Bowman, *Chemistry of Materials* **2013**, *26*, 724-744.
- [60] T. Komnenos, *Liebigs Ann. Chem* **1883**, *218*, 145-169.
- [61] A. Michael, *Advanced Synthesis & Catalysis* **1887**, *35*, 349-356.
- [62] a) J. W. Chan, C. E. Hoyle, A. B. Lowe, M. Bowman, *Macromolecules* **2010**, *43*, 6381-6388; b) B. H. Northrop, S. H. Frayne, U. Choudhary, *Polymer Chemistry* **2015**, *6*, 3415-3430.
- [63] N. Kimura, T. Okegawa, K. Yamazaki, K. Matsuoka, *Bioconjugate chemistry* **2007**, *18*, 1778-1785.
- [64] R. Tedja, A. H. Soeriyadi, M. R. Whittaker, M. Lim, C. Marquis, C. Boyer, T. P. Davis, R. Amal, *Polymer Chemistry* **2012**, *3*, 2743-2751.
- [65] H. Seto, M. Takara, C. Yamashita, T. Murakami, T. Hasegawa, Y. Hoshino, Y. Miura, *ACS applied materials & interfaces* **2012**, *4*, 5125-5133.
- [66] H. Seto, C. Yamashita, S. Kamba, T. Kondo, M. Hasegawa, M. Matsuno, Y. Ogawa, Y. Hoshino, Y. Miura, *Langmuir* **2013**, *29*, 9457-9463.
- [67] P. Gobbo, M. C. Biesinger, M. S. Workentin, *Chemical Communications* **2013**, *49*, 2831-2833.
- [68] H. Fensterbank, K. Baczko, C. Constant, N. Idttalbe, F. Bourdreux, A. Vallée, A.-M. Goncalves, R. Méallet-Renault, G. Clavier, K. Wright, *J. Org. Chem* **2016**, *81*, 8222-8233.
- [69] L. Q. Xu, D. Pranantyo, K.-G. Neoh, E.-T. Kang, G. D. Fu, *ACS Sustainable Chemistry & Engineering* **2016**, *4*, 4264-4272.
- [70] J. Gaitzsch, M. Delahaye, A. Poma, F. Du Prez, G. Battaglia, *Polymer Chemistry* **2016**, *7*, 3046-3055.
- [71] B. Aktan, L. Chambre, R. Sanyal, A. Sanyal, *Biomacromolecules* **2017**, *18*, 490-497.

- [72] V. S. Khire, T. Y. Lee, C. N. Bowman, *Macromolecules* **2007**, *40*, 5669-5677.
- [73] M. W. Jones, G. Mantovani, S. M. Ryan, X. Wang, D. J. Brayden, D. M. Haddleton, *Chemical Communications* **2009**, 5272-5274.
- [74] Y. Gao, R. E. Kieltyka, W. Jesse, B. Norder, A. V. Korobko, A. Kros, *Soft matter* **2014**, *10*, 4869-4874.
- [75] D. Nieves, N. Azmi, R. Xu, R. Levy, E. Yates, D. Fernig, *Chemical Communications* **2014**, *50*, 13157-13160.
- [76] M. Arslan, T. N. Gevrek, J. Lyskawa, S. Szunerits, R. Boukherroub, R. Sanyal, P. Woisel, A. Sanyal, *Macromolecules* **2014**, *47*, 5124-5134.
- [77] B. Schyrr, S. p. Pasche, G. Voirin, C. Weder, Y. C. Simon, E. J. Foster, *ACS applied materials & interfaces* **2014**, *6*, 12674-12683.
- [78] S. Belbekhouche, M. Guerrouache, B. Carbonnier, *Macromolecular Chemistry and Physics* **2016**, *217*, 997-1006.
- [79] G. D. Stynes, T. R. Gengenbach, G. K. Kiroff, W. A. Morrison, M. A. Kirkland, *Journal of Biomedical Materials Research Part A* **2017**, *105*, 1940-1948.
- [80] A. Beloqui, S. Baur, V. Trouillet, A. Welle, J. Madsen, M. Bastmeyer, G. Delaittre, *Small* **2016**, *12*, 1716-1722.
- [81] G. Iucci, C. Battocchio, M. Dettin, F. Ghezzi, G. Polzonetti, *Solid State Sciences* **2010**, *12*, 1861-1865.
- [82] H. Woehlk, J. Steinkoenig, C. Lang, L. Michalek, V. Trouillet, P. Krolla, A. S. Goldmann, L. Barner, J. P. Blinco, C. Barner-Kowollik, *Langmuir* **2018**, *34*, 3264-3274.
- [83] M. Wilchek, E. A. Bayer, in *Methods in enzymology*, Vol. 184, Elsevier, **1990**, pp. 5-13.
- [84] a) N. Deshpande, A. Parulkar, R. Joshi, B. Diep, A. Kulkarni, N. A. Brunelli, *Journal of Catalysis* **2019**, *370*, 46-54; b) G. H. Posner, D. Rogers, *Journal of the American Chemical Society* **1977**, *99*, 8208-8214; c) P. Rani, R. Srivastava, *RSC Advances* **2015**, *5*, 28270-28280; d) M. C. Stuparu, A. Khan, *Journal of Polymer Science Part A: Polymer Chemistry* **2016**, *54*, 3057-3070.
- [85] K. Jin, W. H. Heath, J. M. Torkelson, *Polymer* **2015**, *81*, 70-78.
- [86] a) S. De, A. Khan, *Chemical Communications* **2012**, *48*, 3130-3132; b) S. Binder, I. Gadwal, A. Biemann, A. Khan, *Journal of Polymer Science Part A: Polymer Chemistry* **2014**, *52*, 2040-2046; c) I. Gadwal, S. Binder, M. C. Stuparu, A. Khan, *Macromolecules* **2014**, *47*, 5070-5080; d) A. Brändle, A. Khan, *Polymer Chemistry* **2012**, *3*, 3224-3227.
- [87] a) S. B. Rahane, R. M. Hensarling, B. J. Sparks, C. M. Stafford, D. L. Patton, *Journal of Materials Chemistry* **2012**, *22*, 932-943; b) R. Iwata, R. Satoh, Y. Iwasaki, K. Akiyoshi, *Colloids and Surfaces B: Biointerfaces* **2008**, *62*, 288-298; c) V. Grazú, O. Abian, C. Mateo, F. Batista-Viera, R. Fernández-Lafuente, J. M. Guisán, *Biomacromolecules* **2003**, *4*, 1495-1501.

- [88] a) M. Sangermano, M. Cerrone, G. Colucci, I. Roppolo, R. Acosta Ortiz, *Polymer International* **2010**, *59*, 1046-1051; b) C. F. Carlborg, A. Vastesson, Y. Liu, W. van der Wijngaart, M. Johansson, T. Haraldsson, *Journal of Polymer Science Part A: Polymer Chemistry* **2014**, *52*, 2604-2615; c) F. Saharil, F. Forsberg, Y. Liu, P. Bettotti, N. Kumar, F. Niklaus, T. Haraldsson, W. Van Der Wijngaart, K. B. Gylfason, *Journal of Micromechanics and Microengineering* **2013**, *23*, 025021; d) D. Guzmán, X. Ramis, X. Fernández-Francos, A. Serra, *RSC Advances* **2015**, *5*, 101623-101633; e) Y. Jian, Y. He, Y. Sun, H. Yang, W. Yang, J. Nie, *Journal of Materials Chemistry C* **2013**, *1*, 4481-4489; f) X. Fernández-Francos, A.-O. Konuray, A. Belmonte, S. De la Flor, À. Serra, X. Ramis, *Polymer chemistry* **2016**, *7*, 2280-2290; g) D. Guzmán, X. Ramis, X. Fernández-Francos, A. Serra, *European polymer journal* **2014**, *59*, 377-386; h) M. Pepels, I. Filot, B. Klumperman, H. Goossens, *Polymer Chemistry* **2013**, *4*, 4955-4965.
- [89] a) F. A. Saddique, A. F. Zahoor, S. Faiz, S. A. R. Naqvi, M. Usman, M. Ahmad, *Synthetic Communications* **2016**, *46*, 831-868; b) E. Ertürk, A. S. Demir, *Arkivoc* **2008**, *2*, 160-171; c) C. Wang, H. Yamamoto, *Journal of the American Chemical Society* **2014**, *136*, 6888-6891; d) M. Mauri, N. Tran, O. Prieto, T. Hjertberg, C. Müller, *Polymer* **2017**, *111*, 27-35.
- [90] a) C. I. Schilling, N. Jung, M. Biskup, U. Schepers, S. Bräse, *Chemical Society reviews* **2011**, *40*, 4840-4871; b) A. Procopio, P. Costanzo, R. Dalpozzo, L. Maiuolo, M. Nardi, M. Oliverio, *Tetrahedron Letters* **2010**, *51*, 5150-5153; c) T. Meguro, N. Terashima, H. Ito, Y. Koike, I. Kii, S. Yoshida, T. Hosoya, *Chemical communications* **2018**, *54*, 7904-7907.
- [91] a) J. Ali, J. Najeeb, M. A. Ali, M. F. Aslam, A. Raza, *J. Biosens. Bioelectron* **2017**, *8*, 1-9; b) P. Mehrotra, *Journal of oral biology and craniofacial research* **2016**, *6*, 153-159.
- [92] S. M. M. Dadfar, S. Sekula-Neuner, U. Bog, V. Trouillet, M. Hirtz, *Small* **2018**, *14*, 1800131.
- [93] S. M. M. Dadfar, S. Sekula-Neuner, V. Trouillet, M. Hirtz, *Advanced Materials Interfaces* **2018**, *5*, 1801343.
- [94] a) A. O. Konuray, X. Fernández-Francos, X. Ramis, *Polymer* **2017**, *116*, 191-203; b) A. O. Konuray, X. Fernández-Francos, X. Ramis, *Polymer chemistry* **2017**, *8*, 5934-5947.
- [95] S. Oberhansl, M. Hirtz, A. Lagunas, R. Eritja, E. Martinez, H. Fuchs, J. Samitier, *Small* **2012**, *8*, 541-545.
- [96] a) A. K. Chakraborti, S. Rudrawar, A. Kondaskar, *Organic & biomolecular chemistry* **2004**, *2*, 1277-1280; b) J. Yadav, B. Reddy, A. Basak, A. V. Narsaiah, *Tetrahedron letters* **2003**, *44*, 1047-1050; c) T. Ollevier, G. Lavie-Compin, *Tetrahedron Letters* **2004**, *45*, 49-52; d) A. Kamal, R. Ramu, M. A. Azhar, G. R. Khanna, *Tetrahedron letters* **2005**, *46*, 2675-2678; e) B. Pujala, S. Rana, A. K. Chakraborti, *The Journal of organic chemistry* **2011**, *76*, 8768-8780; f) X. a. Chen, H. Wu, S. Wang, S. Huang, *Synthetic Communications* **2012**, *42*, 2440-2452.
- [97] Q. Xie, X. Weng, L. Lu, Z. Lin, X. Xu, C. Fu, *Biosensors and bioelectronics* **2016**, *77*, 46-50.
- [98] M. Hirtz, W. Feng, H. Fuchs, P. A. Levkin, *Advanced Materials Interfaces* **2016**, *3*, 1500469.
- [99] a) Y. Jeong, K. Choi, J. Kim, D. S. Chung, B. Kim, H. C. Kim, K. Chun, *Sensors and Actuators B: Chemical* **2008**, *128*, 349-358; b) L. Jiang, F. Li, J. Feng, P. Wang, Q. Liu, Y. Li, Y. Dong, Q.

- Wei, *RSC Advances* **2016**, *6*, 24373-24380; c) Y. Li, Y. Zhang, L. Jiang, P. K. Chu, Y. Dong, Q. Wei, *Scientific reports* **2016**, *6*, 22694.
- [100] a) Y. Liu, H. Wang, J. Huang, J. Yang, B. Liu, P. Yang, *Analytica chimica acta* **2009**, *650*, 77-82; b) L. Jiang, J. Han, F. Li, J. Gao, Y. Li, Y. Dong, Q. Wei, *Electrochimica Acta* **2015**, *160*, 7-14; c) W. Li, X. Jiang, J. Xue, Z. Zhou, J. Zhou, *Biosensors and Bioelectronics* **2015**, *68*, 468-474; d) K. Tawa, F. Kondo, C. Sasakawa, K. Nagae, Y. Nakamura, A. Nozaki, T. Kaya, *Analytical chemistry* **2015**, *87*, 3871-3876; e) F. Li, J. Han, L. Jiang, Y. Wang, Y. Li, Y. Dong, Q. Wei, *Biosensors and Bioelectronics* **2015**, *68*, 626-632.
- [101] J. Xu, M. Lynch, S. Nettikadan, C. Mosher, S. Vegasandra, E. Henderson, *Sensors and Actuators B: Chemical* **2006**, *113*, 1034-1041.
- [102] K. L. Parry, A. Shard, R. Short, R. White, J. Whittle, A. Wright, *Surface and Interface Analysis: An International Journal devoted to the development and application of techniques for the analysis of surfaces, interfaces and thin films* **2006**, *38*, 1497-1504.

Appendix A: List of abbreviations

| | |
|---|--------------|
| Alkyne polyethylene glycol silane | ALK-PEG-Si |
| Alpha 1-antitrypsin deficiency | A1AD or AADT |
| Alpha-fetoprotein | AFP |
| Analysis of variance | ANOVA |
| Antibody | Ab |
| Atomic force microscopy | AFM |
| Azadibenzocyclooctyne | ADIBO |
| Benzyl dimethylamine | BDMA |
| Biarylazacyclooctynone | BARAC |
| Bicyclo[6.1.0]nonyne | BCN |
| Biotin polyethylene glycol amine | Biotin-amine |
| Biotin polyethylene glycol thiol | Biotin-thiol |
| Bovine serum albumin | BSA |
| Carbon nanotube | CNT |
| 5-Carboxytetramethylrhodamine-azide | TAMRA-azide |
| Cellulose nanocrystals | CNC |
| Chemical vapor deposition | CVD |
| Constant analyzer energy mode | CAE |
| Copper-catalyzed azide-alkyne cycloaddition | CuAAC |
| Cy5 labeled polyethylene glycol thiol | Cy5 thiol |
| Cytokeratin 19 | CK19 |

| | |
|---|-------------|
| Des-gamma-carboxy prothrombin | DCP |
| Diazabicyclo[4.3.0]non-5-ene | DBN |
| 1,8-diazabicyclo[5.4.0]undec-7-ene | DBU |
| Dibenzoazacyclooctyne | DIBAC |
| Dibenzocyclooctyne-acid | DBCO-acid |
| Dibenzocyclooctyne | DIBO |
| Dibenzylcyclooctyne-PEG4-biotin conjugate | Biotin-DBCO |
| Dibenzylcyclooctyne-PEG4-5/6-FAM | FAM-DBCO |
| Diels-Alder | DA |
| Difluorinated cyclooctyne | DIFO |
| 4-Dimethylaminopyridine | DMAP |
| Dip-pen nanolithography | DPN |
| Dimethyl sulfoxide | DMSO |
| Early Detection Research Network | EDRN |
| Electron-withdrawing groups | EWG |
| Global Cancer Observatory | GCO |
| (3-Glycidyloxypropyl)trimethoxysilane | GPTMS |
| Glypican-3 | GPC-3 |
| Gold nanoparticles | Au NPs |
| Golgi protein 73 | GP73 |
| Hepatitis B virus | HBV |
| Hepatitis C virus | HCV |

| | |
|---|--------------------------------|
| Hepatocellular carcinoma | HCC |
| Magnetic nanoparticles | Fe ₃ O ₄ |
| Maleimide-containing tannic acid | TAMA |
| (3-Mercaptopropyl)trimethoxysilane | MPTMS |
| 1-methylimidazole | 1MI |
| Microchannel cantilevers spotting | μCS |
| MicroRNA | miRNA |
| Midkine | MDK |
| Monofluorinated cyclooctyne | MOFO |
| National Cancer Institute | NCI |
| N,N'-Dicyclohexylcarbodiimide | DCC |
| Nonalcoholic steatohepatitis | NASH |
| Osteopontin | OPN |
| Phosphate buffered saline | PBS |
| Poly(ethylene terephthalate) | PET |
| Poly hydroxyethyl methacrylate | pHEMA |
| Poly(vinyl alcohol) | PVA |
| Root-mean-square | RMS |
| Salmon calcitonin | sCT |
| Silica-bonded S-sulfonic acid | SBSSA |
| Stainless steel | SS |
| Statistical package for the social sciences | SPSS |

| | |
|--|------------------|
| Strain-promoted azide-alkyne cycloaddition | SPAAC |
| Surface patterning tool | SPT |
| Tetramethylrhodamine-5-maleimide | TAMRA-maleimide |
| Thiol-ene coupling | TEC |
| Thiol-ene Michael addition | TEMA |
| Thiol-yne coupling | TYC |
| Titanium oxide | TiO ₂ |
| Triethylamine | TEA |
| X-ray photoelectron spectroscopy | XPS |

Appendix B: List of Figures

- Figure 1.1.** Schematic illustration of soft lithography ^[1h]
- Figure 1.2.** Schematic illustration of electron beam lithography ^[1h]
- Figure 1.3.** Schematic illustration of dip-pen nanolithography ^[1h]
- Figure 1.4.** Dye delivery by microchannel cantilever. The substrate (1) is placed on the stage (2), which can be actuated in the x-, y- and z-direction with a precision of less than 100 nm. The substrate can be brought into contact with the apex of the microchannel cantilever of the SPT (3) By raising the stage in the z-direction ^[2a].
- Figure 1.5.** Schematic of quill-type cantilever-based SPT ^[2b]
- Figure 1.6.** A NLP 2000 System along with related software
- Figure 1.7.** Examples of silane coupling agents used in the silanization technique
- Figure 1.8.** Most significant metal-free click reactions used in the modification of solid surfaces and materials during the last ten years. Newly formed bonds after performing click reaction are highlighted in blue.
- Figure 1.9.** Cancer incidence and mortality statistics worldwide. Number of (a) new cases and (b) deaths in 2018, in 185 countries of the world, for 36 types of cancer, for both sexes and for all ages. These results are available at Global Cancer Observatory (GCO) web site of the International Agency for Research on Cancer (IARC)
- Figure 3.1.** Different types of click chemistry reactions between (a) azide and linear alkyne (CuAAC); (b) azide and cycloalkyne (SPAAC); (c) thiol and linear alkyne and (d) thiol and cycloalkyne.
- Figure 3.2.** Some commonly used cyclooctynes for strain-promoted azide–alkyne cycloaddition (SPAAC)
- Figure 3.3.** Comparison between azide-alkyne and thiol-alkyne click reactions: (a) bare glass; (b) hydroxyl-terminated glass; (c) DBCO-terminated glass; (d) treatment of the DBCO-terminated surface with TAMRA-azide and biotin-azide; (e) treatment of the DBCO-terminated surface with Cy5 thiol and biotin-thiol.
- Figure 3.4.** Characterization of OH-terminated and DBCO-terminated glasses by XPS and contact angle measurement. (a) N 1s XP spectra of OH-terminated (bottom) and DBCO-terminated (top) glasses; (b) Contact angle over time on DBCO- and OH-terminated glass. The experimental data was fitted using MATLAB software. The dashed horizontal line represents the contact angle of the bare glass

which is about 46° . The red dashed line represents a curve of $y = (47.4x+5.1)/(x+3.3)$ and the green dashed curve $y = (63.9x+65.1)/(x+3.1)$, respectively.

Figure 3.5. Array immobilization of TAMRA-azide on the DBCO-terminated glass: (a) Fluorescence microscope images of two micropatterns at two different relative humidities. The inset shows the size distribution of the spots. Scale bars equal $50\ \mu\text{m}$. Dwell time was 0.1 s and exposure time for imaging 10 s; (b) effect of humidity on average radius and fluorescence intensity of the spots. Values with different letters differ significantly ($p < 0.05$), based on Duncan's test.

Figure 3.6. (a) Influence of reaction time and temperature on average fluorescence intensity of the TAMRA-azide spots immobilized on the DBCO-terminated glass through click reaction. For the same temperature, values with different lower case letters and for the same time, values with different capital letters are significantly different ($p < 0.05$), according to Duncan's test; (b) a fluorescence microscope image of micropattern obtained at optimum time (20 min) and temperature ($37\ ^\circ\text{C}$) with a spotting humidity of 20% and dwell time of 0.1 s. The exposure time for the image was 10 s, the inset shows the size distribution of the spots, scale bar equals $50\ \mu\text{m}$; (c) N 1s XP spectra of the DBCO-terminated glass after click reaction with TAMRA-azide at optimum time (20 min) and temperature ($37\ ^\circ\text{C}$) (top) and of DBCO-terminated glass (bottom).

Figure 3.7. Lithography of (a) DBCO-terminated and (b) unfunctionalized glass with TAMRA-azide. Spotting humidity = 20%, dwell time = 0.1 s, reaction time = 4 h, reaction temperature = $37\ ^\circ\text{C}$, and exposure time = 10 s. Scale bars equal $50\ \mu\text{m}$.

Figure 3.8. (a) Influence of reaction time and temperature on average fluorescence intensity of the Cy5 thiol spots immobilized on the DBCO-terminated glass. For the same temperature, values with different lower case letters and for the same time, values with different capital letters are significantly different ($p < 0.05$), according to Duncan's test; (b) fluorescence microscope image of micropattern obtained at optimum time (40 min) and temperature ($37\ ^\circ\text{C}$) with a spotting humidity of 20% and dwell time of 0.1 s. The exposure time for the image was 5 s, the inset shows the size distribution of the spots, scale bar equals $50\ \mu\text{m}$; (c) C 1s XP spectra of the DBCO-terminated glass after click reaction with Cy5 thiol at optimum time (40 min) and temperature ($37\ ^\circ\text{C}$) (top) and DBCO terminated glass (bottom).

Figure 3.9. Fluorescence microscope images of microarrays of (a) biotin-azide conjugate immobilized on the DBCO-terminated glass after incubating with streptavidin-Cy3, click reaction time = 20 min, click reaction temperature = $37\ ^\circ\text{C}$; (b) biotin-thiol immobilized on the DBCO-terminated glass after incubating with streptavidin-Cy3, click reaction time = 40 min, click reaction temperature = $37\ ^\circ\text{C}$. For both microarrays, spotting humidity was 20% and dwell time of 0.1 s was used. The exposure time of both images was 10 s, and the insets show the size distribution of the spots. Scale bars equal

50 μm ; (c) N 1s and (d) S 2p XP spectra of DBCO-terminated glass (bottom), biotin-azide immobilized on DBCO (c, top) and biotin-thiol immobilized on DBCO (d, top).

- Figure 3.10.** Effect of molecular weight / spacer length of biotin-azide or biotin-thiol on the intensity of spots after incubation with fluorescent labeled streptavidin. Molar concentrations of biotin-azide and biotin-thiol solutions were about 2.2 and 0.5 mM, respectively. The numbers in the parentheses present the molecular weight of compounds. Values with the same letters do not differ significantly ($p < 0.05$), based on Duncan's test.
- Figure 4.1.** Examples of catalysts used in the (a) base-catalyzed and (b) nucleophile-catalyzed thiol-en Michael addition reaction.
- Figure 4.2.** Schematic illustration for thiol-terminated surface modification by thiol-yne coupling and thiol-ene Michael addition click reactions. The pink and red squares symbolize non-fluorescent and fluorescent dyes, respectively.
- Figure 4.3.** Characterization of hydroxyl-terminated and thiol-terminated glasses by contact angle measurement; (a) The experimental data of contact angle measurements which were fitted by rational functions using MATLAB software. The red and blue dashed curves are the best fitted curves related to OH-terminated and SH-terminated glasses, respectively. Also, the green horizontal dashed line denotes the contact angle of the bare glass which is about 46° . Values with different letters differ significantly ($p < 0.05$), based on Duncan's test; Images of water droplets on (b) OH-terminated and (c) SH-terminated glasses.
- Figure 4.5.** Influence of reaction time and temperature on average fluorescence intensity of the (a) FAM-DBCO and (b) TAMRA-maleimide spots immobilized on the thiol-terminated glass via click reaction. For the same temperature, values with different lower case letters and for the same time, values with different capital letters are significantly different ($p < 0.05$), according to Duncan's test; Fluorescence microscope images of micropatterns obtained at optimum reaction temperature and time (37°C and 20 min) with a spotting humidity of 20% and dwell time (tip/surface contact time) of 0.1 s for (c) FAM-DBCO and (d) TAMRA-maleimide spots immobilized on the thiol-terminated glass. The exposure time for the images was 10 s, the insets show the size distribution of the spots and the scale bars equal 50 μm .
- Figure 4.6.** Influence of ink concentration on average fluorescence intensity of the (a) biotin-DBCO and (b) biotin-maleimide spots immobilized on the thiol-terminated glass through click reaction after incubating with fluorescently labeled streptavidin. Click reaction time and temperature were 20 min and 37°C , respectively. Values with different letters differ significantly ($p < 0.05$), based on Duncan's test; Fluorescence microscope images of micropatterns for (c) biotin-DBCO and (d)

biotin-maleimide spots immobilized on the thiol-terminated glass at ink concentrations $400 \mu\text{g}\cdot\text{ml}^{-1}$ (c and d; tops) and $2000 \mu\text{g}\cdot\text{ml}^{-1}$ (c and d; bottoms), after incubating with streptavidin. For all microarrays spotting humidity was 20% and dwell time of 0.1 s was used. Also, the exposure time of images was 20 s, the insets show the size distribution of the spots and scale bars equal $50 \mu\text{m}$.

Figure 5.1. (a) Two possible regio-isomers expected from ring opening of epoxy by thiol, amine and azide; proposed literature mechanisms for (b) thiol-epoxy reaction initiated by base catalyst, (c) epoxy-amine reaction and (d) epoxy-azide reaction.

Figure 5.2. Schematic representation of the chemical strategies used for functionalization of epoxy-terminated glasses by different fluorescent and non- fluorescent dyes.

Figure 5.3. Water contact angles over time on hydroxyl- and epoxy-terminated glasses. Graphs of contact angle over time were fitted by rational functions utilizing MATLAB software to give a better guide to the eye. The red and green dashed curves are the best fit for OH-terminated (taken as comparison from [92]) and epoxy-terminated glasses, respectively. The blue horizontal dashed line represents the contact angle of the bare glass at about 46° . Significant changes in contact angle ($p < 0.05$) are marked by different letters.

Figure 5.4. Roughness values determined by AFM test for the hydroxyl-terminated (I) and epoxy-terminated (II) glasses as well as for the epoxy-terminated glasses after coating with Cy5 thiol (III), TAMRA-azide (IX), R6G (X), biotin-thiol (XI), biotin-amine (XII) and biotin-azide (XIII).

Figure 5.5. Arrays of fluorescent-labeled dyes including Cy5 thiol, R6G and TAMRA-azide. For all microarrays spotting humidity was 20% and dwell time of 0.1 s was used. Also, the exposure time of images was 20 s, the insets show the size distribution of the spots and scale bars equal $50 \mu\text{m}$.

Figure 5.6. Arrays of biotin-thiol, biotin-amine and biotin-azide on epoxy-terminated glass after incubating with fluorescent-labeled streptavidin. For all microarrays spotting humidity was 20% and dwell time of 0.1 s was used. Also, the exposure time of images was 20 s and scale bars equal $50 \mu\text{m}$.

Figure 6.1. Biotin immobilization on the hydroxyl-terminated glasses via different click reactions. Hydroxyl-terminated glasses were first functionalized with DBCO-OH (path i), MPTMS (path ii), or GPTMS (path iii), subsequently biotinylated through different click reactions (routes 1-6)

Figure 6.2. Schematic of microarrays prepared for AFP detection. (a) Incubating biotinylated surfaces with streptavidin solution, (b) reaction of the streptavidin on the surface with biotinylated anti-AFP (c) delivery of fluorescent-labeled AFP via μCS and (d) preparation of fluorescent-labeled AFP through reaction between NHS-ester reagent (NHS-rhodamine) and primary amine of antigen (AFP)

- Figure 6.3.** Roughness values determined by AFM test for the bare glass and hydroxyl-, DBCO-, thiol- and epoxy-terminated glasses as well as for samples of routes 1-6. Values with the same letters do not differ significantly ($p < 0.05$), based on Duncan's test.
- Figure 6.4.** XPS characterization of (a) hydroxyl-terminated (bottom) and DBCO-terminated (top) glasses; (b) DBCO-terminated glass (bottom) and sample of route 1 (top); (c) DBCO-terminated glass (bottom) and sample of route 2 (top); (d) hydroxyl-terminated (bottom) and thiol-terminated (top) glasses; (e) thiol-terminated glass (bottom) and sample of route 3 (top); (f) thiol-terminated glass (bottom) and sample of route 4 (top); (g) hydroxyl-terminated (bottom) and epoxy-terminated (top) glasses; (h) epoxy-terminated glass (bottom) and sample of route 5 (top) and (i) epoxy-terminated glass (bottom) and sample of route 6 (top).
- Figure 6.5.** Detection of AFP antigen. (a) Fluorescence intensity of microarrays after incubating fluorescent-labeled AFP spots with anti-AFP on the surfaces at different times (10, 20, 30 and 60 min) and two temperatures (25 and 37 °C). Anti-AFP was immobilized via biotin-streptavidin-biotin sandwich technique on the different biotinylated surfaces (samples of routes 1-6) previously prepared via different click reaction methods. (b-g) fluorescence microscope images of micropatterns obtained at optimum incubation time and temperature. All microarrays were spotted at 20% relative humidity. Ink concentration was 800 $\mu\text{g}\cdot\text{ml}^{-1}$. Dwell and exposure times of all images were 0.1 and 0.4 s, respectively. Spot size distribution is given in the insets. All scale bars equal 100 μm .
- Figure 6.6.** Evaluation of sensitivity of microarrays prepared from sample of route 5 after incubating anti-AFP spots with fluorescent-labeled AFP. (a) Fluorescence intensity of microarrays at different concentrations of fluorescent-labeled AFP (12.5, 25, 50, 100, 200, 400 and 800 $\mu\text{g}\cdot\text{ml}^{-1}$) (b) fluorescence microscope images of micropatterns. All microarrays were spotted at 20% relative humidity. Dwell and exposure times of all images were 0.1 and 0.4 s, respectively. Incubation conditions were 37 °C and 20 min.
- Figure 6.7.** Detection of unlabeled AFP by additional sandwich approach via a second binding of biotinylated antibody and fluorescent-labeled streptavidin
- Figure 6.8.** Fluorescence microscope image of micropattern obtained from unlabeled AFP after implementation of the incubation step with fluorescent-labeled streptavidin
- Figure 7.1.** Diamond surfaces with average roughness of (a) 4 nm and (b) 14 nm
- Figure 7.2.** Contact angle measurement for different types of functionalized diamond
- Figure 7.3.** Fluorescence microscope images of micropatterns of fluorescent inks obtained at optimum reaction

conditions with a spotting humidity of 20%, dwell time (tip/surface contact time) of 2 s and exposure time of 10 s. (a) and (b) Cy5 thiol on the DBCO-terminated surface, (c) and (d) TAMRA-azide on the DBCO-terminated surface, (e) and (f) TAMRA-maleimide on the thiol-terminated surface, (g) and (h) FAM-DBCO on the thiol-terminated surface, (i) and (j) Cy5 thiol on the epoxy-terminated surface, (k) and (l) R6G on the epoxy-terminated surface and (m) and (n) TAMRA-azide on the epoxy-terminated surface. The scale bars equal 50 μm .

Figure 7.4. Fluorescence microscope images of micropatterns non-fluorescent inks after incubation with fluorescent-labeled streptavidin obtained at optimum reaction conditions with a spotting humidity of 20%, dwell time (tip/surface contact time) of 2 s and exposure time of 10 s. (a) and (b) biotin-thiol on the DBCO-terminated surface, (c) and (d) biotin-azide on the DBCO-terminated surface, (e) and (f) biotin-maleimide on the thiol-terminated surface, (g) and (h) biotin-DBCO on the thiol-terminated surface, (i) and (j) biotin-thiol on the epoxy-terminated surface, (k) and (l) biotin-amine on the epoxy-terminated surface and (m) and (n) biotin-azide on the epoxy-terminated surface. The scale bars equal 50 μm .

Appendix C: List of Tables

Table 3.1. Elemental composition determined by XPS

Table 3.2. Static contact angles of water droplets on the bare and functionalized glass surfaces

Table 7.1. Average fluorescence intensity of different fluorescent spots immobilized on the different functionalized diamond via click reaction

Table 7.2. Average fluorescence intensity of different non-fluorescent spots immobilized on the different functionalized diamond via click reaction

Table 9.1 List of the used materials

Curriculum Vitae

Name Seyed Mohammad Mahdi Dadfar
Born 17.02.1987; Iran
Address Leopoldstraße 62, 76344 Eggenstein-Leopoldshafen, Germany
Email mahdi.dadfar@kit.edu
Phone +49(0)1788774992
Family Single



Today Guest scientist at Institute of Nanotechnology (INT)
Karlsruhe Institute of Technology (KIT)
Hermann-von-Helmholtz-Platz 1, 76344 Eggenstein-Leopoldshafen, Germany

Supervisor PD Dr. Dr. Michael Hirtz

Education

2016-2019 Karlsruhe Institute of Technology (KIT)
Karlsruhe, Germany
PhD, Institute of Nanotechnology (INT)
Coupling Chemistry for Surface Immobilization in Scanning Probe Lithography
Grade: Sehr gut (magna cum laude)
Supervisors: PD Dr. Dr. Michael Hirtz and Prof. Dr. Annie Powell

2013-2015 **Working on Projects at Shiraz University instead of Military Service**
Member of Iran's National Elites Foundation
Working on different projects at Shiraz University in the field of biopolymers, synthesis of nanomaterials for drug delivery application and nanocomposites instead of military service under supervision of Prof. Dr. Kavooosi
Collaboration with top universities in Iran
Consulting engineer at some polymer companies

2010-2013 **Shiraz University**
Shiraz, Iran
Master of Science, Department of Food Science and Technology, (GPA: 16.67/20)
Thesis Title: "Production and Investigation of Antibacterial and Physicochemical Properties of Carboxymethyl cellulose, Gelatin and Chitosan based films reinforced with nanosilver"
(grade=19.85)

2005-2009 **Tehran University (Faculty of Food Science)**
Tehran, Iran

Bachelor of Science, (GPA: 16.17/20.0)

2004-2005 **Alameh Jafarie pre-university**
Pre-University Certificate (GPA: 18.1/20)

2001-2004 **Shahed high school**
High-school Diploma (GPA: 18.4/20)

Industrial Experience

Summer 2008 Exir Pharmaceutical Company, Borojerd, Iran, (Worked as a Project Trainee)

Honor/Award

2018 Wining “KHYS Networking Grant” for visiting two international groups including Denmark Technical University (DTU) and University of Twente

2013-2015 Member of “Iran’s National Elites Foundation” (The highest prestige and professional nation foundation for supporting elites) and working on projects at university instead of military service which is mandatory in Iran

2013 M.Sc. thesis proposal approved and supported by the Iran Nanotechnology Initiative Council

2010 Being Accepted to Shiraz University among more than 5,000 for M.Sc in Food Science and Technology

2005 Being Accepted to Faculty of Food Science, Tehran University among 392,048 for B.Sc in Food Science and Technology (Iranian 2th ranked university)

1998-2000 Ranked 1st in Provincial Scientific Exams (2 times)

1993-2005 Ranked 1st during twelve years education of Elementary, Middle, High School, and Pre-University

Research Projects

Production of Light Weight Biocomposite from Different Biopolymers (Gelatin, Cellulose and Polyvinyl alcohol) and Glass Fiber and Investigation of Mechanical and Chemical Properties of Them. As a Successful Project for Mandatory Military Services in Iran

Biodegradable Films Made from Gelatin and Carbon Nanotube for Food Packaging Applications

Environmentally-Friendly Food Packaging Made of Polylactic acid and Organoclay

Patent

Seyed Mohammad Mahdi Dadfar, Gholamreza Kavooosi, and Amin Mohammadi, “Transparent Wound Dressing with Antimicrobial Properties Made of Different Biopolymers Incorporated with Essential Oils”. (granted November, 1, 2012)

Seyed Mohammad Mahdi Dadfar, Gholamreza Kavooosi, and Amin Mohammadi, “Bio polymeric sticking plaster and wound dressing” (granted August, 3, 2013)

Journal Publications

- 1) **Seyed Mohammad Mahdi Dadfar**, Sylwia Sekula-Neuner, Uwe Bog, Vanessa Trouillet, Michael Bruns, and Michael Hirtz. Site-specific surface functionalization via microchannel cantilever spotting (μ CS): comparison between thiol-alkyne and azide-alkyne click chemistry reactions.” *ISI journal of Small (published)*. Vol. 14. 1800131 (2018).
- 2) **Seyed Mohammad Mahdi Dadfar**, Sylwia Sekula-Neuner, Vanessa Trouillet, and Michael Hirtz. A Comparative Study of Thiol-Terminated Surface Modification by Click Reactions: Thiol-yne Coupling versus Thiol-ene Michael Addition.” *ISI journal of advanced material interface. (published)*. 1801343 (2018).
- 3) **Seyed Mohammad Mahdi Dadfar**, Gholamreza Kavooosi, Seyed Mohammad Ali Dadfar,”Investigation of mechanical properties, antibacterial features, and water vapor permeability of polyvinyl alcohol thin films reinforced by glutaraldehyde and multiwalled carbon nanotube”, *ISI Journal of polymer composites. (published)*. Vol. 35.9 (2014) 1736-1743.
- 4) **Seyed Mohammad Mahdi Dadfar**, Gholamreza Kavooosi ”Mechanical and water binding properties of carboxymethyl cellulose/multiwalled carbon nanotube nanocomposites”, *ISI Journal of polymer composites (published)*. Vol. 36.1 (2014) 145-152.
- 5) Gholamreza Kavooosi, **Seyed Mohammad Mahdi Dadfar**, Amin Mohammadi Purfard. ”Mechanical, Physical, Antioxidant, and Antimicrobial Properties of Gelatin Films Incorporated with Thymol for Potential Use as Nano Wound Dressing”, *ISI Journal of food science (published)*. Vol. 78.2 (2013) 244-250. **(most-cited paper of 2013)**
- 6) Gholamreza Kavooosi, **Seyed Mohammad Mahdi Dadfar**, Amin Mohammadi Purfard, Reza Mehrabi. ”antioxidant and antibacterial properties of gelatin films incorporated with carvacrol”, *ISI Journal of food safety (published)*. Vol. 33.4 (2013) 423-432.
- 7) Asgar Farahnaky, **Seyed Mohammad Mahdi Dadfar**, Mahdiyaz Shahbazi,”Physical and mechanical properties of gelatin-clay nanocomposite”, *ISI Journal of food Engineering (published)*. Vol. 122 (2014) 78–83
- 8) Gholamreza Kavooosi, **Seyed Mohammad Mahdi Dadfar**, Seyed Mohammad Ali Dadfar, Farhad Ahmadi, Mehrdad Niakosari, ” Investigation of gelatin/multi-walled carbon nanotube nanocomposite films as packaging materials”, *ISI Journal of food science and nutrition. (published)*. Vol. 2. 1 (2014) 65-73
- 9) Gholamreza Kavooosi, Aytak rahmatollahi, **Seyed Mohammad Mahdi Dadfar**, Amin Mohammadi Purfard. ” Effects of essential oil on the water binding capacity, physico-mechanical properties, antioxidant and antibacterial activity of gelatin films” *ISI Journal of food science and technology. (published)*. Vol. 57.2 (2014) 556-561.
- 10) Gholamreza Kavooosi, Behroz nateghpoor, **Seyed Mohammad Mahdi Dadfar** and Seyed Mohammad Ali Dadfar. “Antioxidant, antifungal, water binding, and mechanical properties of poly(vinyl alcohol) film incorporated with essential oil as a potential wound dressing material”, *ISI journal of applied polymer science Vol. 131.20 (2014)*.
- 11) Gholamreza Kavooosi, Amin Shakiba, Mahmood Ghorbani. **Seyed Mohammad Mahdi Dadfar**, Amin Mohammadi Purfard. “Antioxidant, Antibacterial, Water Binding Capacity and Mechanical Behavior of Gelatin-Ferula Oil Film as a Wound Dressing Material”, *ISI journal of Galen medical (published)*. Vol. 4.2 (2015) 103-114.
- 12) Gholamreza Kavooosi, Zarintaj Bordbar, Seyed Mohammad Ali Dadfar, **Seyed Mohammad Mahdi Dadfar**. “Preparation and characterization of a novel gelatin–poly (vinyl alcohol) hydrogel film loaded with Zataria multiflora essential oil for antibacterial–antioxidant wound-dressing applications” *ISI journal of applied polymer science (published)*. Vol. 134.39 (2017).

13) **Seyed Mohammad Mahdi Dadfar**, Sylwia Sekula-Neuner, Vanessa Trouillet, Hui-Yu Liu, Ravi Kumar, Annie K. Powell, Michael Hirtz. "Evaluation of click chemistry microarrays for immunosensing of alpha-fetoprotein (AFP)". *Submitted*

14) **Seyed Mohammad Mahdi Dadfar**, Sylwia Sekula-Neuner, Vanessa Trouillet, Annie K. Powell, Michael Hirtz. "Ring opening of epoxy by thiol, amine and azide". *will be submitted soon*

Conference Presentations

Seyed Mohammad Mahdi Dadfar, Sylwia Sekula-Neuner, Uwe Bog, Vanessa Trouillet, Michael Bruns, and Michael Hirtz, Design and manufacturing of nanobiosensors suitable for protein detection, "Nanotech and Nanobiotechnology" conference in Paris, France, 2018

Seyed Mohammad Mahdi Dadfar, Sylwia Sekula-Neuner, Uwe Bog, Vanessa Trouillet, Michael Bruns, and Michael Hirtz, "international school of nanomedicine" conference in Palermo, Italy, April 2018

Seyed Mohammad Mahdi Dadfar, Sylwia Sekula-Neuner, Uwe Bog, Vanessa Trouillet, Michael Bruns, and Michael Hirtz, Site-specific surface modification of glass with fluorescent TAMRA-azide via microchannel cantilever spotting (μ CS), 5th KIT PhD Symposium, KIT, Karlsruhe, Germany, 2017

Seyed Mohammad Mahdi Dadfar, G. Kavooosi, A. Mohammadi Purfard," Transparent Wound Dressing with Antimicrobial Properties Made of Different Biopolymers Incorporated with Essential Oils, "submitted and presented in Mashhad Azad University Congress, October 2012.

Devices Proficiency

Atomic Force Microscopy (AFM)

Dip-Pen Nanolithography (DPN)

Desktop Nanolithography Platform (DNP)

Fluorescence Microscope

Extracurricular Activities

Refereeing Football, Watching Movies; Playing Soccer; Table Tennis, Hiking, Swimming and chess

Language

| | |
|---------|---------------|
| Farsi | Mother Tongue |
| English | Fluent |
| German | B1 |

References

1. PD Dr. Dr. Michael Hirtz (Current Supervisor)

Associate Professor

Karlsruhe Institute of Technology (KIT), Eggenstein-Leopoldshafen, Germany

E-mail: Michael.hirtz@kit.edu

3. Prof. Dr. Annie Powell

Professor

Institute of Inorganic Chemistry and Institute of Nanotechnology, Karlsruhe Institute of Technology,

76131 Karlsruhe, Germany

E-mail: annie.powell@kit.edu

2. Prof. Dr. Harald Fuchs

Professor

Physikalisches Institut Wilhelm-Klemm Str. 10

48149 Münster, Germany

E-mail: fuchsh@uni-muenster.de

4. Prof. Dr. Gholamreza Kavooosi

Associate Professor

Shiraz University, Shiraz, Iran

E-mail: ghkavooosi@shirazu.ac.ir

List of publications

- 1) **Seyed Mohammad Mahdi Dadfar**, Sylwia Sekula-Neuner, Uwe Bog, Vanessa Trouillet, Michael Bruns, and Michael Hirtz. Site-specific surface functionalization via microchannel cantilever spotting (μ CS): comparison between thiol-alkyne and azide-alkyne click chemistry reactions.” *ISI journal of Small (published)*. Vol. 14. 1800131 (2018).
- 2) **Seyed Mohammad Mahdi Dadfar**, Sylwia Sekula-Neuner, Vanessa Trouillet, and Michael Hirtz. A Comparative Study of Thiol-Terminated Surface Modification by Click Reactions: Thiol-yne Coupling versus Thiol-ene Michael Addition.” *ISI journal of advanced material interface. (published)*. 1801343 (2018).
- 3) **Seyed Mohammad Mahdi Dadfar**, Gholamreza Kavooosi, Seyed Mohammad Ali Dadfar,”Investigation of mechanical properties, antibacterial features, and water vapor permeability of polyvinyl alcohol thin films reinforced by glutaraldehyde and multiwalled carbon nanotube”, *ISI Journal of polymer composites. (published)*. Vol. 35.9 (2014) 1736-1743.
- 4) **Seyed Mohammad Mahdi Dadfar**, Gholamreza Kavooosi ”Mechanical and water binding properties of carboxymethyl cellulose/multiwalled carbon nanotube nanocomposites”, *ISI Journal of polymer composites (published)*. Vol. 36.1 (2014) 145-152.
- 5) Gholamreza Kavooosi, **Seyed Mohammad Mahdi Dadfar**, Amin Mohammadi Purfard. ”Mechanical, Physical, Antioxidant, and Antimicrobial Properties of Gelatin Films Incorporated with Thymol for Potential Use as Nano Wound Dressing”, *ISI Journal of food science (published)*. Vol. 78.2 (2013) 244-250. (**most-cited paper of 2013**)
- 6) Gholamreza Kavooosi, **Seyed Mohammad Mahdi Dadfar**, Amin Mohammadi Purfard, Reza Mehrabi. ”antioxidant and antibacterial properties of gelatin films incorporated with carvacrol”, *ISI Journal of food safety (published)*. Vol. 33.4 (2013) 423-432.
- 7) Asgar Farahnaky, **Seyed Mohammad Mahdi Dadfar**, Mahdiyar Shahbazi,”Physical and mechanical properties of gelatin-clay nanocomposite”, *ISI Journal of food Engineering (published)*. Vol. 122 (2014) 78–83
- 8) Gholamreza Kavooosi, **Seyed Mohammad Mahdi Dadfar**, Seyed Mohammad Ali Dadfar, Farhad Ahmadi, Mehrdad Niakosari, ” Investigation of gelatin/multi-walled carbon nanotube nanocomposite films as packaging materials”, *ISI Journal of food science and nutrition. (published)*. Vol. 2. 1 (2014) 65-73
- 9) Gholamreza Kavooosi, Aytak rahmatollahi, **Seyed Mohammad Mahdi Dadfar**, Amin Mohammadi Purfard. ” Effects of essential oil on the water binding capacity, physico-mechanical properties, antioxidant and antibacterial activity of gelatin films” *ISI Journal of food science and technology. (published)*. Vol. 57.2 (2014) 556-561.
- 10) Gholamreza Kavooosi, Behroz nateghpoor, **Seyed Mohammad Mahdi Dadfar** and Seyed Mohammad Ali Dadfar. “Antioxidant, antifungal, water binding, and mechanical properties of poly(vinyl alcohol) film incorporated with essential oil as a potential wound dressing material”, *ISI journal of applied polymer science Vol. 131.20 (2014)*.
- 11) Gholamreza Kavooosi, Amin Shakiba, Mahmood Ghorbani. **Seyed Mohammad Mahdi Dadfar**, Amin Mohammadi Purfard. “Antioxidant, Antibacterial, Water Binding Capacity and Mechanical Behavior of Gelatin-Ferula Oil Film as a Wound Dressing Material”, *ISI journal of Galen medical (published)*. Vol. 4.2 (2015) 103-114.
- 12) Gholamreza Kavooosi, Zarintaj Bordbar, Seyed Mohammad Ali Dadfar, **Seyed Mohammad Mahdi Dadfar**. “Preparation and characterization of a novel gelatin–poly (vinyl alcohol) hydrogel film loaded with Zataria multiflora essential oil for antibacterial–antioxidant wound-dressing applications” *ISI journal of applied polymer science (published)*. Vol. 134.39 (2017).
- 13) **Seyed Mohammad Mahdi Dadfar**, Sylwia Sekula-Neuner, Vanessa Trouillet, Hui-Yu Liu, Ravi Kumar, Annie K. Powell, Michael Hirtz. “Evaluation of click chemistry microarrays for immunosensing of alpha-fetoprotein (AFP)”. *Submitted*
- 14) **Seyed Mohammad Mahdi Dadfar**, Sylwia Sekula-Neuner, Vanessa Trouillet, Annie K. Powell, Michael Hirtz. “Ring opening of epoxy by thiol, amine and azide”. *will be submitted soon*